UNIVERSITY OF SOUTHERN CALIFORNIA
DEPARTMENT OF CIVIL ENGINEERING

EMPIRICAL MODELS OF THE DURATION OF STRONG EARTHQUAKE GROUND MOTION BASED ON THE MODIFIED MERCALLI INTENSITY

by

Elena I. Novikova and Mihailo D. Trifunac

Report No. CE 94-01

Los Angeles, California
May, 1994

ABSTRACT

In this work, the duration of the strong motion part of a function $f(t)$ describing ground motion at a site (acceleration, velocity or displacement) is defined as the sum of the time intervals during which the integral $\int_0^t f^2(\tau)d\tau$ gains a significant portion of its final value. To determine frequency dependent duration, we filtered the signal through 12 narrow band-pass channels, and evaluated the duration separately in each channel. The main purpose of this work is to develop new empirical regression models of the so defined duration of strong earthquake ground motion in terms of the Modified Mercalli intensity observed at the recording site and of the recording site conditions. The duration is considered as being composed of two parts: (1) the duration of strong motion if the recording station was located on basement rocks and (2) the prolongation of this duration if the station is located on sediments.

We present a variety of the regression models of duration which differ from those in the literature by considering new model parameters and by the larger and more complete database used in the regression analysis. The model appropriate for each particular case can be chosen among those presented. The choice depends on the availability of information about the source, the propagation path, the intensity of shaking and the site conditions.

A distribution function of the residuals of the predicted duration is proposed. This, for example, allows to estimate the strong ground motion duration which will not be exceeded with a given confidence level, if the intensity at the site (and, preferably, some site properties) are known.

ACKNOWLEDGEMENTS

This report summarizes a part of our effort in establishing the basis for development of empirical scaling equations for duration of strong earthquake shaking for use in seismic design in Southern California. This work has been supported in part by the joint project of the California Department of Transportation and the City and County of Los Angeles. This project is entitled "The Characteristics of Earthquake Ground Motion for Seismic Design." This report addresses the topic in Task H-4 of the above project and deals with the "Duration of Strong motion shaking in Southern California." The financial support from the California Department of Transportation and the City and County of Los Angeles, as well as the organizational support from the Southern California Earthquake Center, are gratefully acknowledged.

TABLE OF CONTENTS

Page No.

ABSTRACT i

ACKNOWLEDGEMENTS ii

TABLE OF CONTENTS iii

I. INTRODUCTION 1

I.1 About this study 1

I.2 The definition of duration 3

I.3 The strong ground motion database 8

II. THE TERMS INVOLVED IN THE DURATION MODELS 14

II.1 "Basic duration" 14

II.2 Prolongation due to site conditions 34

III. THE REGRESSION MODELS 40

III.1 Models $dur = dur(I_{MM}, \Delta', I_{MM}\Delta')$ and $dur = dur(I_{MM})$ 40

III.2 Models $dur = dur(I_{MM}, \Delta', I_{MM}\Delta', s)$, $dur = dur(I_{MM}, s)$ 53

III.3 Models $dur(I_{MM}, \Delta', I_{MM}\Delta', s, s_L)$ and $dur = dur(I_{MM}, s, s_L)$ 59

III.4 Models $dur = dur(I_{MM}, \Delta', I_{MM}\Delta', h, R, hR, R^2, h^2, \varphi)$ and $dur = dur(I_{MM}, h, R, hR, R^2, h^2\varphi)$ 66

III.5 Models $dur = dur(I_{MM}, \Delta', I_{MM}\Delta', R, R^2, \varphi)$, $dur = dur(I_{MM}, R, R^2, \varphi)$, $dur = dur(I_{MM}, \Delta', I_{MM}\Delta', h, h^2)$ and $dur = dur(I_{MM}, h, h^2)$ 81

III.6 How to choose the proper model 97

III.7 Distribution function of the residuals 97

IV. CONCLUSIONS 104

V. REFERENCES 106

I. INTRODUCTION

I.1. About this Study

Instrumental data are essential for all kinds of investigations of the amplitude and the duration characteristics of strong ground motion. However, it takes time to accumulate sufficient and homogeneous data on regional estimates of the magnitude scale. As a substitute for the instrumental data, a qualitative description of the earthquake effects in terms of the Modified Mercalli Intensity (MMI) scale (Wood and Neumann, 1931) or its equivalents can be used.

This work investigates the relationship between the frequency dependent duration of strong ground motion and the Modified Mercalli intensity at the recording site, I_{MM}. Regression equations, relating the duration of strong motion to I_{MM} can be found in the literature (Trifunac and Westermo, 1976, 1977, 1982; Westermo and Trifunac, 1978, 1979). In this work, we use more abundant database, and we present models which include new parameters and consider more detailed analyses.

As in the studies of Trifunac and Brady (1975a), Trifunac and Westermo (1977, 1982), Westermo and Trifunac (1979), Theofanopulos and Watabe (1989) and our previous work (Novikova and Trifunac, 1993), we consider the duration of the strong ground motion, *dur*, as the sum of the duration of the rupture process at the source, τ_0, the prolongation due to dispersion along the propagation from the source to the station, τ_Δ, and the prolongation due to the multiple scattering in sediments and/or soft soils near the recording site, $\tau_{\text{region and site}}$:

$$dur = \tau_0 + \tau_\Delta + \tau_{\text{region and site}}. \tag{1.1}$$

The first two terms, $\tau_0 + \tau_\Delta$, we call "the basic duration." It can be modeled in terms of the magnitude of the earthquake and the source-to-station distance (Trifunac and Brady, 1975a; Trifunac and Westermo, 1982; Westermo and Trifunac, 1978; Theofanopulos and Watabe, 1989; Novikova and Trifunac, 1993) or in terms of the Modified Mercalli intensity of shaking at the recording site (Trifunac and Westermo, 1977, 1982; Westermo and Trifunac, 1979). In this work, we develop two groups of regression equations. One group considers the "basic duration" as a function of both the Modified Mercalli intensity and the source-to-station distance. The second group of models does not include the source-to-station distance in the model parameters. The models from the first, more descriptive group, can be compared to the empirical equations, relating the duration to the magnitude of the earthquake and the epicentral distance (Novikova and Trifunac, 1993). The comparison allows us to study the MMI scale through several narrow frequency "windows," and find for which frequencies and distances the MMI is governed more by the magnitude of an earthquake, than by the attenuation with distance. Historically, the MMI scale has evolved dealing with description of the earthquake effects on older structures. The damage of the modern and in particular long-period (tall) structures, long span bridges or large dams is hard to describe by the MMI scale, because such

structures are not even mentioned in the definition of the scale. Thus, the correlations of the frequency dependent duration of strong ground shaking with I_{MM} should be useful not only for the duration studies, but also because of the possibility to understand better the "new" characteristics of the MMI scale at low frequencies.

The third term in Eq. (1.1), $\tau_{\text{region and site}}$ (in what follows, we will shorten this notation to τ_{rs}), can be expressed, for example, through the simplified geological classification parameter s ($s = 2$ for basement rock sites, $s = 0$ for sites located on sediments and $s = 1$ for intermediate sites, as in Trifunac and Brady, 1975b), and the local soil parameter s_L (as in Seed et al., 1976, $s_L = 2$ for deep soil sites, $s_L = 1$ for stiff soil sites and $s_L = 0$ for the sites located on local "rock"). This representation of τ_{rs} was used by Novikova and Trifunac (1993) in the models of frequency dependent duration with the "basic duration" expressed through the earthquake magnitude and the epicentral distance. When the Modified Mercalli intensity is used as the "main" parameter in the scaling equations (Trifunac and Westermo, 1976, 1977), the geological conditions at the recording site have been also shown to influence the duration of strong motion. In this work, we expand such analyses to include the scaling in terms of the local soil conditions as well.

The s- and s_L-description of the recording site conditions may, however, appear to be too rough to adequately describe the effects causing the prolongation of the duration at stations located on sediments. Westermo and Trifunac (1978, 1979) and Trifunac and Westermo (1982) used the depth of sediments under the recording site, h, instead of the parameter s for description of the geological conditions at the site and their influence on the duration. In these works, τ_{rs} was considered as a linear function of h, although it was mentioned that such a dependence may not be physically meaningful. Novikova and Trifunac (1993) developed another, more detailed, representation of the term τ_{rs} as a function of (a) the depth of sediments, h, under the recording station, (b) the characteristic horizontal dimension of the valley R—the distance from the station to the rocks, which reflect seismic waves coming from the source, in the direction of the station, and, thus produce some prolongation of the duration of strong motion, and (c) the angle, subtended at the station by those rocks, φ, which characterize the overall "power" of the horizontal reflections. The last two parameters, R and φ, can be estimated, for example, from the "Map showing distribution and configuration of basement rocks in California" by Smith (1964). It was found that τ_{rs} can be modeled by a sum of a linear function of φ and a coupled quadratic function of R and h. The latter corresponds to the qualitative analysis of how the duration should depend on the horizontal and the vertical dimensions of the sedimentary deposits. The duration increases with the increase of these dimensions up to some intermediate values of h and R because of the delayed arrivals of the waves which experienced reflections inside or at the boundaries of the sedimentary valley. Further increase of h and R causes a decrease of the duration due to attenuation of the late arrivals, which propagate along longer paths. In Novikova and Trifunac (1993) the described form of τ_{rs} was used together with the "basic duration" $\tau_0 + \tau_\Delta$ expressed in terms of the earthquake magnitude and the epicentral distance. In

this work, we utilize this same form of τ_{rs} in models of the duration with intensity-type "basic duration."

It is of interest in practical applications not only to the be able to predict the expected value of the duration of strong ground motion, but also to evaluate the probability of exceedance of any given duration at a particular frequency. One can estimate this probability from the distribution functions of the residuals. We use here the same distribution function of the residuals as the one used by Novikova and Trifunac (1993). The coefficients of this function are adjusted for each model at each frequency band.

The regression equations and the distributions of the residuals presented in this work are fully applicable only in the region were the strong motion data used in the regression analyses were collected, i.e. in the Western United States and, in particular, in California. It might (and it will) happen that a different geological environment can change the prevailing earthquake mechanism, the distribution of the hypocentral depths of the sources, the velocities and the attenuation factors, and other possible conditions that influence the values of the regression coefficients. Also, the intensity scales used in other parts of the world are significantly different from the MMI scale. Another restriction in the application of our models comes from the "completeness" of the database we used for the regression analysis. The database covers only a restricted range of earthquake magnitudes, distances to the epicenter, intensity at the site and other parameters. We assume that only predictions coming from interpolation, not extrapolation, may be acceptable. However, our equations can probably serve as a starting point for analysis of data from other regions and other databases. The proper adjustments of the frequency dependent coefficients in our models may appear to be sufficient to get the regression equation suited for a different region. This releases the investigator from the lengthy work of searching for a physically justified empirical model, and requires only the effort of implementing the regression analysis with already existing equations. Also, the database necessary to develop the regression equations should be more abundant than the database required for the adjustment of the existing models to the new region.

I.2 The Definition of Duration

The first studies of the dependence of the duration on magnitude (Housner, 1965) and on epicentral distance and magnitude (Esteva and Rosenblueth, 1964) did not present quantitative definitions of duration. Page et al. (1972) define the duration to be the time interval between the first and the last time when the acceleration exceeds the level of 0.05 g ("bracketed" duration). Husid et al. (1969) define the duration as the time interval during which 95% of the total energy (eventually observed at the site) is coming to the recording station. Trifunac and Brady (1975a) define the duration of the excitation function $f(t)$, which can be acceleration, velocity or displacement, as the shortest time interval during which 90% of the integral $\int_0^{t_0} f^2(\tau)d\tau$ is achieved (t_0 designates the length of the digitized record). Bolt (1973) suggested that the duration

of strong ground motion should be considered separately in several narrow frequency bands, as it is physically a frequency dependent quantity. Trifunac and Westermo (1976, 1977, 1982) and Westermo and Trifunac (1978, 1979) followed this idea and developed frequency dependent definition of duration, based on the earlier work of Trifunac and Brady (1975a). Kawashima and Aizawa (1989) studied the bracketed and introduced the normalized duration, which they defined as the elapsed time between the first and the last acceleration excursions greater than μ times the peak acceleration ($0 < \mu < 1$). McCann and Shah (1979) based their definition of the duration on the time dependent root-mean square acceleration, $a_{\rm rms}(t)$. The derivative of $a_{\rm rms}(t)$ identifies the time after which $a_{\rm rms}(t)$ is always decreasing, and this time is used as the upper cut-off time of the strong motion portion. The lower cut-off time can be obtained by applying the above procedure to the record with reversed time. Vanmarcke and Lai (1980) introduced a definition of duration of strong ground shaking using an idealization of the earthquake as a segment of limited duration of a random process with constant spectral density function. Their definition relates the Arias intensity, the maximum acceleration at the site, the predominant period of earthquake excitation and the root-mean square acceleration to the duration of strong ground motion. Mohraz and Peng (1989) introduced the structural frequency and the damping into the definition of duration and used a low-pass filter for computing the duration.

The definition of duration, as used by different investigators, progressed from the simple "bracketed" duration towards the frequency dependent, structural response oriented functionals. The seismic energy and the rate of the seismic energy input are considered now as the main tools in the definition of duration. Many definitions utilize the integral of the type $\int_0^t f^2(\tau)d\tau$, where $f(t)$ is acceleration, velocity or displacement. These integrals can and do have specific physical meaning. For example, $\int_0^t v^2(\tau)d\tau$ is proportional to the total energy, transmitted by the seismic waves past the recording point. The time derivative of this integral gives the power of the seismic excitation as a function of time. The time derivative of $\int_0^t a^2(\tau)d\tau$ gives $a^2_{\rm rms}(t)$. The functional $\int_0^{t_0} a^2(\tau)d\tau$ is proportional to the work (per unit mass) done during the time interval from $t = 0$ to $t = t_0$ by all the forces acting on a single-degree of freedom viscously damped oscillator, exited by the acceleration $a(t)$. When the length of the record t_0 is sufficient to capture all significant motions at the recording site, the functional $\int_0^{t_0} a^2(\tau)d\tau$ is related to the Arias intensity. The probabilistic prediction of the response, $f(t)$, of a multi-degree of freedom structure can be characterized in terms of the number of peaks of $f(t)$ during the entire history of the excitation, the width of the power spectrum of $f(t)$ and the value of $(1/t_0)\cdot\left(\int_0^{t_0} f^2(\tau)d\tau\right)^{1/2}$ (Udwadia and Trifunac, 1974; Amini and Trifunac, 1985; Gupta and Trifunac, 1987, 1988, 1990a,b, 1991, 1992).

The portions of the record where $\int_0^t f^2(\tau)d\tau$ has its fastest growth can be related to the definition of the strong motion part of the excitation. Such definition of the strong motion duration can then be linked to various physical phenomena, whose description involves integrals of this type. Hence, following the works of Trifunac and Westermo, we will accept the definition of the strong motion duration of a function $f(t)$, where $f(t)$

is acceleration, velocity or displacement, as the sum of time intervals during which the integral $\int_0^t f^2(\tau)d\tau$ has the steepest slope and gains a significant portion (90%) of its final value.

The duration of strong ground shaking depends on the frequency of the motion. We account for this by studying the duration as a function of various parameters in 12 separate frequency bands, here called "channels." The central frequencies of these channels cover the span from $f_0 = 0.075$ Hz to $f_0 = 21$ Hz. The signal corresponding to each channel is obtained by band-pass filtering the original (wide-band) records by the Ormsby filters. The values of the roll-off and the cut-off frequencies of the Ormsby filters and their central frequencies f_0 are listed in Table 1.1. Band-pass filtering is applied to each component of acceleration, velocity and displacement.

The definition of duration we use in this report is of the "relative" type, i.e. it does not include information about the absolute level of acceleration, while the "absolute" definitions, like the one of Page et al. (1972) and Bolt (1973) do carry this information. However, the knowledge of the frequency dependent duration in this "relative" sense combined with the information about the Fourier spectral amplitudes at all frequencies (Trifunac, 1989a,b,c) provide a fairly complete description of the strong motion.

A useful feature of our definition is that, unlike some other physically related definitions (McCann and Shah, 1979; Vanmarcke and Lai, 1980), it considers the strong motion part as being composed of several separate strong motion portions, and the beginnings and the ends of all of these portions (pulses) can be specified. The definition of the duration of strong motion as one continuous time interval is not meaningful for some records. The information on the arrival time of each separate strong motion pulse and on its duration can be used to study the source of the earthquake and the related wave propagation phenomena (Novikova and Trifunac, 1993). Note also that this additional information about the "structure" of the strong motion can be used in further development of the definition of the strong motion duration. Thus, considering the energy dissipated by the structure in the time "gap" between two strong motion pulses and the root-mean square amplitude of the excitation function in this gap and in the pulses, one can determine whether the structure is going the "see" two consecutive strong ground motion pulses as one continuous strong excitation.

The procedure for calculating the frequency dependent duration in each channel of the recorded (and narrow-band-filtered) acceleration (and of the velocity and displacement obtained from it, Trifunac and Lee, 1979) is summarized in Fig. 1.1. The band-pass filtered $f(t)$ is shown at the top of the figure. The result of integration $I(t) = \int_0^t f^2(t)dt$ is shown in the center together with its smoothed version, $I_{\rm sm}(t)$. The reasons for the smoothing of the integral are discussed in detail by Novikova and Trifunac (1993). The values chosen for the corner frequencies of the smoothing filters in each channel are listed in Table 1.1. Note that the actual width of the pulses shorter than about 3 sec cannot be measured even in the high frequency channels after such a smoothing. We are primarily interested in the applications to structural response. When a lightly damped

Table 1.1 The properties of the filters used in the two-step process of calculating the frequency dependent duration of strong ground motion.

	Step one: bandpass filtering		**Step two:** smoothing of $\int_0^t f^2(\tau)\, d\tau$
Channel number	Central freq. f_0	Cut-off and roll-off frequencies of the bandpass filter, (Hz)	Corner freq. f_c
1	0.075 Hz	.05 - .07 ; .08 - .10	0.038 Hz
2	0.12 Hz	.08 - .10 ; .15 - .17	0.06 Hz
3	0.21 Hz	.15 - .17 ; .27 - .30	0.11 Hz
4	0.37 Hz	.27 - .30 ; .45 - .50	0.14 Hz
5	0.63 Hz	.45 - .50 ; .80 - .90	0.17 Hz
6	1.1 Hz	.80 - .90 ; 1.30 - 1.50	0.20 Hz
7	1.7 Hz	1.30 - 1.50 ; 1.90 - 2.20	0.23 Hz
8	2.5 Hz	1.90 - 2.20 ; 2.80 - 3.50	0.26 Hz
9	4.2 Hz	2.80 - 3.50 ; 5.00 - 6.00	0.28 Hz
10	7.2 Hz	5.00 - 6.00 ; 8.75 - 10.25	0.30 Hz
11	13 Hz	8.75 - 10.25 ; 16.00 - 18.00	0.32 Hz
12	21 Hz	16.00 - 18.00 ; 25.00 - 27.00	0.35 Hz

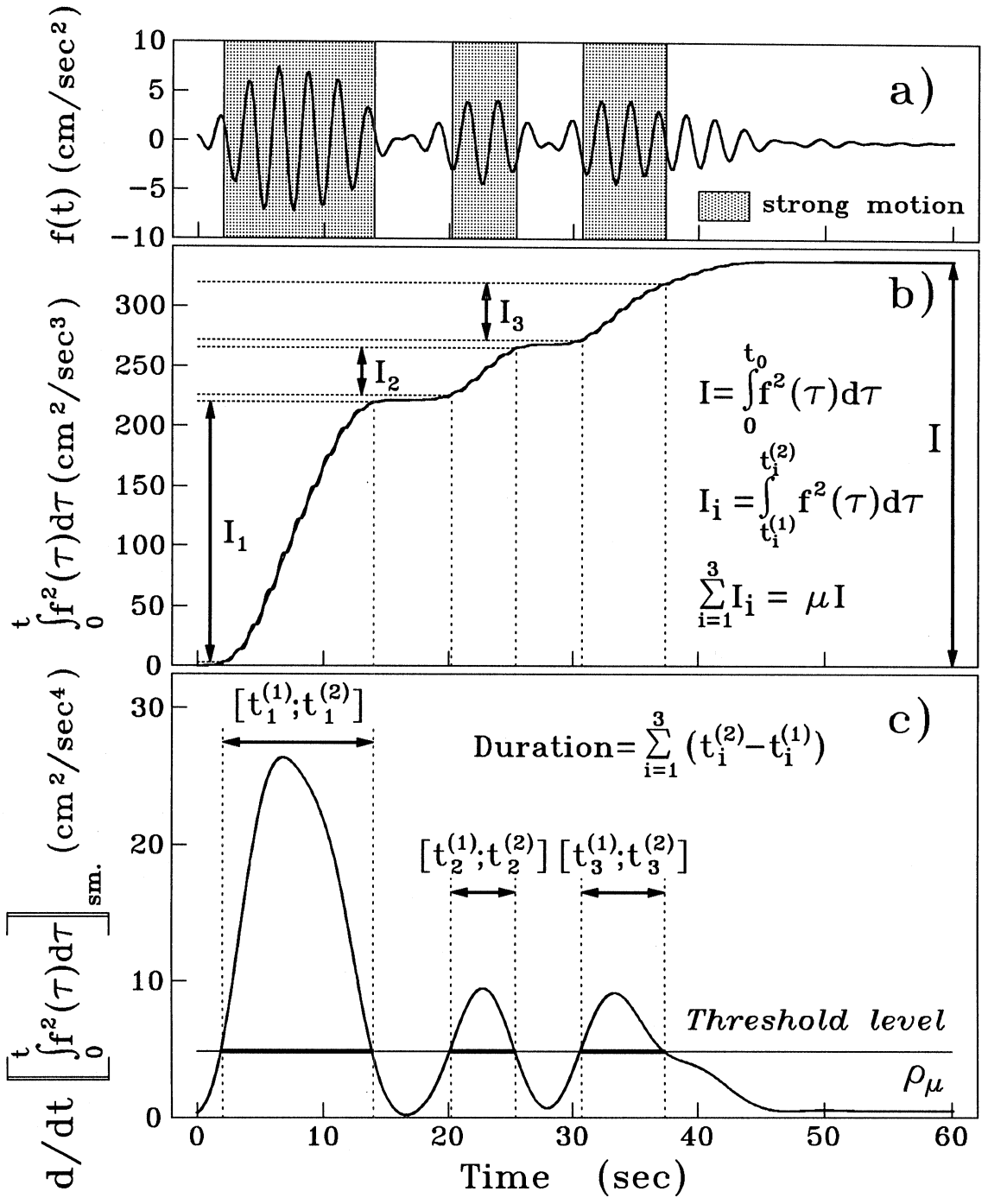

Fig. 1.1 The definition of the duration illustrated for the east acceleration component of the Morgan Hill earthquake, band-pass filtered by the channel #4 filters (central frequency 0.37 Hz):

a) a time history f(t) with the strong motion intervals shaded;

b) $\int_0^t f^2(\tau)d\tau$ and its smoothed version;

c) the derivative of the smoothed integral of $f^2(t)$ and its threshold level ρ_μ. Time intervals giving contribution to duration with $\mu = 0.9$ are highlighted.

structure is exited by the strong ground motion, the short pulses of the excitation function with short time gaps of "silence" inbetween them are smoothed out in the response. Being concerned primarily with the relatively long pulses of strong motion, we apply the smoothing filter to the exitation function. The duration of strong ground motion, *dur*, is then defined as the sum of several time intervals $[t_i^{(1)}; t_i^{(2)}]$, in which $I_{\rm sm}(t)$ has the steepest slope. The sum of the gains of $I(t)$ in those time intervals is equal to the fraction μ of the total integral $I(t_0)$, where t_0 is the length of the strong motion record. The portions of the record with the steepest slope of $I_{\rm sm}(t)$ are identified as those time intervals where the derivative $d\left[I_{\rm sm}(t)\right]/dt$ is bigger than some threshold level ρ_μ (bottom of the Fig. 1.1). The value of ρ_μ can be obtained in each case when μ is specified. In this study, we assumed $\mu = 0.9$. Some empirical models were tested with $\mu = 0.75$ and $\mu = 0.95$, and no significant differences in the major overall trends were found. From this point on, we will refer to the duration obtained by the procedure described above as "observed" duration.

I.3 The Strong Ground Motion Database

We used the uniformly processed data consisting of the three component "free field" acceleration records obtained in the Western U.S. (Lee and Trifunac, 1987). Each component of every record was digitized, integrated (to get velocity and acceleration) and filtered to be noise-free inside a frequency band which depends on the quality of the record, but is not wider than $[0.05 \div 25]$ Hz. The methods used in the digitization and the processing of these records are described by Trifunac and Lee (1979) and by Lee and Trifunac (1984, 1990). This database has 486 vertical and 984 horizontal components of acceleration, velocity and displacement, generated by 106 earthquakes and recorded at 283 different sites.

Large number of these records was generated by the San Fernando earthquake in 1971, which had magnitude $M = 6.4$. Excluding this event, the database has relatively uniform converge of magnitudes from $M = 4.0$ to $M = 6.5$ with just a few records available for $M \sim 3$ and $M \geq 7$ (Trifunac, 1991). Epicentral distances are uniformly represented in the range $\Delta \leq 50$ km with the number of available records progressively diminishing beyond $\Delta = 60$ km. The determination of the hypocentral depth is generally not reliable in the region with a shallow seismogenic zone (in California, the depth of the seismogenic zone is about 20 km). The hypocentral depth can be obtained accurately only if the earthquake happens to be recorded by a dense array, which is not always the case. All the earthquakes recorded in 1930's through 1950's were reported to have focal depth of 16 km. This results from the old practice to assign the location of hypocenters to some selected "standard" depths. In our database, the hypocentral depth of the majority of the events is ≤ 16 km.

The following information about the recording sites is available. Roughly, the geological conditions at the site are described by the parameter s (Trifunac and Brady, 1975b). Sites located on sediments are marked by $s = 0$, sites located on geological

(basement) rock are labeled by $s = 2$, and $s = 1$ stands for the intermediate sites. We will also use the soil classification factor s_L (Seed et al., 1976), which describes the sites on a "local scale," once the properties on the "geological scale" are specified in terms of the parameter s. For deep soil sites $s_L = 2$ (soil layer deeper than 100m), and $s_L = 1$ for stiff soil sites (soil layer $15 \div 70$ m deep). In both cases, the shear wave velocity in the soil should be less than 800 m/sec. If the shear wave velocity in the soil exceeds 800 m/sec, the site is classified as "rock," $s_L = 0$. The distribution of sites among different s and s_L is not even, with a small number of stations located on geological basement rock and at "rock" soil sites. Also, at present, the parameter s_L is not known for some stations.

For many of the sites, a more detailed geological description is available. The depth of sediments under the stations varies from $h = 0$ to $h = 7$ km. The parameters, characterizing the geometry of the basement rocks, appearing on the earths surface, were obtained from the Smith's map (1964). The angle, subtended at the recording site by the rocks, capable of producing reflections of the seismic waves towards the station, ranges from 5° to 300°, with the majority of cases having $\varphi < 180°$. The distance from the recording station to those rocks varies from $R = 1$ to $R = 75 \div 80$ km. A more detailed description of the data set can be found in Novikova and Trifunac (1993).

The site intensity is the main parameter in our models, and it deserves a special attention. The database covers the range of the Modified Mercalli intensity, I_{MM}, from II to X. The coverage is, however, not uniform: 90% of the data points have I_{MM} equal to V, VI or VII (Fig. 1.2). Only about one third of all the records have the Modified Mercalli intensity, I_{MM}, actually recorded at the site. The missing values were estimated from the equation, proposed by Lee and Trifunac (1985).

$$I_{MM} = 1.5 \cdot M + 1.12 - 0.856 \cdot \ln \tilde{\Delta} - 0.015 \cdot \tilde{\Delta} - 0.26 \cdot s, \tag{1.2a}$$

where $\tilde{\Delta}$ is "representative distance"

$$\tilde{\Delta} = \sqrt{\Delta^2 + H^2 + L^2}. \tag{1.2b}$$

Δ designates the epicentral distance, H is the hypocentral depth, L stands for the source dimension, and s is the geological classification parameter. The estimate of the source dimension was obtained from

$$L = L(M) \left\{ 1 - \exp\left(\frac{\Delta \cdot \ln 0.1}{L(M)} \right) \right\}, \tag{1.2c}$$

where $L(M)$ is an empirically determined linear function of magnitude, M, such that

$$\begin{aligned} \text{for } M = 3 \quad & L(M) = 0.2 \text{ km}, \\ \text{for } M = 6.5 \quad & L(M) = 17.5 \text{ km}. \end{aligned} \tag{1.2d}$$

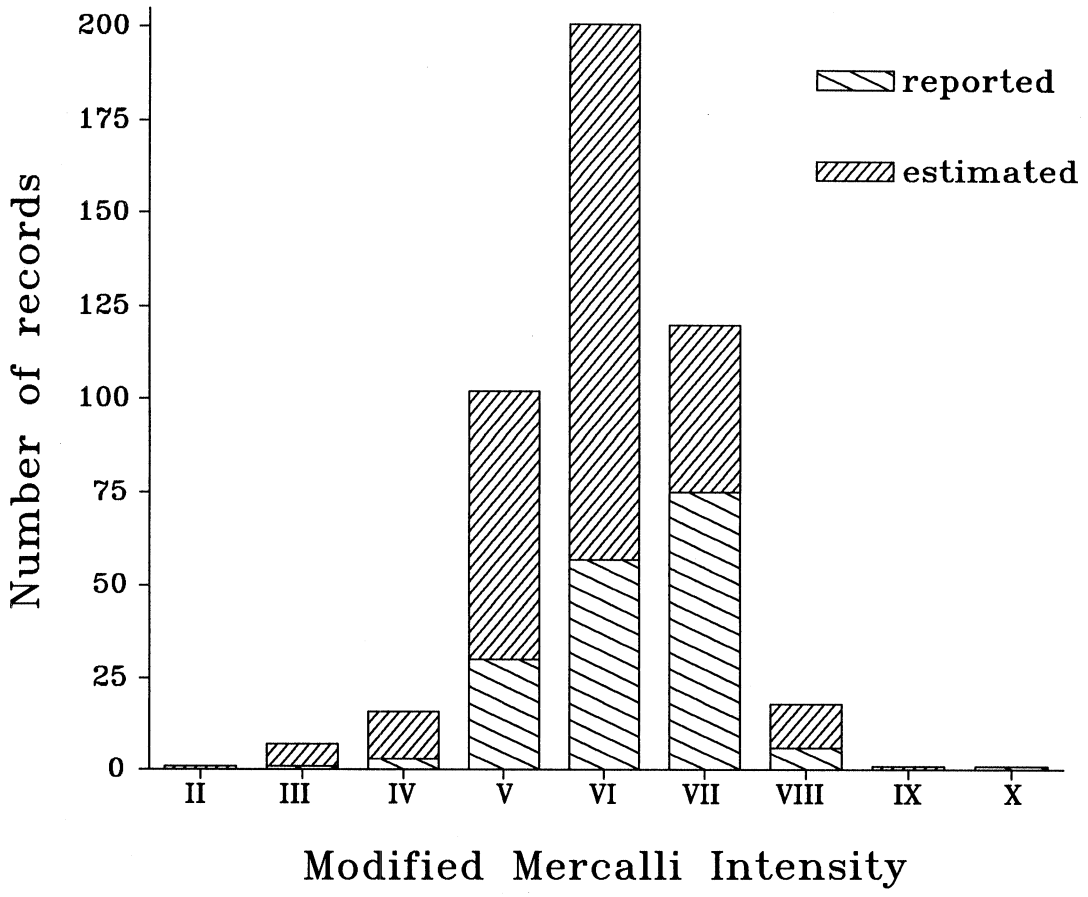

Fig. 1.2 Distribution of 3-component records in the database with respect to the Modified Mercalli intensity.

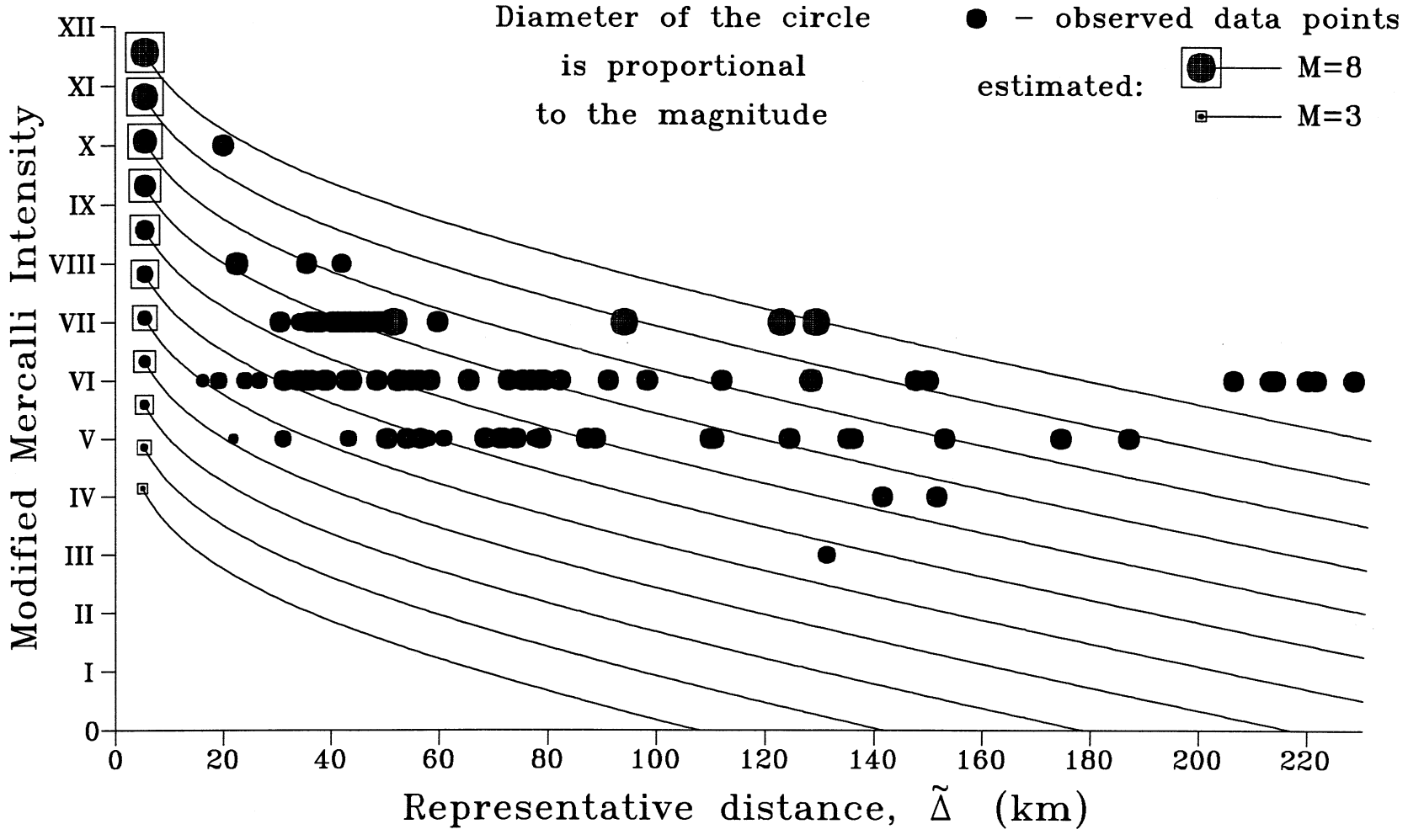

Fig. 1.3 The observed data (shaded circles) and the estimate of the Modified Mercalli intensity by Eq. (1.2) for hypocentral depth $H = 5$ km and $s = 2$ (basement rock site). Each line corresponds to one magnitude and is marked by a shaded circle of an appropriate size, enclosed by a square to distinguish it from the observed data ($M = 3$, 3.5, 4, 4.5, 5, 5.5, 6, 6.5, 7, 7.5 and 8).

All lengths related to the source are measured in km. The logic that leads to Eq. (1.2c) is as follows (Trifunac and Lee, 1985, 1990). It is reasonable to assume that if the site is "far enough," relative to the size of the fault, the whole fault will be "felt" at this site. It may be questionable, however, that the same assumption can be true for small distances from the fault. This is related to the fact that the fault size is not present in the expression of Fourier amplitudes of the near field motion (Brune, 1970; Trifunac, 1973). So, in Eq. (1.2), the "effective" size of the fault, L, is obtained by scaling the estimate of the fault length, $L(M)$, by some factor. This factor is equal to zero when the epicentral distance is zero. At $\Delta = L(M)$, the factor is equal to 0.9 which means that 90% of the fault size is "felt." When the epicentral distance grows, the value of this factor gradually approaches 1.

Eq. (1.2) fits the data for short and intermediate epicentral distances (say, up to 160 km), and underestimates I_{MM} for large epicentral distance. Eq. (1.2) was obtained by the regression analysis on the same data set used in this work. The quality of the fit is shown on Fig. 1.3. The observed intensities are plotted versus the representative distance $\widetilde{\Delta}$. Each data point is shown as a shaded circle, with the diameter of the circle proportional to the earthquake magnitude. The estimate of I_{MM} from Eq. (1.2) is presented by a family of solid lines, each line corresponding to a certain magnitude. The range of magnitudes is from $M = 3$ to $M = 8$, with increments of 0.5. The beginning of each line is marked by a circle in a square box, with the diameter of the circle proportional to the magnitude the line corresponds to. The estimates are shown for $H = 5$ km and for recording stations located on basement rock ($s = 2$). As only a few records in our database were obtained at epicentral distances greater than 160 km, and because many of those were not considered in the regression models of the duration of the earthquake related strong ground motion, due to their low signal to noise ratio, we assumed that Eq. (1.2) can be used to estimate the missing data on the Modified Mercalli intensity. These estimates, together with the reported I_{MM}, can be used in one homogeneous data set in the studies of the relation between the duration of strong ground motion and the Modified Mercalli intensity.

The subset of data that could be used in the study of the duration was carefully selected from the original database. The selection procedure we used is based on simple physical considerations and is described by Novikova and Trifunac (1993). Each channel of acceleration, velocity and displacement of each record was analyzed separately. Cases, where the duration of strong motion was obviously longer than the length of the recording, were not included in the analysis. Also, cases with low signal to noise ratio were disregarded (we used more stringent criteria than those used by Trifunac and Lee, 1979, in the initial data processing during the compilation of the database). Fig. 1.4 shows the number of accepted acceleration, velocity and displacement band-pass filtered records at each channel, separately for horizontal and vertical components. At each channel, data from all three functions (acceleration, velocity and displacement) were used in the subsequent analysis as one uniform data set. The justification for this procedure is discussed by Novikova and Trifunac (1993).

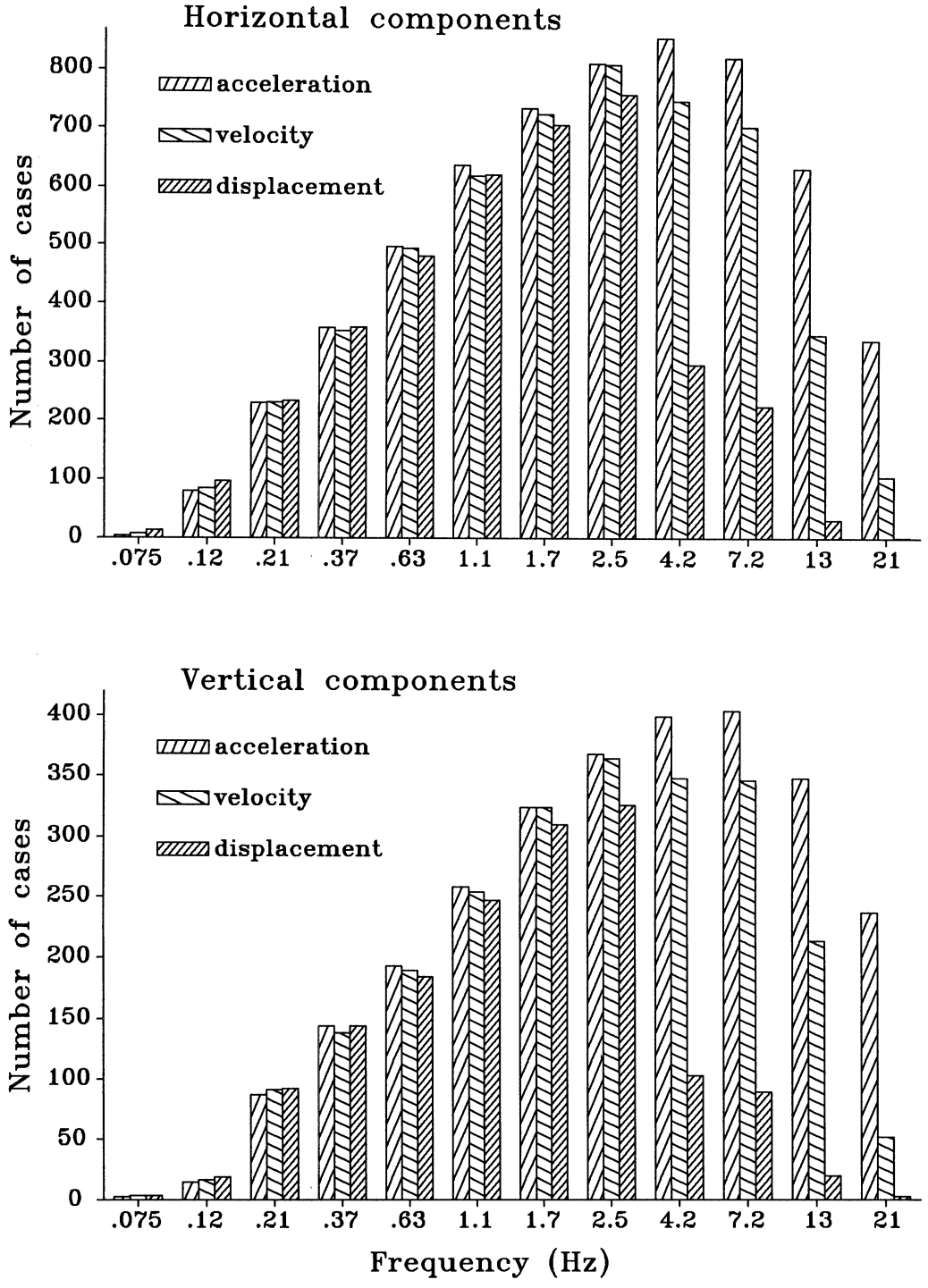

Fig. 1.4 Number of adopted components of band-pass filtered acceleration, velocity and displacement, available at each frequency band (channel). The channels are identified by their central frequency.

II. THE TERMS INVOLVED IN THE DURATION MODELS

The purpose of this Chapter is to introduce the terms used to represent the "basic duration," $\tau_0 + \tau_\Delta$, and the "prolongation due to site conditions," τ_{rs}, from Eq. (1.1). Later, in Chapter III, we will use these terms in our models of the duration of strong motion. The numbering of the unknown (regression) coefficients is chosen to be consistent with our previous work (Novikova and Trifunac, 1993). Table 2.1 at the end of this Chapter summarizes the notation used.

II.1 "Basic Duration"

In the empirical models of the duration in terms of the earthquake magnitude and epicentral distance, the terms τ_0 and τ_Δ have specific physical meaning. Thus, τ_0 represents the duration of the rupture process of the source and it can be modelled through the earthquake magnitude. The term τ_Δ gives the prolongation of the duration due to dispersion (at low and moderate frequencies) and due to scattering (at high frequencies). This is confirmed by (1) the good agreement of the estimates of the source dimension as a function of magnitude, obtained from τ_0, with the results of other authors, and by (2) meaningful estimates of the regional wave velocities, obtained from τ_Δ at intermediate frequencies (Novikova and Trifunac, 1993). In the models of the duration in terms of the Modified Mercalli intensity, however, these two terms, τ_0 and τ_Δ, should be treated together, because the source and the propagation effects cannot be uncoupled when the shaking at a site is measured by the MMI scale.

We will consider two representations of the "basic duration." In the first representation, a simple possible form of the dependence of the duration, *dur*, on the intensity at the site, I_{MM}, is assumed:

$$\tau_0 + \tau_\Delta = a_1(f) + a_{19}(f) \cdot I_{MM}, \tag{2.1}$$

where a_1 and a_{19} are unknown frequency dependent coefficients. These coefficients have"contradicting" nature. From Fig.1.3, it can be seen that larger MMI may mean larger magnitude of the earthquake or shorter epicentral distance. However, larger magnitude implies longer duration, and shorter epicentral distance implies shorter duration. So on one hand, the duration of strong ground motion should be longer when I_{MM} increases due to the assumed increase in the magnitude of the event, and on the other hand, it should be shorter, when I_{MM} increases due to a decrease in the epicentral distance. As a result, different trends prevail at different frequency bands. That can be noticed in Fig. 2.1, which shows the observed duration as a function of the Modified Mercalli intensity for all 12 channels. At low frequencies, the duration of strong motion tends to decrease when the intensity increases. At high frequencies, the duration grows with an increase of the intensity level.

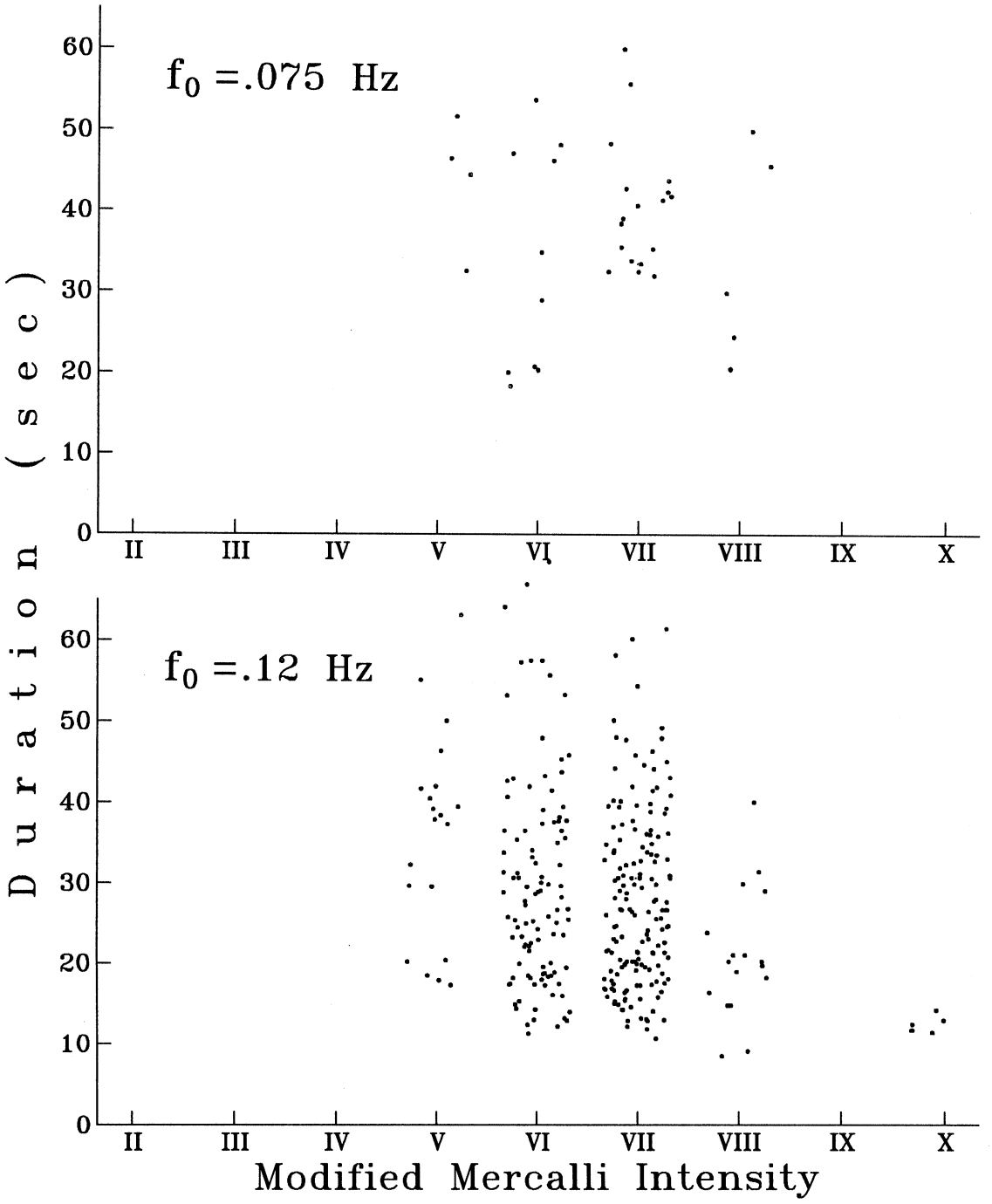

Fig. 2.1a Channels #1 and #2: the duration of strong ground motion as determined from band-pass filtered acceleration, velocity and displacement, is plotted versus the Modified Mercalli intensity. The vertical and horizontal components are shown combined for each channel. For the clarity of this figure, a stripe of finite width on the horizontal axis is assigned to each intensity level I_{MM}, and the abscissa of each data point, corresponding to this I_{MM}, is chosen arbitrarily within this stripe.

At low frequencies, the duration tends to decrease when the intensity increases. At high frequencies, the duration grows with the increase of the intensity level.

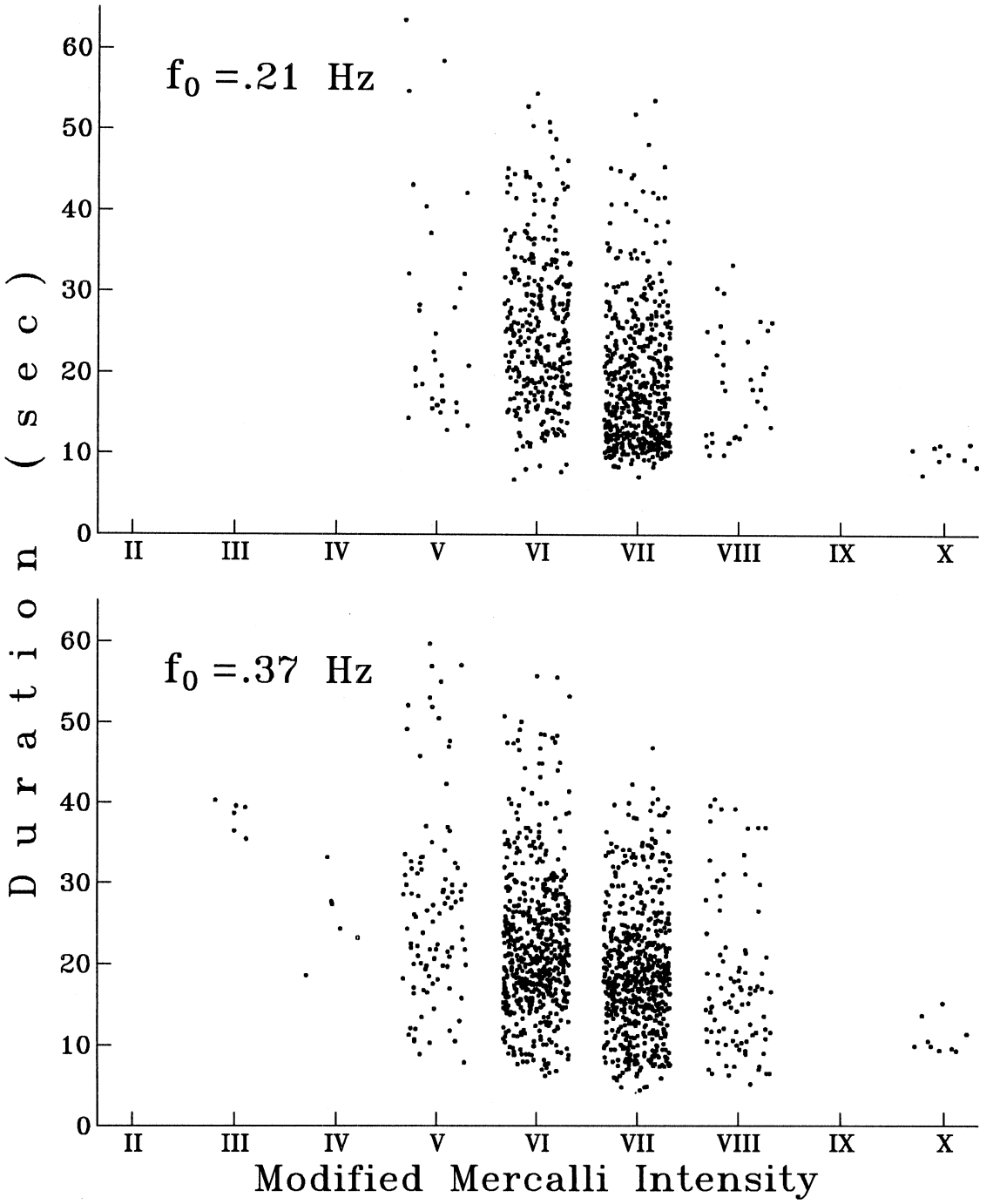

Fig. 2.1b Channels #3 and #4: the duration of strong ground motion as determined from band-pass filtered acceleration, velocity and displacement, is plotted versus the Modified Mercalli intensity. The vertical and horizontal components are shown combined for each channel. For the clarity of this figure, a stripe of finite width on the horizontal axis is assigned to each intensity level I_{MM}, and the abscissa of each data point, corresponding to this I_{MM}, is chosen arbitrarily within this stripe.

At low frequencies, the duration tends to decrease when the intensity increases. At high frequencies, the duration grows with the increase of the intensity level.

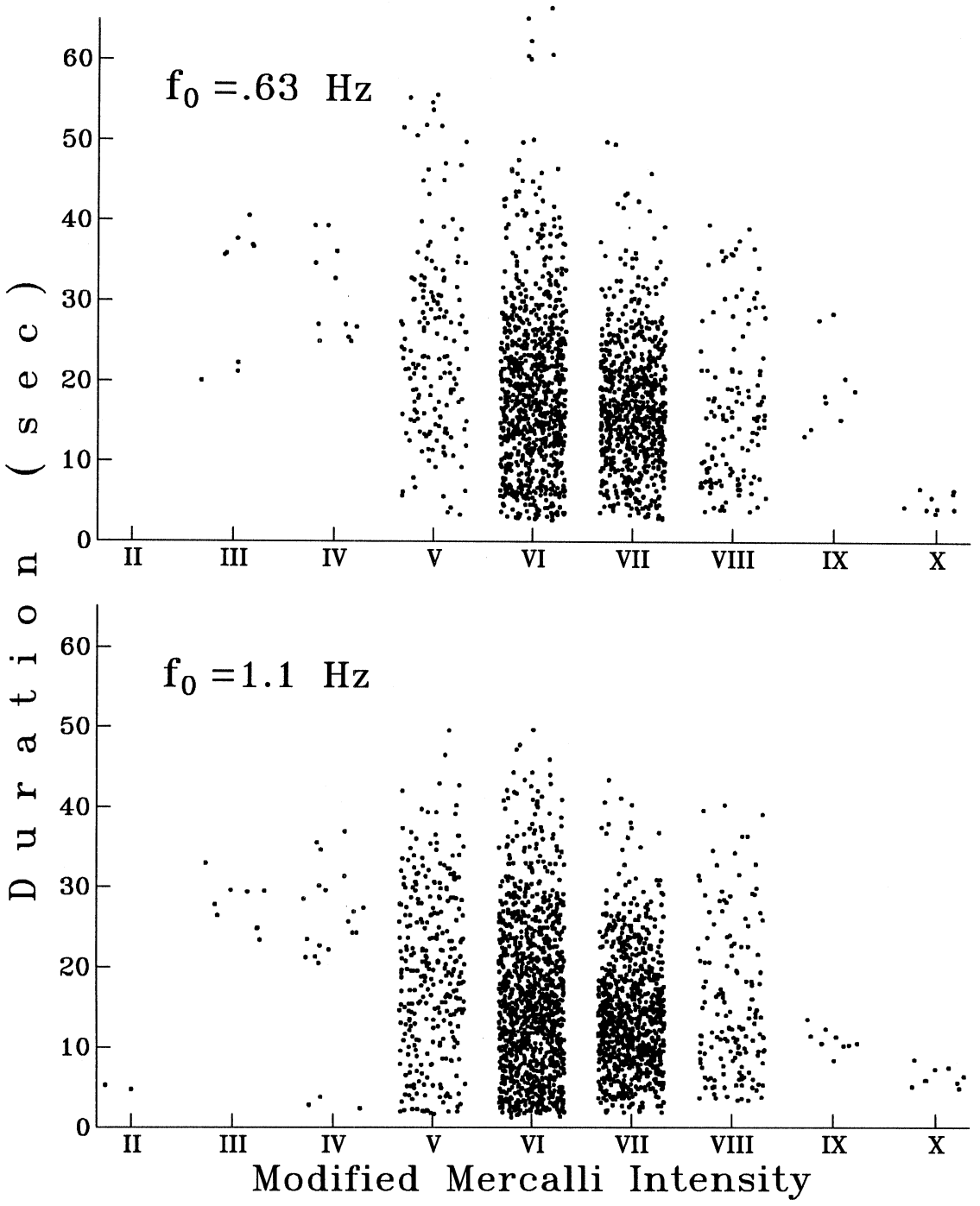

Fig. 2.1c Channels #5 and #6: the duration of strong ground motion as determined from band-pass filtered acceleration, velocity and displacement, is plotted versus the Modified Mercalli intensity. The vertical and horizontal components are shown combined for each channel. For the clarity of this figure, a stripe of finite width on the horizontal axis is assigned to each intensity level I_{MM}, and the abscissa of each data point, corresponding to this I_{MM}, is chosen arbitrarily within this stripe.

At low frequencies, the duration tends to decrease when the intensity increases. At high frequencies, the duration grows with the increase of the intensity level.

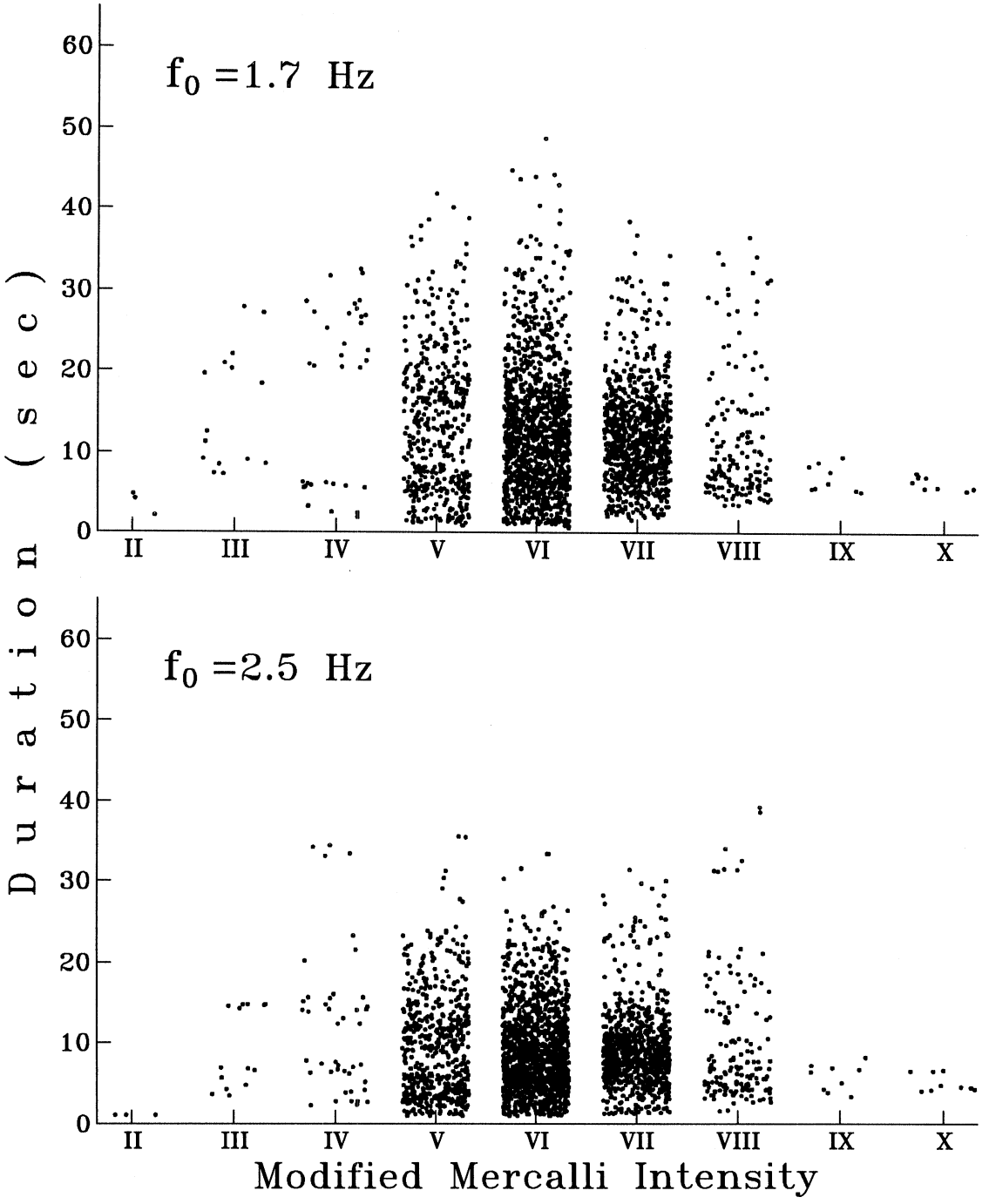

Fig. 2.1d Channels #7 and #8: the duration of strong ground motion as determined from band-pass filtered acceleration, velocity and displacement, is plotted versus the Modified Mercalli intensity. The vertical and horizontal components are shown combined for each channel. For the clarity of this figure, a stripe of finite width on the horizontal axis is assigned to each intensity level I_{MM}, and the abscissa of each data point, corresponding to this I_{MM}, is chosen arbitrarily within this stripe.

At low frequencies, the duration tends to decrease when the intensity increases. At high frequencies, the duration grows with the increase of the intensity level.

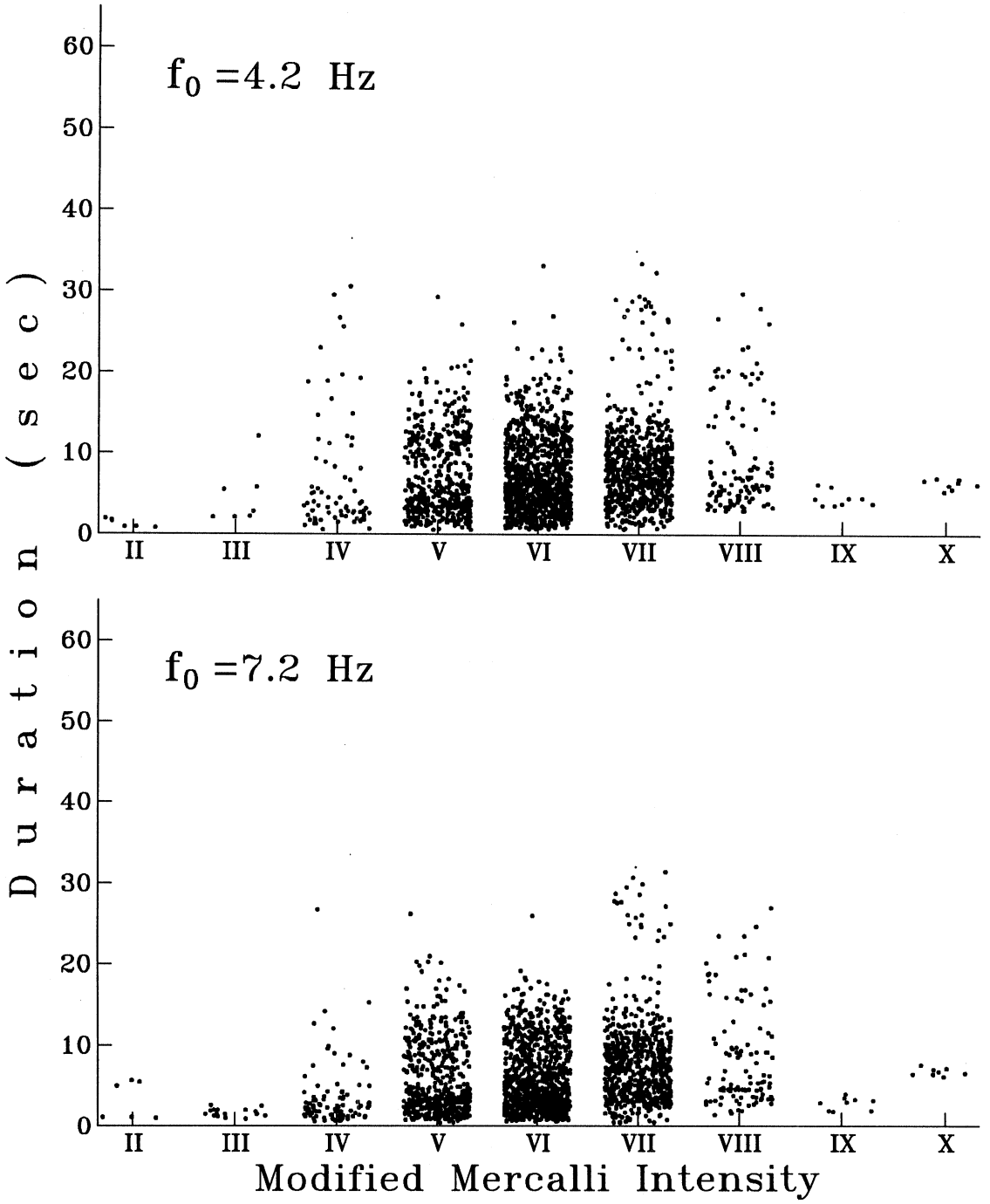

Fig. 2.1e Channels #9 and #10: the duration of strong ground motion as determined from band-pass filtered acceleration, velocity and displacement, is plotted versus the Modified Mercalli intensity. The vertical and horizontal components are shown combined for each channel. For the clarity of this figure, a stripe of finite width on the horizontal axis is assigned to each intensity level I_{MM}, and the abscissa of each data point, corresponding to this I_{MM}, is chosen arbitrarily within this stripe.

At low frequencies, the duration tends to decrease when the intensity increases. At high frequencies, the duration grows with the increase of the intensity level.

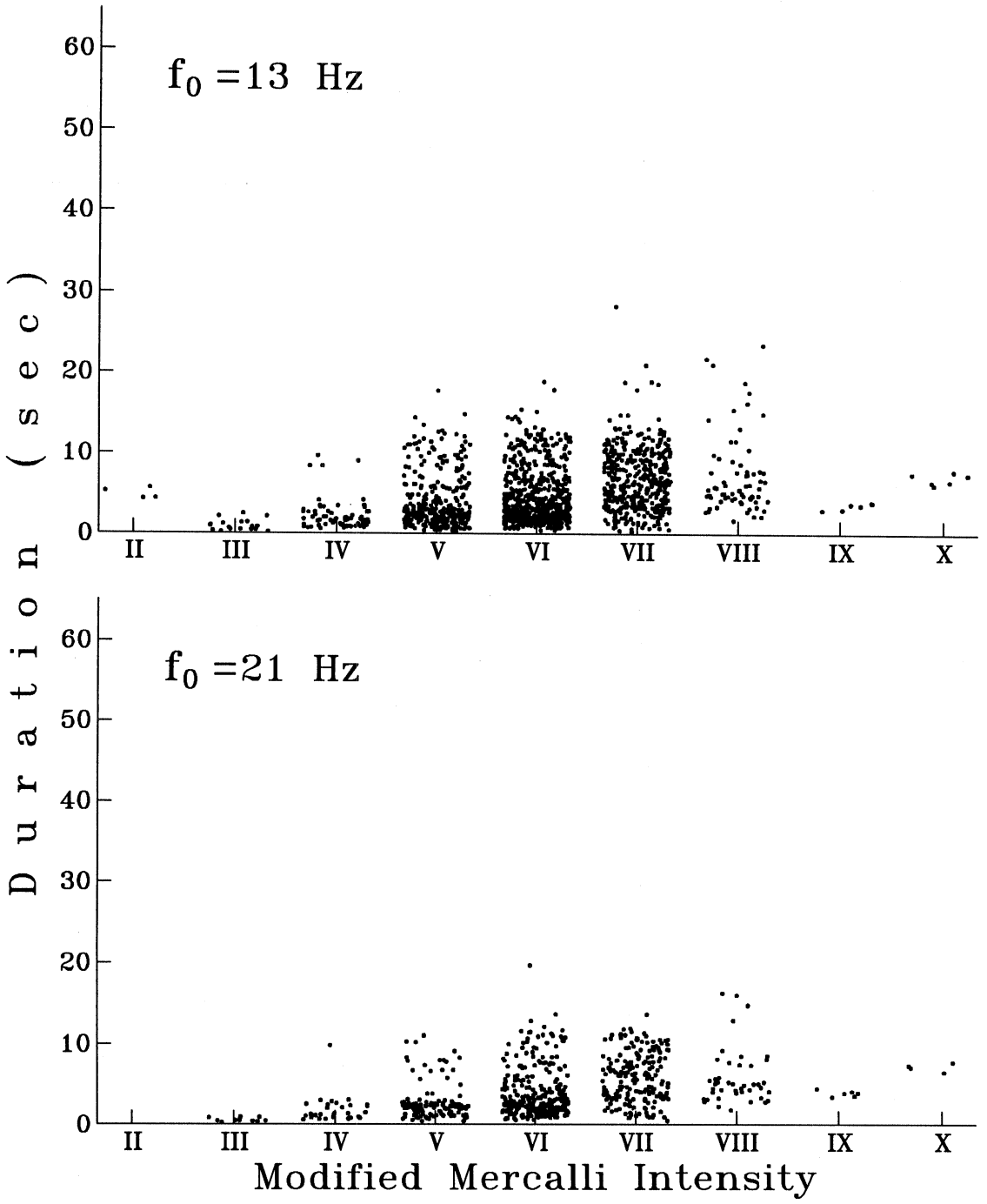

Fig. 2.1f Channels #11 and #12: the duration of strong ground motion as determined from band-pass filtered acceleration, velocity and displacement, is plotted versus the Modified Mercalli intensity. The vertical and horizontal components are shown combined for each channel. For the clarity of this figure, a stripe of finite width on the horizontal axis is assigned to each intensity level I_{MM}, and the abscissa of each data point, corresponding to this I_{MM}, is chosen arbitrarily within this stripe.

At low frequencies, the duration tends to decrease when the intensity increases. At high frequencies, the duration grows with the increase of the intensity level.

The other representation of the "basic duration" includes the distance to the source as one of the model parameters. Although we assume that no instrumental data are available, the models where $\tau_0 + \tau_\Delta$ depends on both the intensity at the site and the source to site distance are worth considering. First, these models can provide some useful information on the nature of the MMI scale. Second, the position of the epicenter can be approximately located even if no instrumental data are available, by creating the map of the Modified Mercalli intensities and finding the point where I_{MM} reaches its maximum.

What kind of distance should this be and in what manner should it be included in the regression equations? The answer to this question depends on the correlations of the Modified Mercalli intensity with the earthquake magnitude and on various definitions of the distance: epicentral, hypocentral, closest distance to the fault, and others. Only about one third of the database had the Modified Mercalli intensity actually observed at the recording site (Fig. 1.2). The remaining two thirds of the data on I_{MM} were estimated using Eq. (1.2) and the "representative distance" in Eq. (1.2b) in particular. Thus, it is logical to use this "representative distance" from the source to the site in our regression equations, which relates the duration of strong ground motion and the Modified Mercalli intensity at the site. To take advantage of the "representative distance," an estimate of the source dimension $L(M)$ should be available. However, we do not wish to use the earthquake magnitude in the development of the models of duration in terms of the Modified Mercalli intensity. The use of magnitude would contradict the assumption that no instrumental data are available. Thus, this restriction prevents us from taking advantage of the "representative distance" $\widetilde{\Delta}$, and the best we can do is to consider the hypocentral distance $\Delta' = \sqrt{\Delta^2 + H^2}$ as an approximation to $\widetilde{\Delta}$. The use of the hypocentral distance requires knowledge of the hypocentral depth H, which would not be available if there was no instrumental record on the earthquake. However, in the regions with seismogenic zone which can be described reasonably well (like San Andreas fault system in Central and Southern California), the prevailing hypocentral depth can be estimated. Also, the detailed studies of the rate of attenuation of the intensity with distance may be used to estimate the hypocentral depth (e.g. Shebalin, 1969; Trifunac and Todorovska, 1989). In our case we assumed $H = 5$ km for all the sources with unknown hypocentral depth. This particular value comes from the distribution of records produced by the sources with known H.

The functional form of the dependence of $\tau_0 + \tau_\Delta$ on I_{MM} and Δ' can be obtained by combining Eq. (1.2a) with the established functional dependence of τ_0 on the magnitude M

$$\tau_0 = a_1 + a_2 \cdot M + a_3 \cdot M^2, \tag{2.2}$$

and the functional dependence of τ_Δ on the epicentral distance Δ

$$\tau_\Delta = a_4 \cdot \Delta, \tag{2.3}$$

where a_i, $i = 1 \div 4$, are frequency dependent regression coefficients (Novikova and Trifunac, 1993). From the analysis of the Eqs. (1.2a), (2.2) and (2.3), it is also seen that

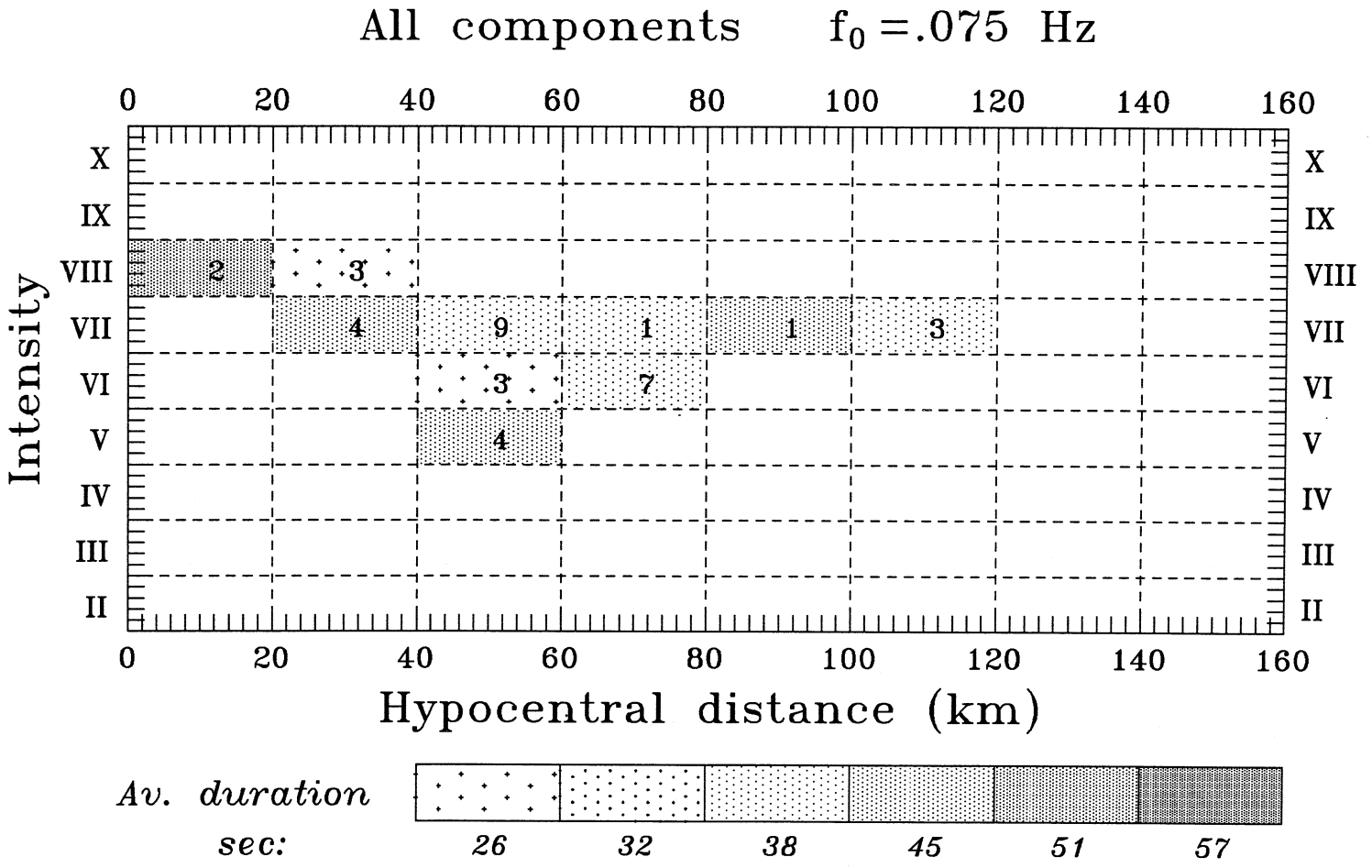

Fig. 2.2a Channel #1: the observed duration of strong ground motion as a function of the hypocentral distance, Δ', and the Modified Mercalli intensity, I_{MM}. The duration is shown averaged in the ranges of Δ' and I_{MM}, specified by the dashed mesh. Longer duration corresponds to a denser shade. The numbers in the dashed "boxes" give the number of the data points available for the particular range of Δ' and I_{MM}. The horizontal and the vertical components are shown together.

It is seen that, in some frequency bands, the behavior of the duration as a function of I_{MM} is different for different Δ'.

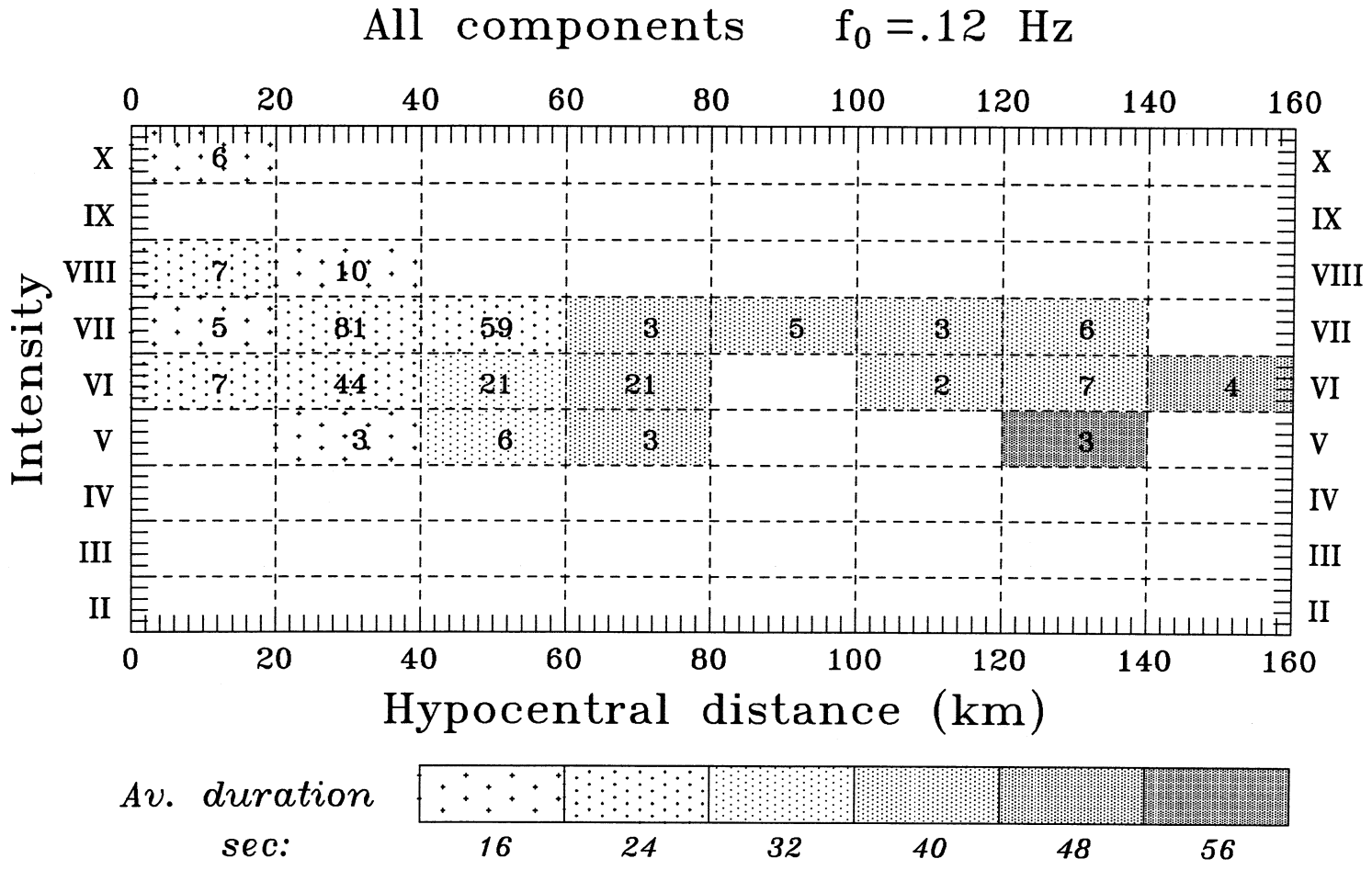

Fig. 2.2b Channel #2: the observed duration of strong ground motion as a function of the hypocentral distance, Δ', and the Modified Mercalli intensity, I_{MM}. The duration is shown averaged in the ranges of Δ' and I_{MM}, specified by the dashed mesh. Longer duration corresponds to a denser shade. The numbers in the dashed "boxes" give the number of the data points available for the particular range of Δ' and I_{MM}. The horizontal and the vertical components are shown together.

It is seen that, in some frequency bands, the behavior of the duration as a function of I_{MM} is different for different Δ'.

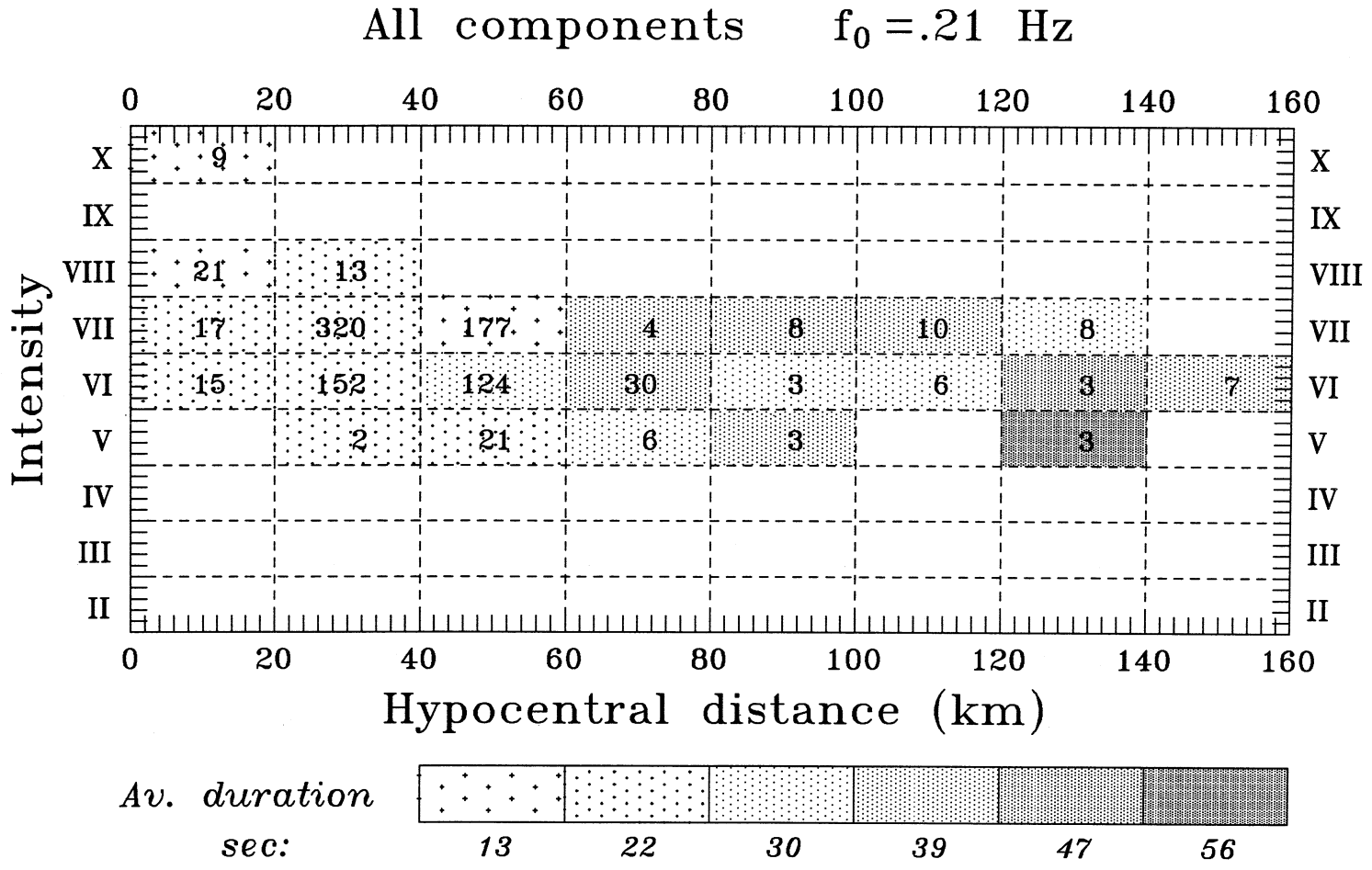

Fig. 2.2c Channel #3: the observed duration of strong ground motion as a function of the hypocentral distance, Δ', and the Modified Mercalli intensity, I_{MM}. The duration is shown averaged in the ranges of Δ' and I_{MM}, specified by the dashed mesh. Longer duration corresponds to a denser shade. The numbers in the dashed "boxes" give the number of the data points available for the particular range of Δ' and I_{MM}. The horizontal and the vertical components are shown together.

It is seen that, in some frequency bands, the behavior of the duration as a function of I_{MM} is different for different Δ'.

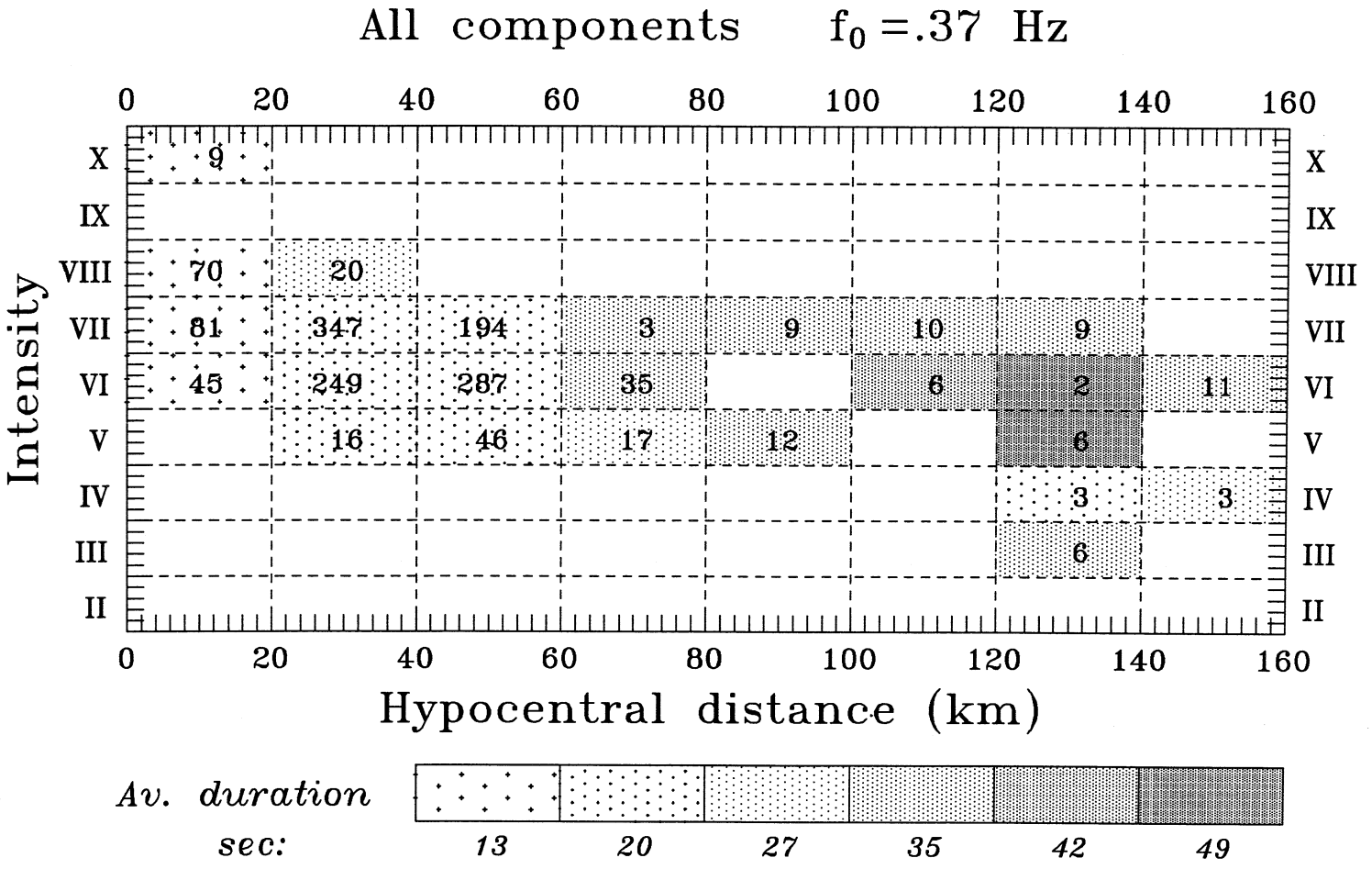

Fig. 2.2d Channel #4: the observed duration of strong ground motion as a function of the hypocentral distance, Δ', and the Modified Mercalli intensity, I_{MM}. The duration is shown averaged in the ranges of Δ' and I_{MM}, specified by the dashed mesh. Longer duration corresponds to a denser shade. The numbers in the dashed "boxes" give the number of the data points available for the particular range of Δ' and I_{MM}. The horizontal and the vertical components are shown together.

It is seen that, in some frequency bands, the behavior of the duration as a function of I_{MM} is different for different Δ'.

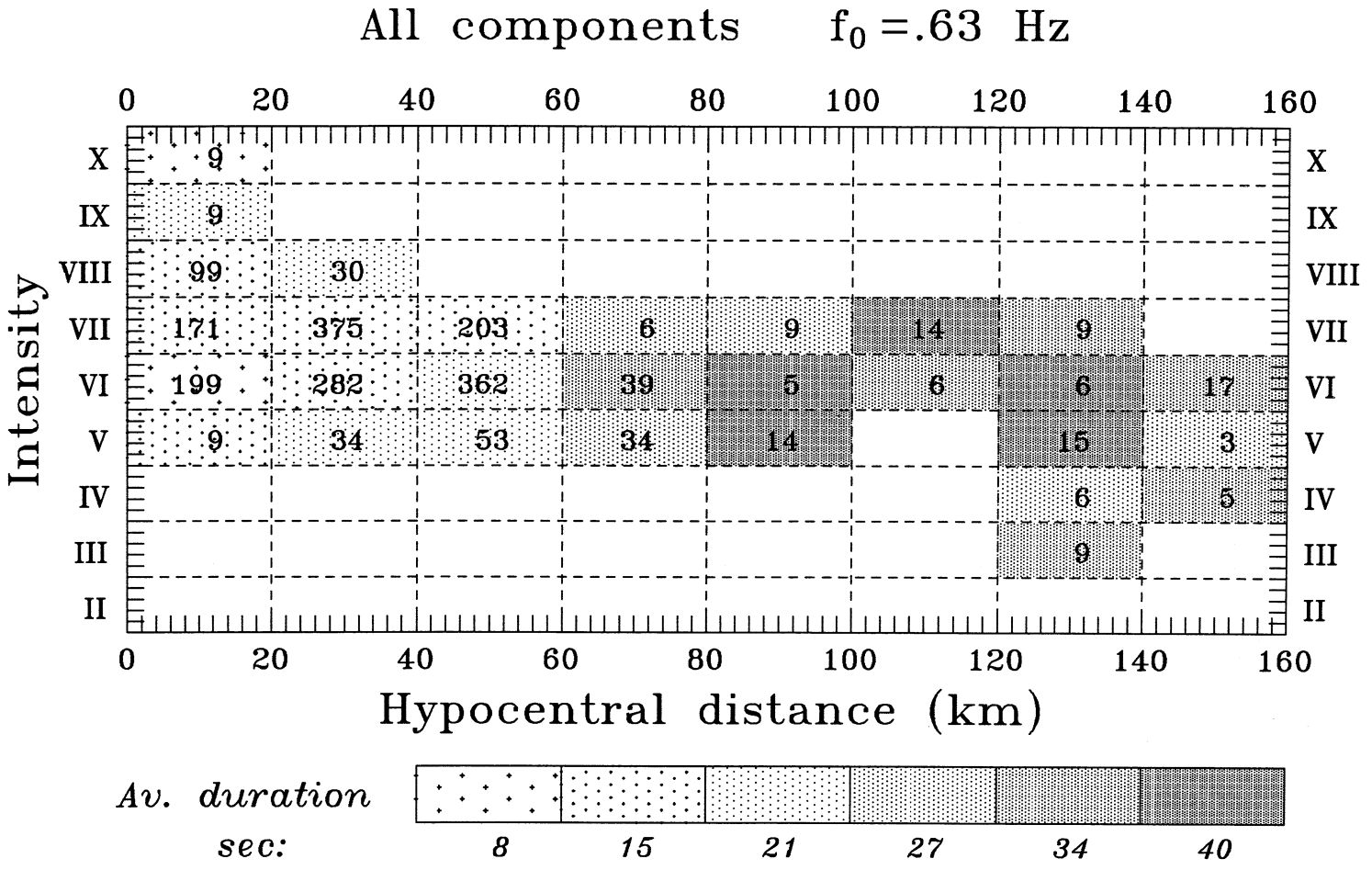

Fig. 2.2e Channel #5: the observed duration of strong ground motion as a function of the hypocentral distance, Δ', and the Modified Mercalli intensity, I_{MM}. The duration is shown averaged in the ranges of Δ' and I_{MM}, specified by the dashed mesh. Longer duration corresponds to a denser shade. The numbers in the dashed "boxes" give the number of the data points available for the particular range of Δ' and I_{MM}. The horizontal and the vertical components are shown together.

It is seen that, in some frequency bands, the behavior of the duration as a function of I_{MM} is different for different Δ'.

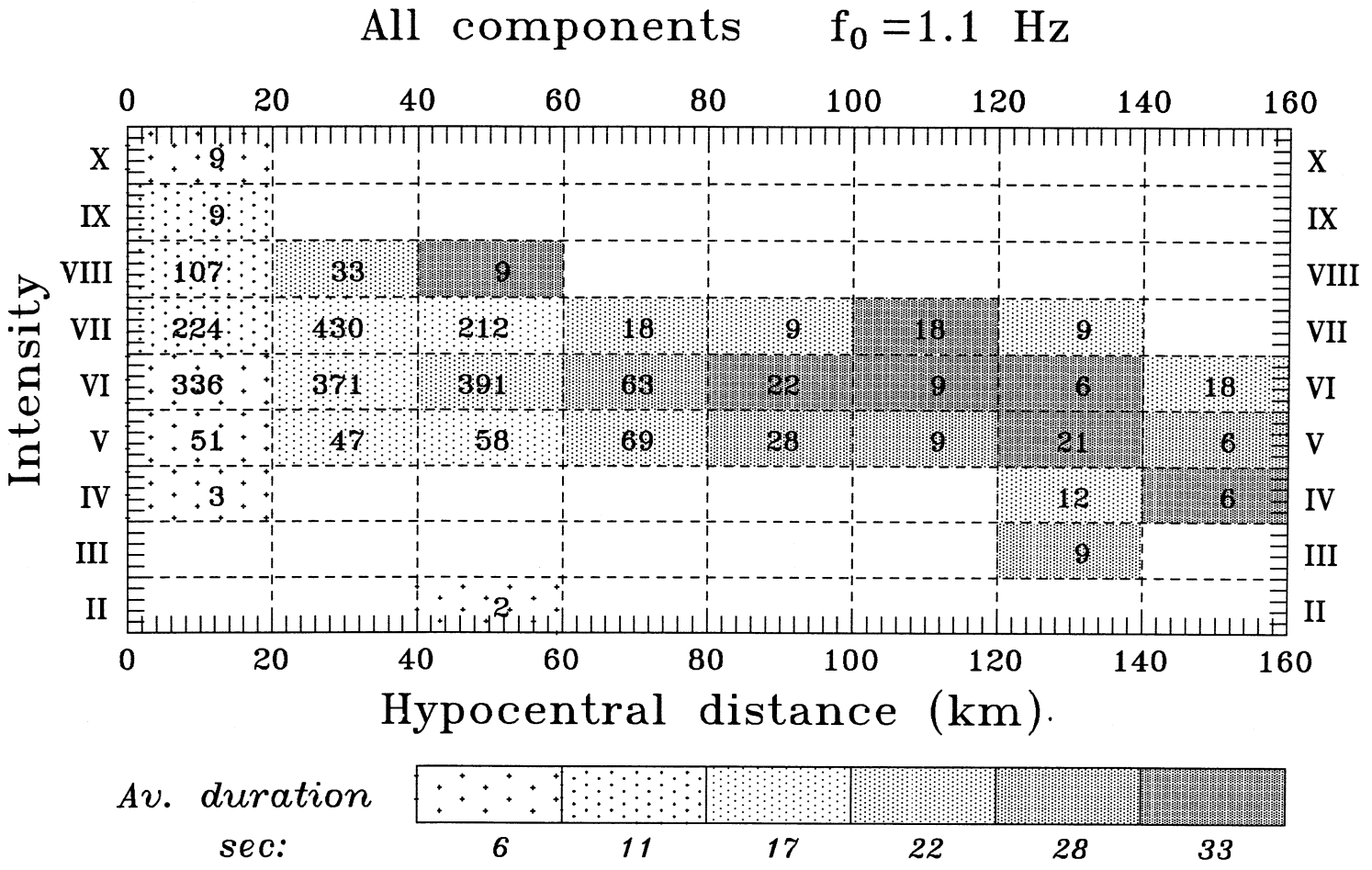

Fig. 2.2f Channel #6: the observed duration of strong ground motion as a function of the hypocentral distance, Δ', and the Modified Mercalli intensity, I_{MM}. The duration is shown averaged in the ranges of Δ' and I_{MM}, specified by the dashed mesh. Longer duration corresponds to a denser shade. The numbers in the dashed "boxes" give the number of the data points available for the particular range of Δ' and I_{MM}. The horizontal and the vertical components are shown together.

It is seen that, in some frequency bands, the behavior of the duration as a function of I_{MM} is different for different Δ'.

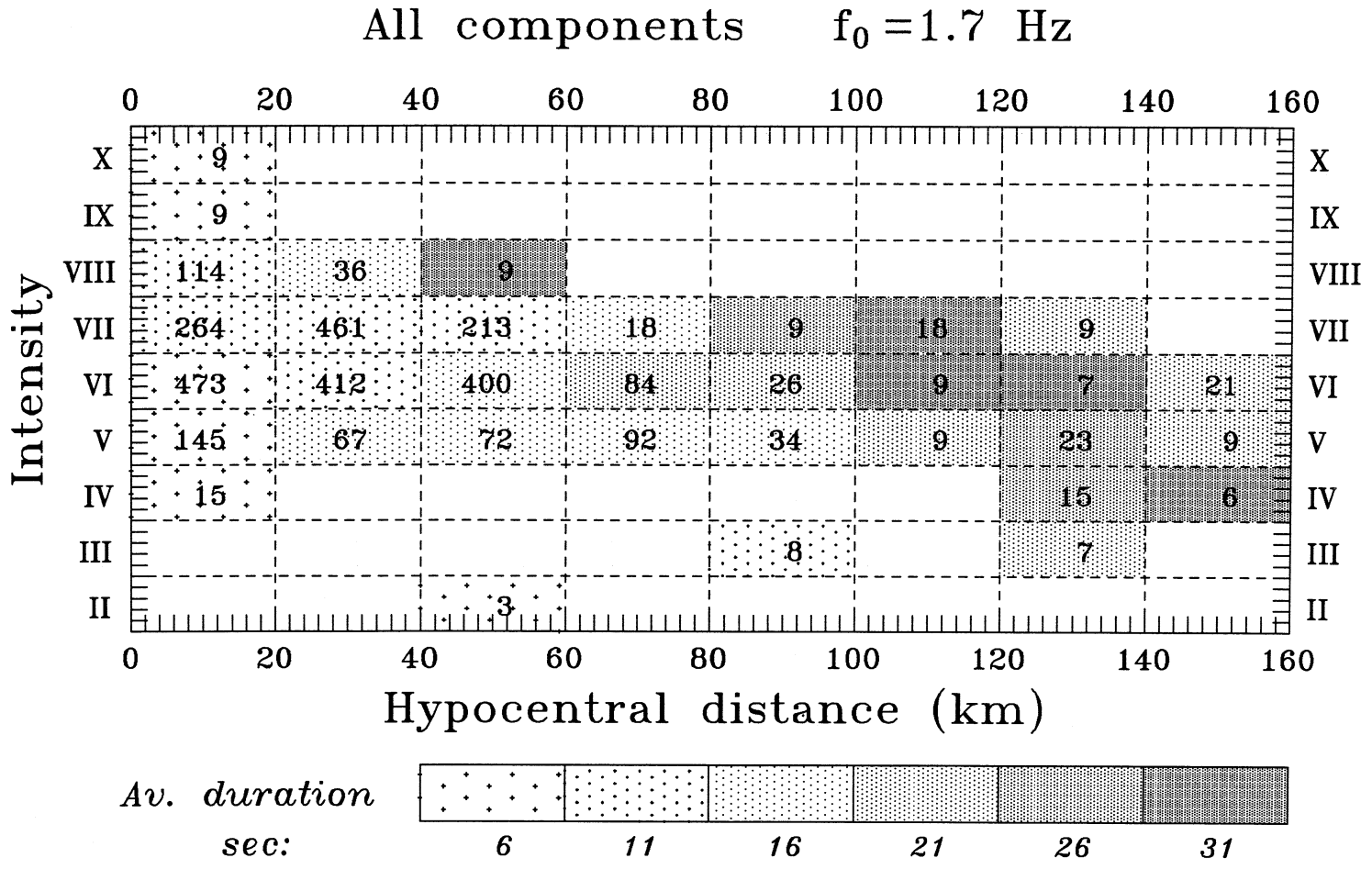

Fig. 2.2g Channel #7: the observed duration of strong ground motion as a function of the hypocentral distance, Δ', and the Modified Mercalli intensity, I_{MM}. The duration is shown averaged in the ranges of Δ' and I_{MM}, specified by the dashed mesh. Longer duration corresponds to a denser shade. The numbers in the dashed "boxes" give the number of the data points available for the particular range of Δ' and I_{MM}. The horizontal and the vertical components are shown together.

It is seen that, in some frequency bands, the behavior of the duration as a function of I_{MM} is different for different Δ'.

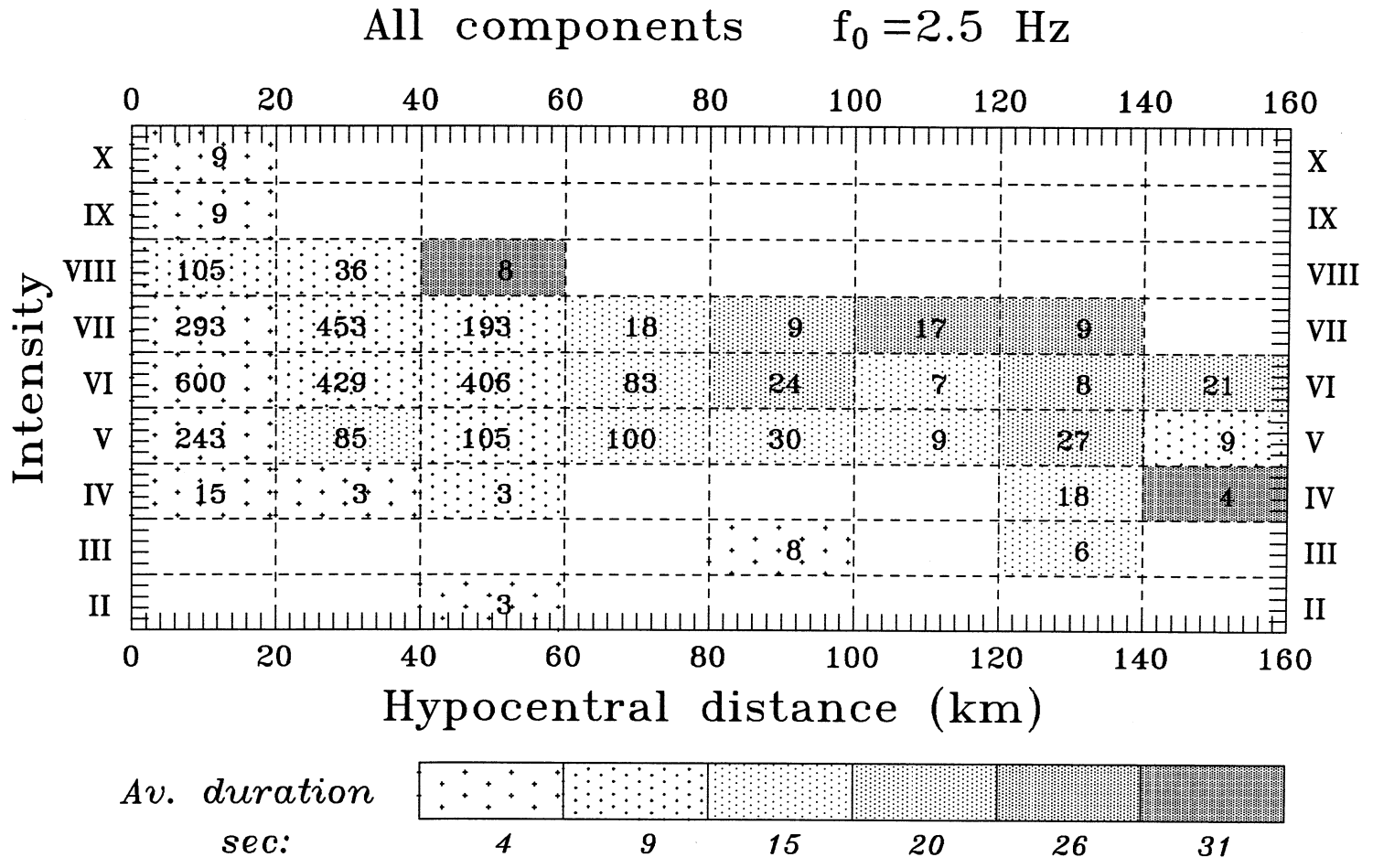

Fig. 2.2h Channel #8: the observed duration of strong ground motion as a function of the hypocentral distance, Δ', and the Modified Mercalli intensity, I_{MM}. The duration is shown averaged in the ranges of Δ' and I_{MM}, specified by the dashed mesh. Longer duration corresponds to a denser shade. The numbers in the dashed "boxes" give the number of the data points available for the particular range of Δ' and I_{MM}. The horizontal and the vertical components are shown together.

It is seen that, in some frequency bands, the behavior of the duration as a function of I_{MM} is different for different Δ'.

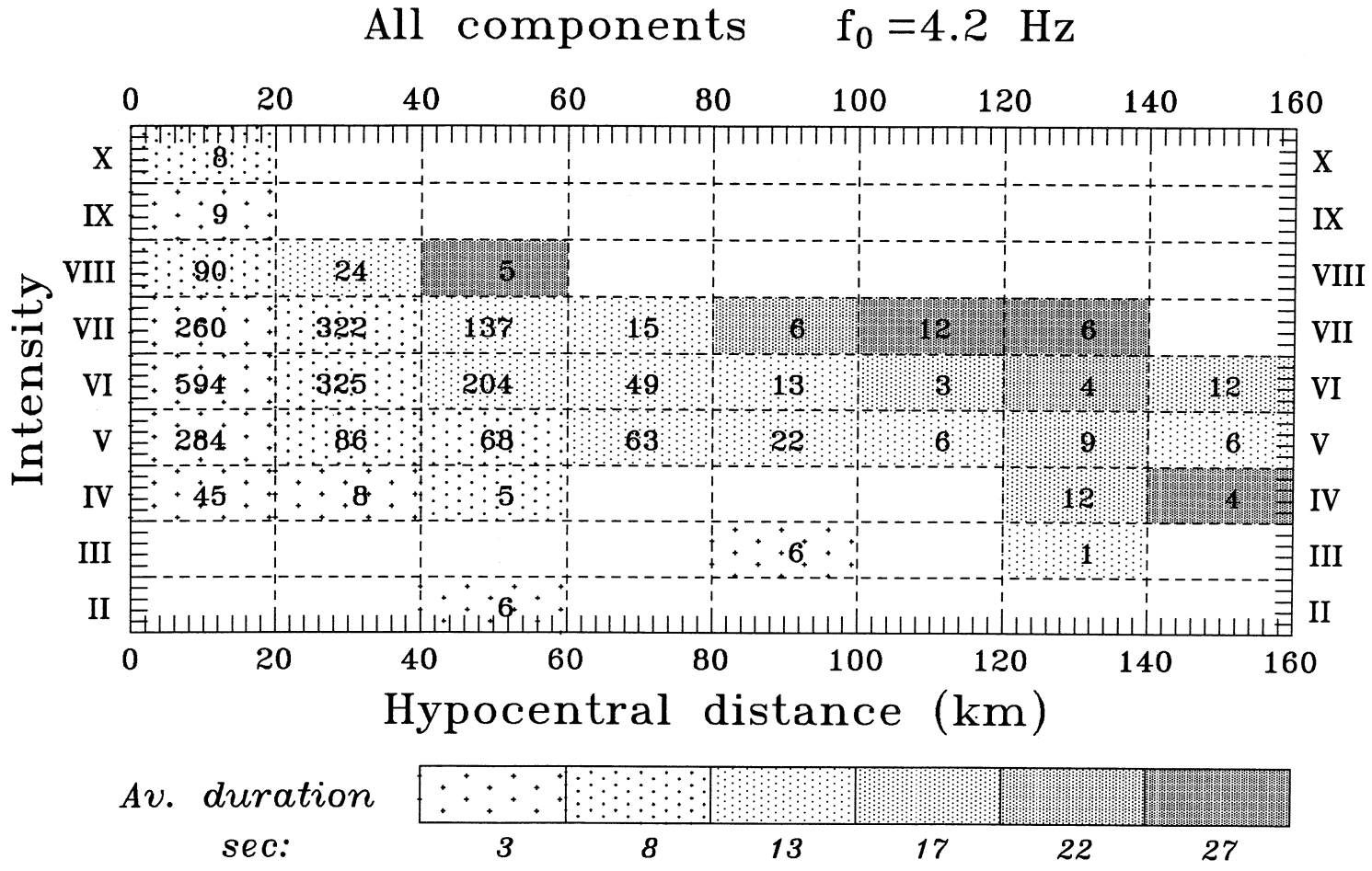

Fig. 2.2i Channel #9: the observed duration of strong ground motion as a function of the hypocentral distance, Δ', and the Modified Mercalli intensity, I_{MM}. The duration is shown averaged in the ranges of Δ' and I_{MM}, specified by the dashed mesh. Longer duration corresponds to a denser shade. The numbers in the dashed "boxes" give the number of the data points available for the particular range of Δ' and I_{MM}. The horizontal and the vertical components are shown together.

It is seen that, in some frequency bands, the behavior of the duration as a function of I_{MM} is different for different Δ'.

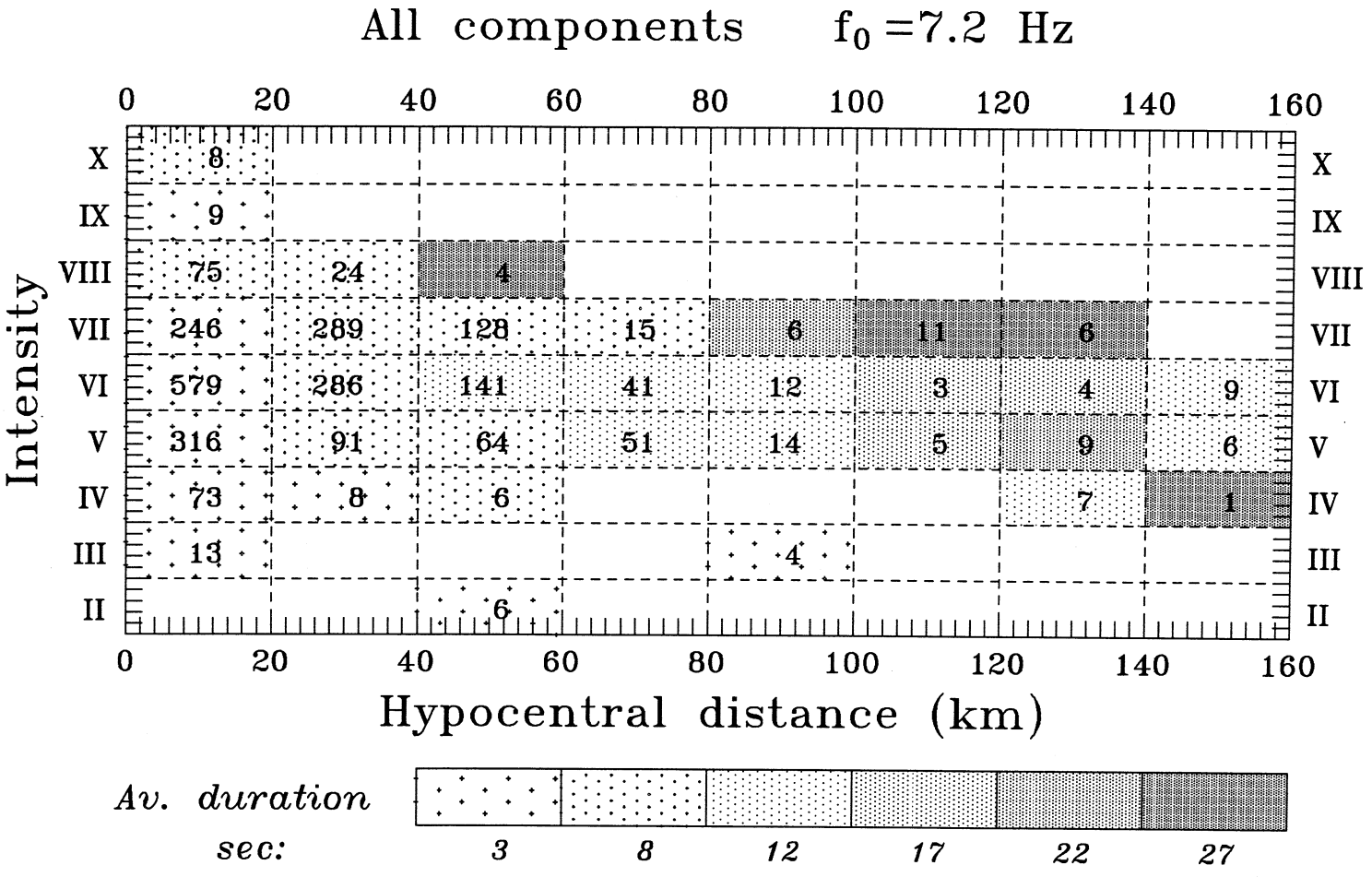

Fig. 2.2j Channel #10: the observed duration of strong ground motion as a function of the hypocentral distance, Δ', and the Modified Mercalli intensity, I_{MM}. The duration is shown averaged in the ranges of Δ' and I_{MM}, specified by the dashed mesh. Longer duration corresponds to a denser shade. The numbers in the dashed "boxes" give the number of the data points available for the particular range of Δ' and I_{MM}. The horizontal and the vertical components are shown together.

It is seen that, in some frequency bands, the behavior of the duration as a function of I_{MM} is different for different Δ'.

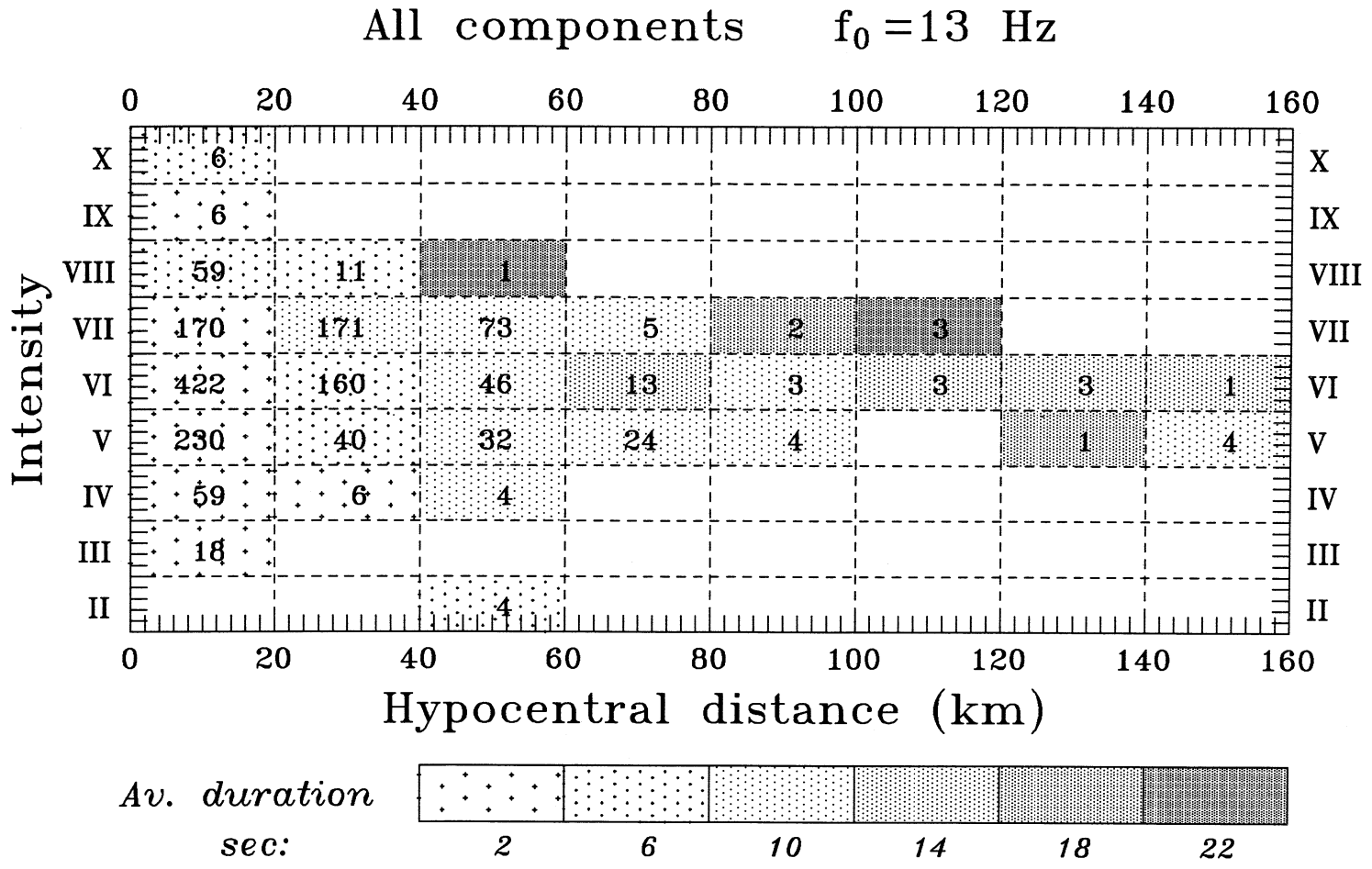

Fig. 2.2k Channel #11: the observed duration of strong ground motion as a function of the hypocentral distance, Δ', and the Modified Mercalli intensity, I_{MM}. The duration is shown averaged in the ranges of Δ' and I_{MM}, specified by the dashed mesh. Longer duration corresponds to a denser shade. The numbers in the dashed "boxes" give the number of the data points available for the particular range of Δ' and I_{MM}. The horizontal and the vertical components are shown together.

It is seen that, in some frequency bands, the behavior of the duration as a function of I_{MM} is different for different Δ'.

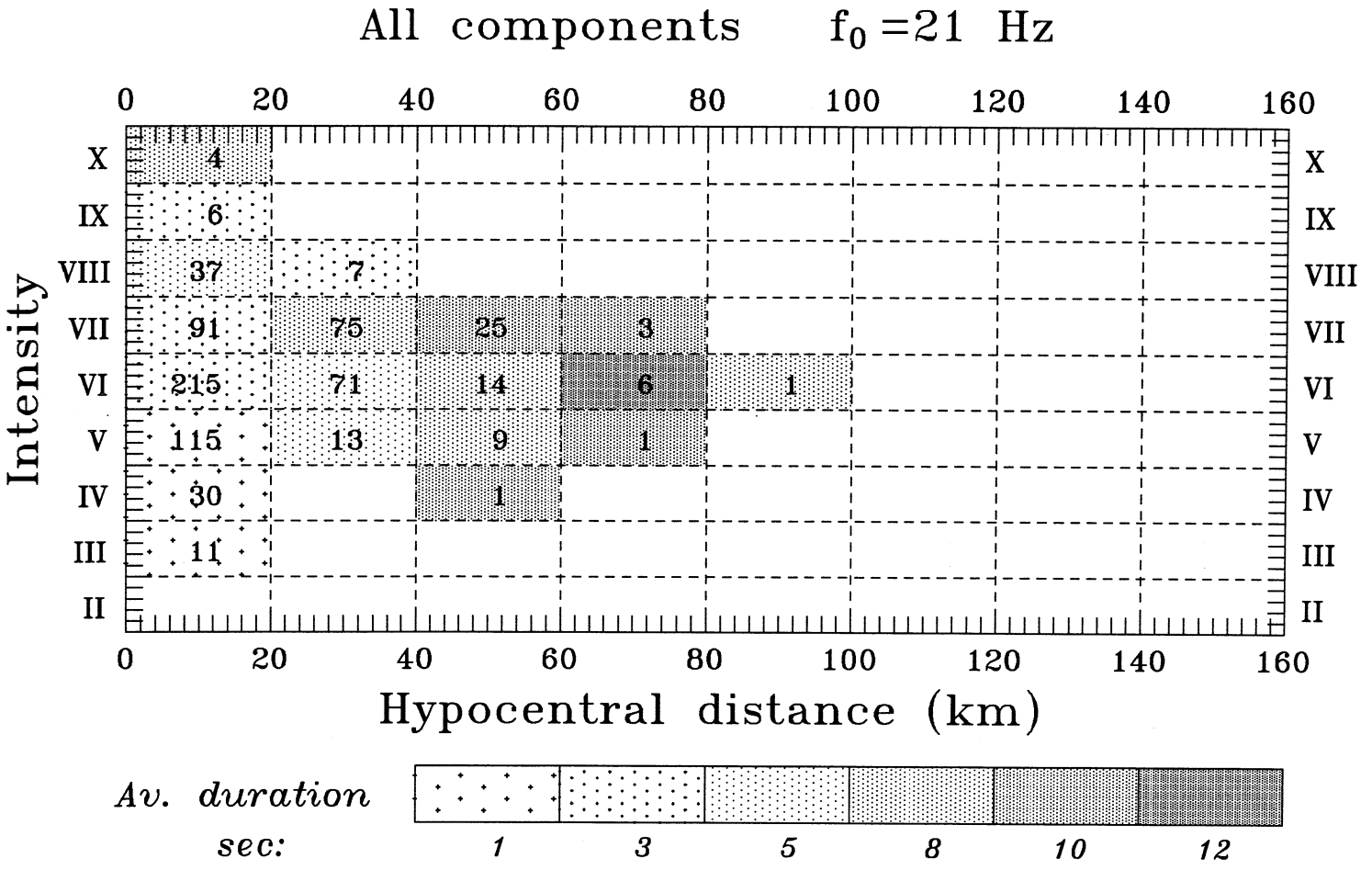

Fig. 2.21 Channel #12: the observed duration of strong ground motion as a function of the hypocentral distance, Δ', and the Modified Mercalli intensity, I_{MM}. The duration is shown averaged in the ranges of Δ' and I_{MM}, specified by the dashed mesh. Longer duration corresponds to a denser shade. The numbers in the dashed "boxes" give the number of the data points available for the particular range of Δ' and I_{MM}. The horizontal and the vertical components are shown together.

It is seen that, in some frequency bands, the behavior of the duration as a function of I_{MM} is different for different Δ'.

the dependence of $\tau_0 + \tau_\Delta$ on the intensity and on the distance should be coupled. To avoid the usually unstable nonlinear regression analysis and to use the simplest possible functional form for $\tau_0 + \tau_\Delta$ which would allow such coupling, we consider

$$\tau_0 + \tau_\Delta = a_1(f) + a_{19}(f) \cdot I_{MM} + a_4(f) \cdot \Delta' + a_{20}(f) \cdot I_{MM} \Delta', \qquad (2.4)$$

where a_1, a_{19}, a_4, and a_{20} are some unknown frequency dependent coefficients. The data (related to the functional form in Eq. (2.4)), are displayed in Fig. 2.2. For each channel separately, the observed duration is shown as a function of two parameters: the Modified Mercalli intensity at the recording site and the hypocentral distance. The data for the horizontal and for the vertical components are displayed together. The duration is shown averaged over the ranges of Δ' and I_{MM} given by

$$\begin{cases} \Delta'_l \le \Delta' < \Delta'_{l+1}, & \Delta'_l = 20 \cdot l, & l = 0 \div 8 \\ (I_{MM}) = (I_{MM})_k, & (I_{MM})_k = k + 2, & k = 0 \div 8 \end{cases}$$

The intervals of Δ'_l and $(I_{MM})_k$ are shown by the dashed mesh, with the density of shade inside every "box" proportional to the averaged duration. The scale of shades used is also shown. As it can be seen from the data, the behavior of the duration as a function of I_{MM} is different for different hypocentral distances Δ'.

II.2 Prolongation due to Site Conditions

To model the "prolongation" term τ_{rs} in Eq. (1.1), we consider two descriptions of the recording site conditions: a "detailed" description of the geometry of the sedimentary basin where the site is located, and a "rough" description of the geological and the local soil conditions through the qualitative parameters s and s_L.

As it was shown by Novikova and Trifunac (1993), the prolongation of the duration at sites on sediments can be modelled by

$$\tau_{rs}(f) = a_5(f) \cdot h + a_6(f) \cdot R + a_7(f) \cdot hR + a_8(f) \cdot R^2 + a_9(f) \cdot h^2 + a_{10}(f) \cdot \varphi, \qquad (2.5)$$

where h is the depth of sediments under the station (vertical dimension of the valley). R in the above equation is the distance from the station to the rocks or clusters of rocks, appearing on the earth's surface and capable of reflecting the seismic waves towards the station. The intensity of these secondary (reflected) waves is governed by the angle φ, subtended at the station by the surface of the rocks which actually reflect some considerable amount of the seismic energy to the station. For given site, parameters R and φ may depend on the source position. The values for R and φ for each record (each pair source–station) were measured from the Smith's map (1964). An example of such measurements is shown in Fig. 2.3

The form of the dependence of τ_{rs} on R, h and φ as in Eq. (2.5) was chosen for the following reasons. We consider the φ-term first. If the angle φ is small, the reflected wave

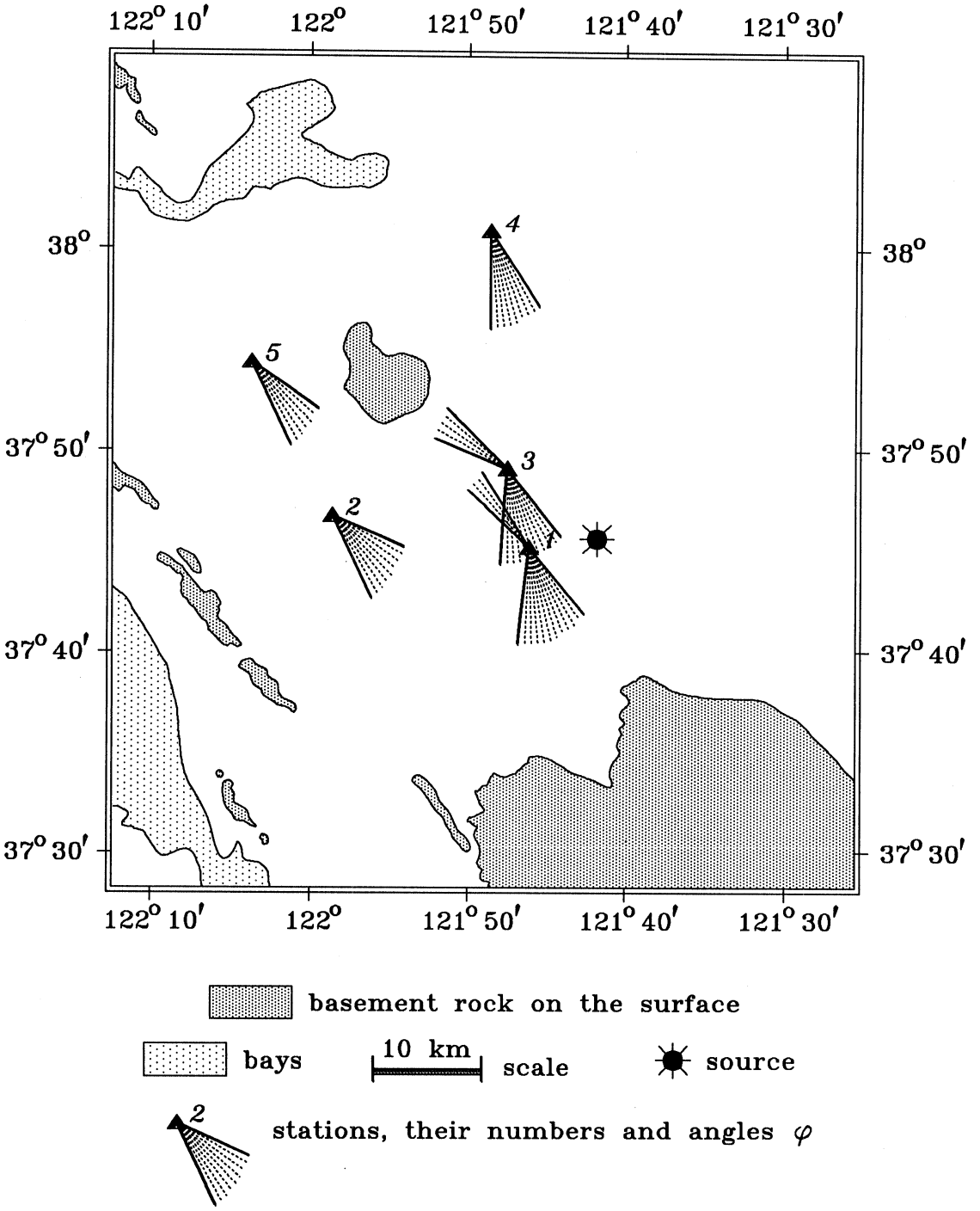

Fig. 2.3 Determination of the parameters for the horizontal reflections (the angle φ, subtended at the recording station by the surface of the rocks from which reflections occur, and the characteristic horizontal distance to these rocks, R) for the Livermore earthquake, January 26, 1980, recorded in the San Francisco bay area. Distribution and configuration of the basement rocks are taken from the Smith's (1964) map. With superscripts, corresponding to the station number, $R^{(1)} = 20$ km, $R^{(2)} = 30$ km, $R^{(3)} = 25$ km, $R^{(4)} = 45$ km, $R^{(5)} = 45$ km and $\varphi^{(1)} = 70°$, $\varphi^{(2)} = 40°$, $\varphi^{(3)} = 70°$, $\varphi^{(4)} = 40°$, $\varphi^{(5)} = 30°$.

carries little energy and cannot be noticed relative to the background of the other waves. An increase of φ leads to an increase of the duration of the reflected pulses, because larger φ implies longer reflecting surface and increases the variety of the sampled lengths of the source-rock-station propagation paths. These considerations suggest that τ_{rs} is an increasing function of φ. The data (see Novikova and Trifunac, 1993) suggest that the dependence τ_{rs} on φ can be assumed to be linear.

The dependence on R is more complex. Suppose first that R is small. Then the time intervals which correspond to the initial pulse (of duration dur_1) and the reflected pulse (of duration dur_2) will be observed at the station almost simultaneously without producing significant increase in the duration of the strong motion. Next, we increase R. The time delay between the two pulses of energy causes separation of the corresponding intervals of strong motion in the accelerogram, and the total duration is longer now and equal to $dur_1 + dur_2$. Further increase of R causes an increase of the time which the reflected surface waves spend travelling through the dispersing medium. This causes an increase of dur_2, and results in further prolongation of the total duration $dur_1 + dur_2$. Next we make R very big. The second pulse, the one that was generated by reflection from the remote rock, has experienced strong attenuation and is now so weak that it can be hardly noticed in the background of the scattered waves. The further the rock is, the weaker the pulse will become. Therefore, two ranges of the horizontal characteristic dimension (distance to the reflecting rock) exist: small R, where the duration of strong motion grows with increasing R, and large R, where the effect is just the opposite. The simplest way to describe such a dependence on R is to use a parabolic function, $const_1 + const_2 \cdot R + const_3 \cdot R^2$, where $const_i$, $i = 1, 2, 3$ are some constants, and we expect $const_3 < 0$.

The dependence of τ_{rs} on h is similar to that on R, with only difference in the scale, due to the fact that h describes the dimension perpendicular to the predominant direction of the strong motion wave propagation. It can be described by another parabolic function, $const_4 + const_5 \cdot h + const_6 \cdot h^2$, where $const_i$, $i = 4, 5, 6$ are some constants, and we expect $const_6 < 0$.

Due to the complex geometry of the sedimentary deposits, the dependence of τ_{rs} on R and h is coupled. Thus, renaming the coefficients and excluding the constant term (which belongs to the "basic duration" term in the regression equations), we arrive at the representation of τ_{rs} by Eq. (2.5). If not all of three parameters R, h and φ are available, the "truncated" term τ_{rs}

$$\tau_{rs}(f) = a_6(f) \cdot R + a_8(f) \cdot R^2 + a_{10}(f) \cdot \varphi \tag{2.6}$$

or

$$\tau_{rs}(f) = a_5(f) \cdot h + a_9(f) \cdot h^2 \tag{2.7}$$

can be used.

If none of the parameters R, h or φ are available, the site can be roughly described by the geological classification parameter s ($s = 0$ for sites on sediments, $s = 2$ for sites

on basement rock, and $s = 1$ for sites on intermediate geology), and by the local soil parameter s_L ($s_L = 2$ for deep soil sites, $s_L = 1$ for stiff soil sites, and $s_L = 0$ for local "rock" sites). We consider τ_{rs} to be composed of two parts, the prolongation due to the presence of sediments under the station, $\tau_{rs}^{(s)}$, and the prolongation due to the local soils, $\tau_{rs}^{(s_L)}$.

The parameters s and s_L, are qualitative variables (each takes on only three discrete values) and so need to be considered in a different way than the conventional quantitative variables (Montgomery and Peck, 1982). The term accounting for the local soil effects can be written in the form:

$$\tau_{rs}^{(s_L)} = a_{11}(f)\cdot S_L^{(1)} + a_{12}(f)\cdot S_L^{(2)}, \tag{2.8}$$

where

$$\begin{aligned} S_L^{(1)} &= \begin{cases} 1, & \text{if } s_L = 1, \\ 0, & \text{if } s_L \neq 1, \end{cases} \\ S_L^{(2)} &= \begin{cases} 1, & \text{if } s_L = 2, \\ 0, & \text{if } s_L \neq 2. \end{cases} \end{aligned} \tag{2.9}$$

In this representation, the coefficient a_{11} describes the change in the duration of strong motion in the case of a site being on stiff soil conditions as compared with the "rock" sites ($s_L = 0$). The coefficient a_{12} accounts for deep soil sites, comparing those with stations located on "rock." This means that positive a_{12} would show that the duration of strong motion is longer at deep soil sites, than on "rock" sites. Positive a_{11} would indicate the same in the case of stiff soil sites. By comparing a_{11} and a_{12}, conclusions about the degree of these prolongations can be made. Thus, $a_{12} > a_{11}$ would show that the duration of strong motion is, on the average, longer at deep soil sites, than at stiff soil sites, for example.

We consider the influence of the geological conditions in a similar manner:

$$\tau_{rs}^{(s)} = a_{13}(f)\cdot S^{(1)} + a_{14}(f)\cdot S^{(0)}, \tag{2.10}$$

where

$$\begin{aligned} S^{(1)} &= \begin{cases} 1, & \text{if } s = 1, \\ 0, & \text{if } s \neq 1, \end{cases} \\ S^{(0)} &= \begin{cases} 1, & \text{if } s = 0, \\ 0, & \text{if } s \neq 0, \end{cases} \end{aligned} \tag{2.11}$$

Here a_{13} shows the change in duration for the intermediate ($s = 1$) sites compared with the basement rock sites ($s = 2$). The coefficient a_{14} displays the difference between sedimentary sites ($s = 0$) and basement rock sites. The reason for considering $S^{(0)}$ instead of $S^{(2)}$ (as it was done in Eq. (2.9) for the case of local soil conditions) is that we

Table 2.1 Terms involved in the modelling of the duration of strong ground motion and the assigned regression coefficients.

	"Basic duration" term				"Prolongation due to site conditions" term											
					Detailed description of the geometry of the sedimentary valley						Rough description of the site conditions					
											Soil			Geology		
Number	1	19	20	4	5	6	7	8	9	10	11	12	16	13	14	15
Parameter	1	I_{MM}	$I_{MM}\Delta'$	Δ'	h	R	hR	R^2	h^2	φ	$S_L^{(1)}$	$S_L^{(2)}$	s_L	$S^{(1)}$	$S^{(0)}$	s
Coefficient	a_1	a_{19}	a_{20}	a_4	a_5	a_6	a_7	a_8	a_9	a_{10}	a_{11}	a_{12}	a_{16}	a_{13}	a_{14}	a_{15}

Here: I_{MM}—Modified Mercalli intensity,
Δ'—hypocentral distance (km),
h—depth of sediments at the recording site (km),
R—characteristic horizontal dimension of the sedimentary valley (distance to the reflecting rock), (km),
φ—angle subtended at the station by the reflecting rock (degrees),
s—geological site conditions,
s_L—local soil site conditions,
$S^{(1)}$ and $S^{(0)}$—see Eq. (2.11),
$S_L^{(1)}$ and $S_L^{(2)}$—see Eq. (2.9).

The numbers 2, 3, 17 and 18 were reserved for the source parameters (magnitude and hypocentral depth), see Novikova and Trifunac (1993).

wish to disable all the site effects taking the rock sites (basement rock for the geological classification and local "rock" for the soil classification) as reference.

The complete "prolongation due to site conditions" term, τ_{rs}, can be obtained now as the sum of $\tau_{rs}^{(s)}$ and $\tau_{rs}^{(s_L)}$. Unfortunately, simultaneous implementation of Eqs. (2.8)–(2.11) causes instability in the regression analysis. This is related to the highly uneven distribution of the records among the rocky and the sedimentary sites. In the case where the use of Eqs. (2.8)–(2.11) is impossible, the simplified (but rough) versions of $\tau_{rs}^{(s)}$ and $\tau_{rs}^{(s_L)}$ can be used:

$$\tau_{rs}^{(s)} = a_{15}(f)\cdot(2-s), \tag{2.12}$$

$$\tau_{rs}^{(s_L)} = a_{16}(f)\cdot s_L. \tag{2.13}$$

Table 2.1 summarizes the notation and the numbering of the regression coefficients used in this and in the next Chapter in the development of the empirical models of the frequency dependent duration of strong earthquake ground motion. The terms described by the Eqs. (2.1) and (2.4)–(2.13) are included in the Table 2.1.

III. THE REGRESSION MODELS

In this Chapter, 12 empirical regression models of the frequency dependent duration of strong ground motion in terms of the Modified Mercalli intensity and other parameters are presented. The algorithm for choosing the proper model, depending on the parameters available, is proposed. Also, the distribution functions of the residuals for all the models are presented.

Regarding the notation used in this Chapter, the duration estimated from any of the models is called the "estimated duration," or the "predicted duration." The value obtained from the data (acceleration, velocity or displacement) according to our definition of the duration is called the "observed duration." As before, we designate the observed and the predicted duration of strong ground motion as *dur*. When we want to show explicitly what the parameters of the model considered are, we list those in parenthesis. For example, $dur = dur\ (I_{MM},\ s)$ should be read as "the total duration of strong ground motion as a function of the Modified Mercalli intensity observed at the site and the geological site conditions described by parameter s" (a constant term is always included in the formula by default).

III.1 Models $dur = dur(I_{MM}, \Delta', I_{MM}\Delta')$ and $dur = dur(I_{MM})$

The first model only includes the dependence of the duration of strong ground motion on the Modified Mercalli intensity and the distance to the source in the form of Eq. (2.1). That is, we consider first the case when no information about the site parameters is available:

$$dur = a_1(f) + a_{19}(f)\cdot I_{MM} + a_4(f)\cdot\Delta' + a_{20}(f)\cdot I_{MM}\Delta'. \tag{3.1}$$

Eq. (3.1) was first fit to the data separately for the horizontal and for the vertical components. No significant differences in the behavior of the frequency dependent coefficients $a_{19}(f), a_4(f)$ and $a_{20}(f)$ for the horizontal and for the vertical motion were observed. However, the constant coefficient $a_1(f)$ was found to be different in these two cases. Also, the estimated duration appears to be negative at high frequencies for small hypocentral distances and for very small intensities. This can be explained by the lack of data for this combination of parameters. The final equation for the first model is then:

$$\begin{Bmatrix} dur^{(h)}(f) \\ dur^{(v)}(f) \end{Bmatrix} = \max\left[\left(\begin{Bmatrix} a_1^{(h)}(f) \\ a_1^{(v)}(f) \end{Bmatrix} + a_{19}(f)\cdot I_{MM} + a_4(f)\cdot\Delta' + a_{20}(f)\cdot I_{MM}\Delta'\right), 1\right] \tag{3.2}$$

The hypocentral distance Δ' is measured in kilometers. The superscripts (h) and (v) correspond to the horizontal and to the vertical components of motion respectively.

Table 3.1 Results of the regression analysis of the model in Eq. (3.2).

Channel number	f_0 (Hz)	# of data points N(f)	Coefficients a_i and their accuracy ("σ–interval")					σ_{dur} (sec)	dur_{av} (sec)
			$a_1^{(h)}$ $\pm\sigma_1^{(h)}$	$a_1^{(v)}$ $\pm\sigma_1^{(v)}$	a_{19} $\pm\sigma_{19}$	a_4 $\pm\sigma_4$	a_{20} $\pm\sigma_{20}$		
1	0.075	37	40.8 ±2.0	32.5 ±3.1	.0	.0	.0	10.2	38.3
2	0.12	311	27.7 ±5.4	28.2 ±5.7	-1.30 ±.75	.182 ±.019	.0	10.1	28.3
3	0.21	962	33.3 ±2.7	35.3 ±2.7	-3.17 ±.37	.195 ±.012	.0	7.8	21.4
4	0.37	1499	23.8 ±2.6	24.2 ±2.6	-1.73 ±.39	.084 ±.040	.018 ±.007	7.4	21.0
5	0.63	2035	13.7 ±2.1	15.6 ±2.1	-.62 ±.32	.134 ±.033	.012 ±.006	7.8	18.7
6	1.1	2636	10.0 ±1.6	12.8 ±1.6	-.44 ±.25	.089 ±.025	.016 ±.004	7.0	15.6
7	1.7	3119	5.1 ±1.0	7.8 ±1.0	-.03 ±.16	.046 ±.018	.021 ±.003	5.4	12.4
8	2.5	3418	4.4 ±0.7	6.2 ±0.7	-.11 ±.11	-.018 ±.013	.025 ±.002	4.0	9.1
9	4.2	2739	1.7 ±0.6	3.1 ±0.6	.16 ±.10	-.043 ±.013	.030 ±.002	3.3	7.6
10	7.2	2576	1.0 ±0.5	1.6 ±0.5	.18 ±.08	-.070 ±.012	.035 ±.002	2.8	6.4
11	13	1584	-1.1 ±0.5	-1.0 ±0.5	.46 ±.08	-.028 ±.017	.027 ±.003	2.3	5.1
12	21	735	-3.4 ±0.7	-3.3 ±0.7	.75 ±.12	.118 ±.038	.005 ±.006	2.0	4.2
			1 horiz	1 vert	I_{MM}	Δ'	$I_{MM}\Delta'$		
			Corresponding parameters						

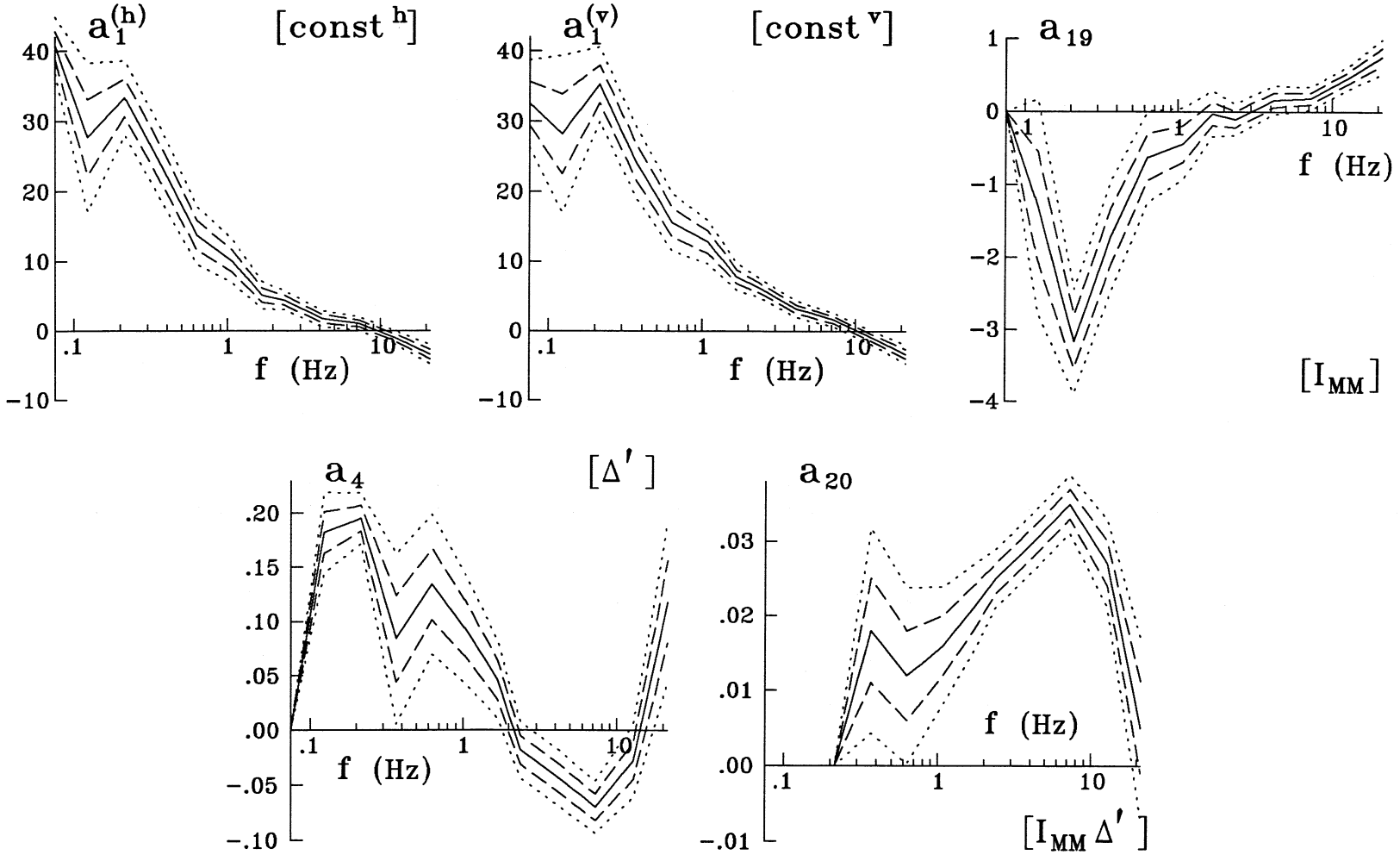

Fig. 3.1 The coefficients $a_i(f)$ in the model in Eq. (3.2), plotted versus the central frequency of the channels (solid lines). The coefficients are bounded by their "σ-intervals" (dashed lines) and by their estimated 95% confidence intervals (dotted lines).

Eq. (3.2) was fit to the data in two steps. In the first iteration, instead of the formula $dur = \max[(\cdot), 1]$, the simple equation $dur = (\cdot)$ (i.e., Eq. (3.1)) was considered and the coefficients $\{a_1(f), a_4(f), a_{19}(f), a_{20}(f)\}_{first}$ were calculated. This first set was used in the second iteration for the evaluation of the quantity $(\cdot)$. The data points for which $(\cdot) < 1$ sec were not included in the second iteration of the regression analysis. The set $\{a_1(f), a_{19}(f), a_4(f), a_{20}(f)\}_{second}$ is almost same as $\{a_1(f), a_{19}(f), a_4(f), a_{20}(f)\}_{first}$, and either of them can serve as a solution. The similarity between those two sets of coefficients follows from the fact that the database does not include many cases for which $(\cdot) < 1$ sec.

Table 3.1 gives the regression coefficients of the model in Eq. (3.2) as $a_i(f) \pm \sigma_i(f)$, where $\sigma_i^2(f)$ are the variances of the values found. Zero values for a coefficient correspond to the cases when $|\sigma_i/a_i| > 1$. The number of the available data points $N(f)$ is very different at each channel, reflecting the statistical reliability of the regression analysis performed. The average observed duration, $dur_{\rm av}$, and the standard deviation of the estimated duration from the observed value, $\sigma_{\rm dur}$, are also listed. Note the strong dependence of $dur_{\rm av}$ on frequency.

Graphical representation of the regression coefficients, plotted versus the central frequency of the channels, is shown in Fig. 3.1. The duration of strong ground motion does not depend on the Modified Mercalli intensity level for low frequencies of motion ($f \lesssim 0.1$ Hz). At these frequencies, the duration of the source rupture is shorter than the period of the wave used to measure it. This results also in absence of the dependence of duration of strong motion on the earthquake magnitude (Novikova and Trifunac, 1993). There is no dependence on the distance to the source either, because essentially only one mode of propagation of surface waves exists for such low frequencies (at local distances), and no dispersion can be noticed (Novikova and Trifunac, 1993). Thus, no dependence of the duration on the Modified Mercalli intensity should be expected.

The isolines of the strong motion duration at higher frequencies, ($f \gtrsim 0.1$ Hz), as predicted by Eq. (3.2), are shown for the horizontal component of motion in Fig. 3.2. For a fixed intensity, the duration grows with distance due to the dispersion of the seismic waves (Novikova and Trifunac, 1993). The dependence of the duration of strong motion on the intensity at the site, for a fixed distance is more complex. The intensity, by itself, is a function of the earthquake magnitude and of the distance to the source. Being directly proportional to the magnitude, the intensity grows when the magnitude increases. The intensity also grows when the distance to the source decreases. These two trends result in what might seem as a "contradictory" behavior of the duration of strong motion as a function of the intensity at the site. On one hand, the duration should increase when the intensity increases, when the increase in intensity corresponds to an increase of the magnitude. On the other hand, the duration should decrease with increasing intensity, because the increase of intensity could correspond to a shorter distance (with no change in magnitude). The resulting picture depends on which of those two effects prevails. One should also remember that the intensity at a site is often assigned by estimating the damage to structures sensitive to the short period part of

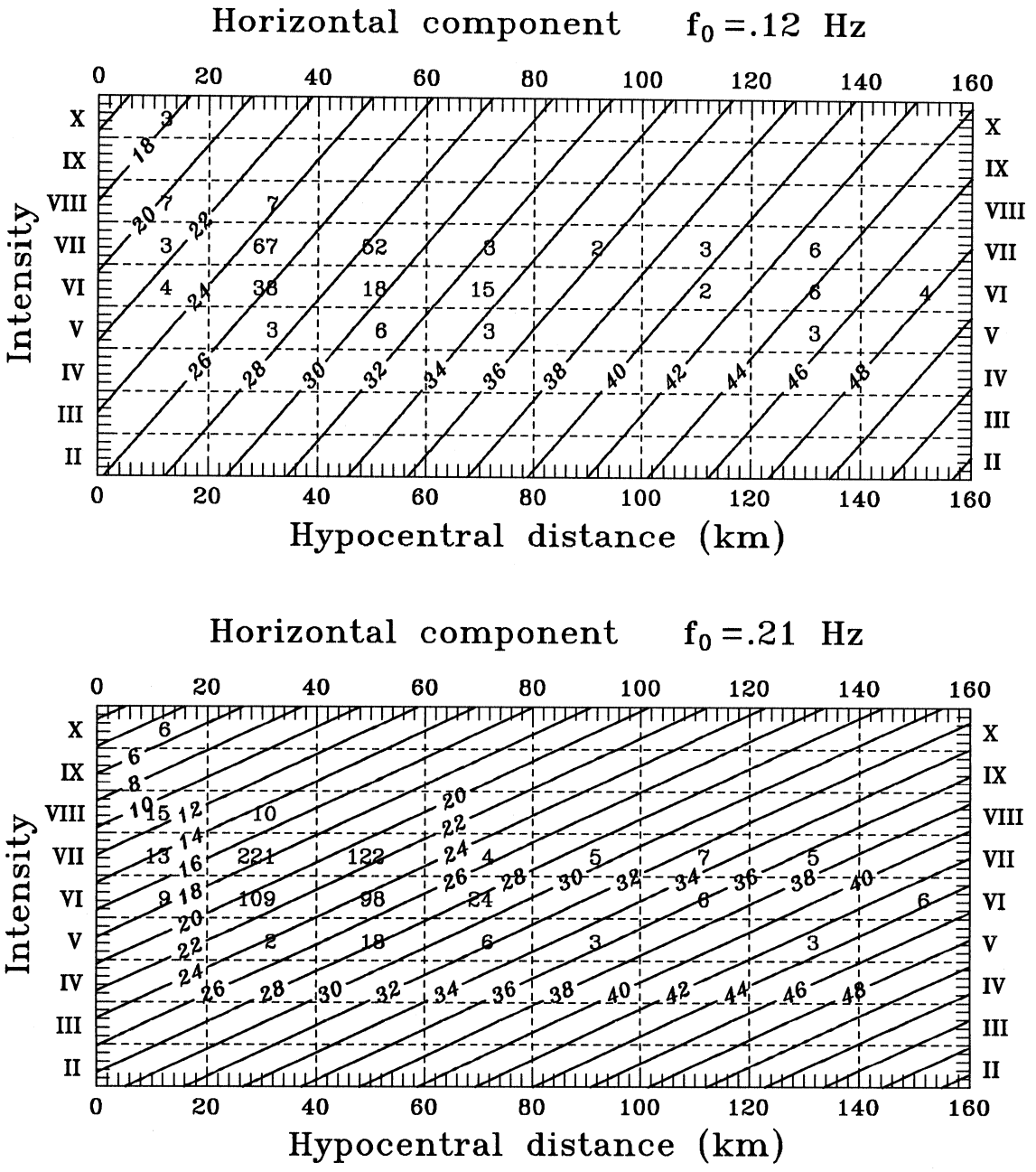

Fig. 3.2a Channels #2 and #3: isolines of the duration (in seconds) of the horizontal component of strong earthquake ground motion as predicted by the model in Eq. (3.2). The numbers in the dashed "boxes" designate the number of the data points used in the analysis for the particular range of intensities, I_{MM}, and hypocentral distances, Δ'.

For each fixed I_{MM}, the duration grows with Δ'. The dependence of the duration on the intensity for fixed hypocentral distance depends on the frequency and on the distance: the duration grows with I_{MM} for the high frequency channels and decreases for the low frequency channels. A smooth transition from one pattern to another can be seen for the intermediate channels, where *dur* grows with increasing I_{MM} for large Δ', and decreases with increasing I_{MM} for small Δ'. See Fig. 2.2 for comparison with the actual data.

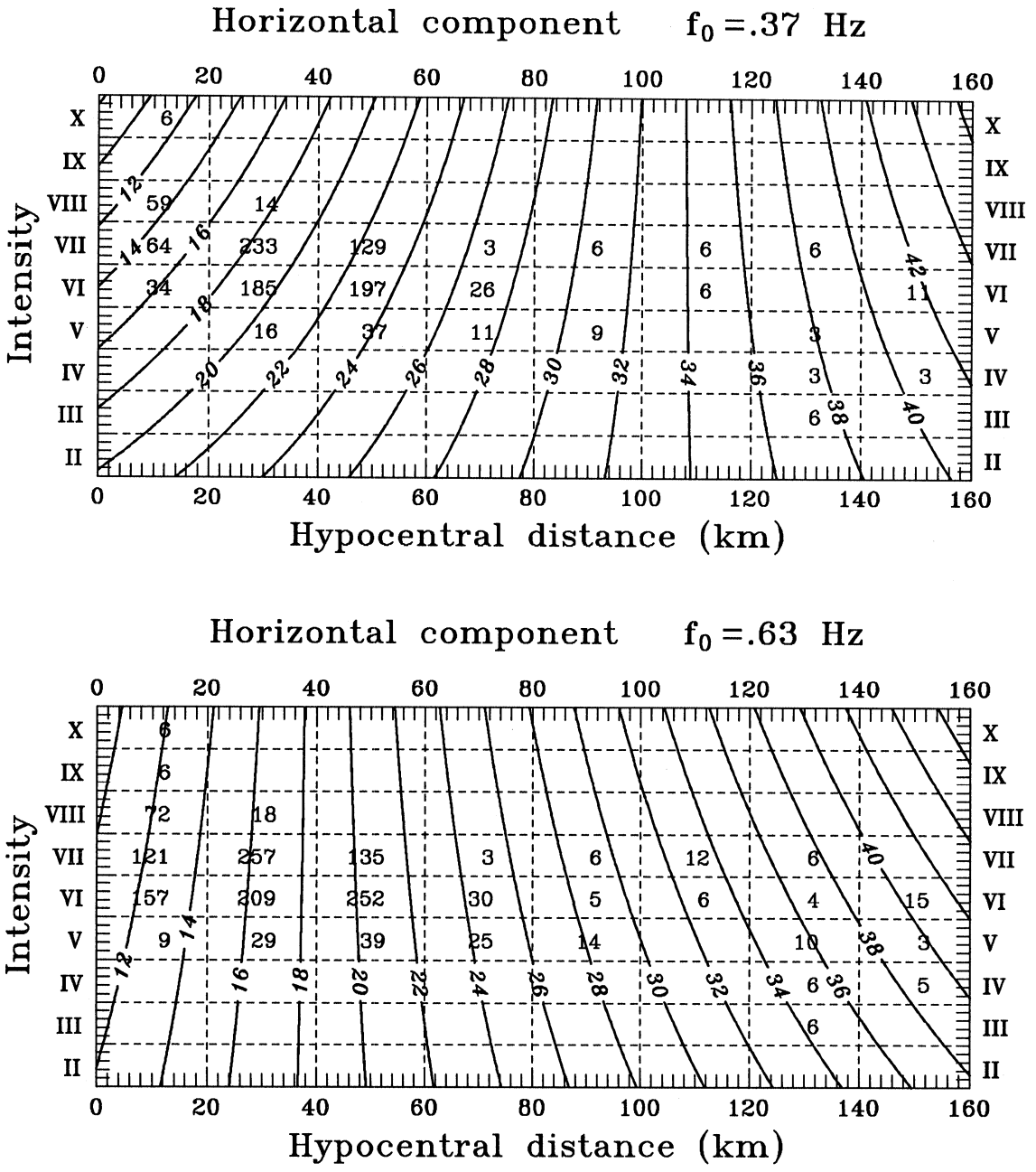

Fig. 3.2b Channels #4 and #5: isolines of the duration (in seconds) of the horizontal component of strong earthquake ground motion as predicted by the model in Eq. (3.2). The numbers in the dashed "boxes" designate the number of the data points used in the analysis for the particular range of intensities, I_{MM}, and hypocentral distances, Δ'.

For each fixed I_{MM}, the duration grows with Δ'. The dependence of the duration on the intensity for fixed hypocentral distance depends on the frequency and on the distance: the duration grows with I_{MM} for the high frequency channels and decreases for the low frequency channels. A smooth transition from one pattern to another can be seen for the intermediate channels, where *dur* grows with increasing I_{MM} for large Δ', and decreases with increasing I_{MM} for small Δ'. See Fig. 2.2 for comparison with the actual data.

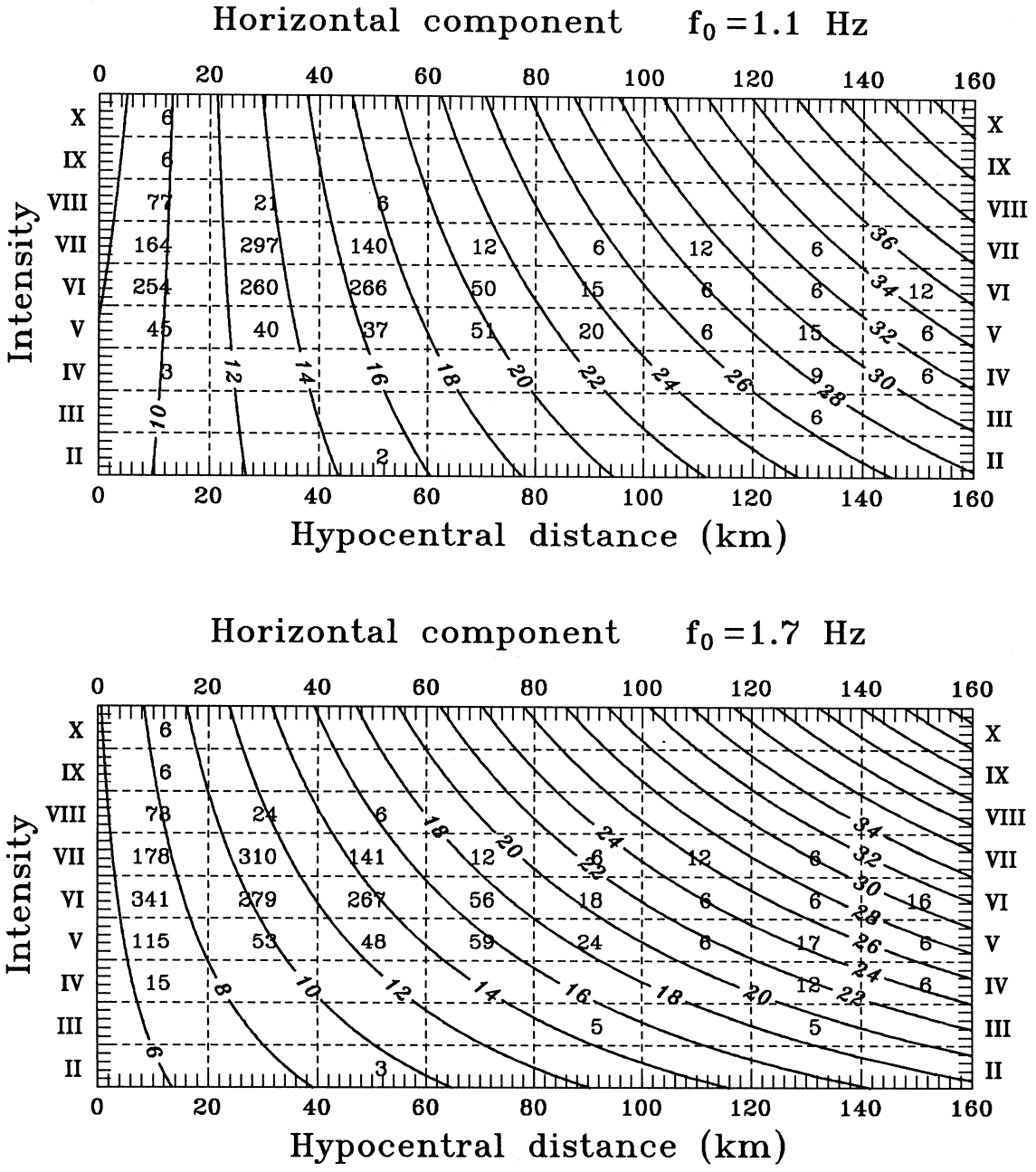

Fig. 3.2c Channels #6 and #7: isolines of the duration (in seconds) of the horizontal component of strong earthquake ground motion as predicted by the model in Eq. (3.2). The numbers in the dashed "boxes" designate the number of the data points used in the analysis for the particular range of intensities, I_{MM}, and hypocentral distances, Δ'.

For each fixed I_{MM}, the duration grows with Δ'. The dependence of the duration on the intensity for fixed hypocentral distance depends on the frequency and on the distance: the duration grows with I_{MM} for the high frequency channels and decreases for the low frequency channels. A smooth transition from one pattern to another can be seen for the intermediate channels, where *dur* grows with increasing I_{MM} for large Δ', and decreases with increasing I_{MM} for small Δ'. See Fig. 2.2 for comparison with the actual data.

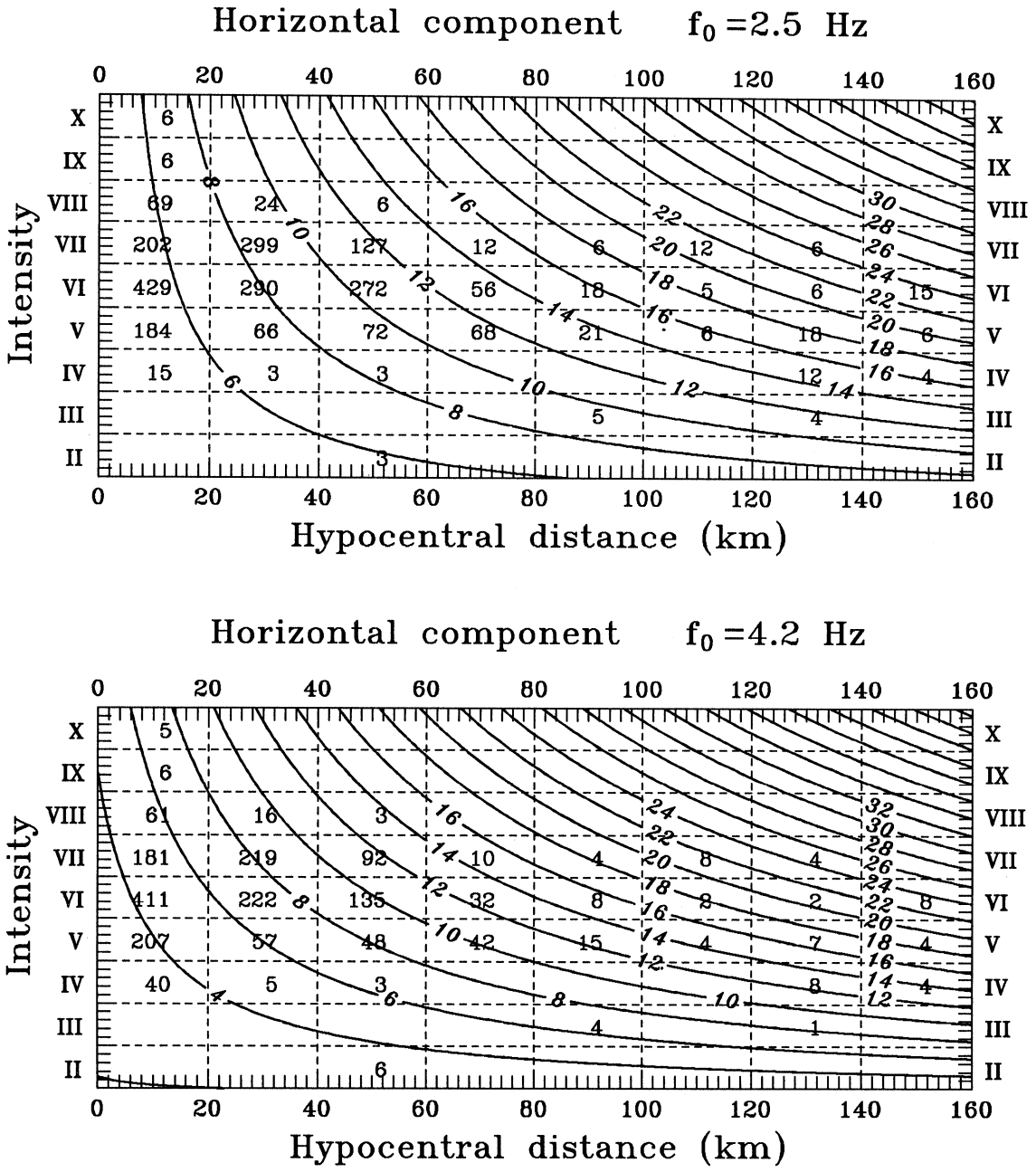

Fig. 3.2d Channels #8 and #9: isolines of the duration (in seconds) of the horizontal component of strong earthquake ground motion as predicted by the model in Eq. (3.2). The numbers in the dashed "boxes" designate the number of the data points used in the analysis for the particular range of intensities, I_{MM}, and hypocentral distances, Δ'.

For each fixed I_{MM}, the duration grows with Δ'. The dependence of the duration on the intensity for fixed hypocentral distance depends on the frequency and on the distance: the duration grows with I_{MM} for the high frequency channels and decreases for the low frequency channels. A smooth transition from one pattern to another can be seen for the intermediate channels, where *dur* grows with increasing I_{MM} for large Δ', and decreases with increasing I_{MM} for small Δ'. See Fig. 2.2 for comparison with the actual data.

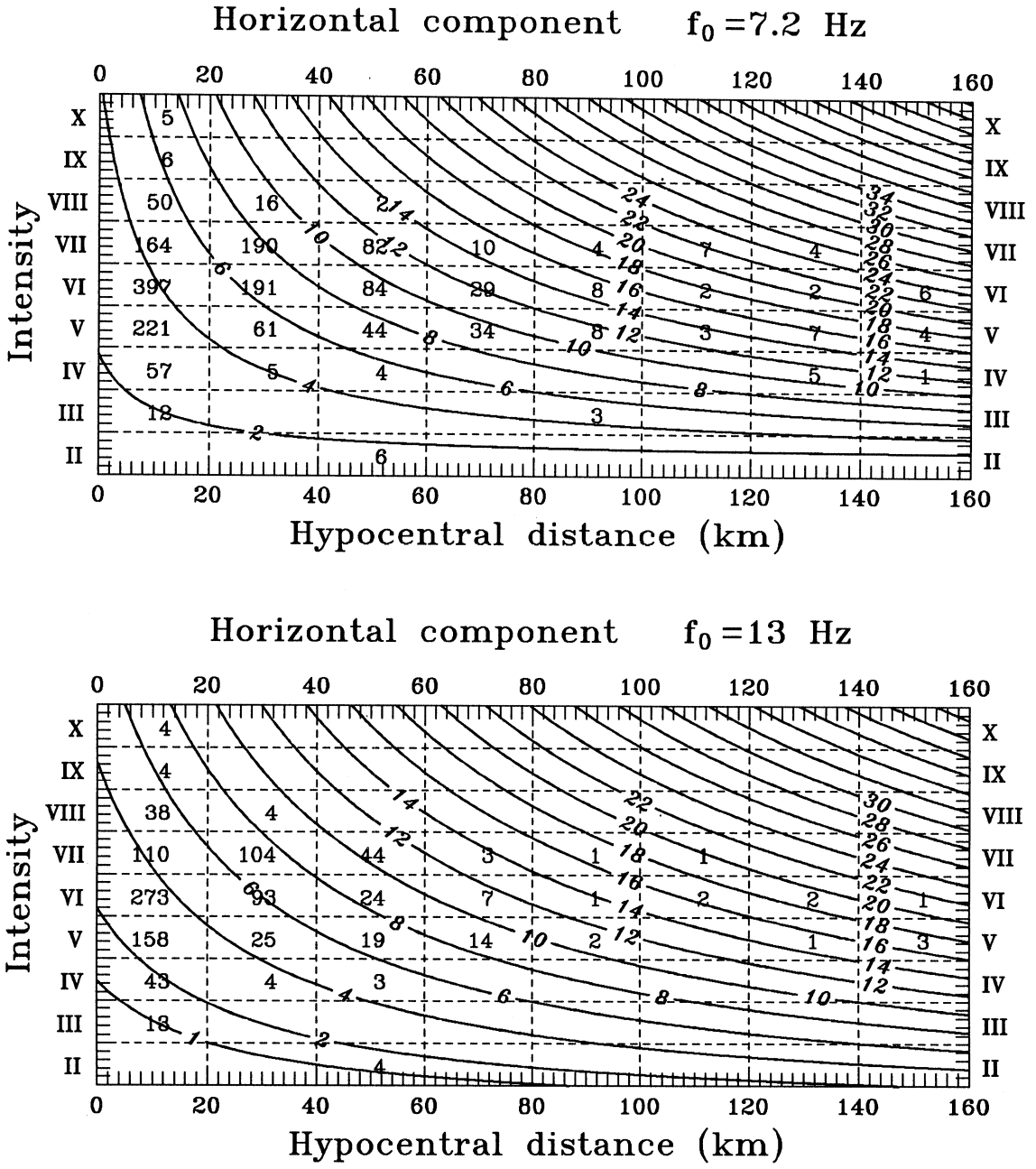

Fig. 3.2e Channels #10 and #11: isolines of the duration (in seconds) of the horizontal component of strong earthquake ground motion as predicted by the model in Eq. (3.2). The numbers in the dashed "boxes" designate the number of the data points used in the analysis for the particular range of intensities, I_{MM}, and hypocentral distances, Δ'.

For each fixed I_{MM}, the duration grows with Δ'. The dependence of the duration on the intensity for fixed hypocentral distance depends on the frequency and on the distance: the duration grows with I_{MM} for the high frequency channels and decreases for the low frequency channels. A smooth transition from one pattern to another can be seen for the intermediate channels, where *dur* grows with increasing I_{MM} for large Δ', and decreases with increasing I_{MM} for small Δ'. See Fig. 2.2 for comparison with the actual data.

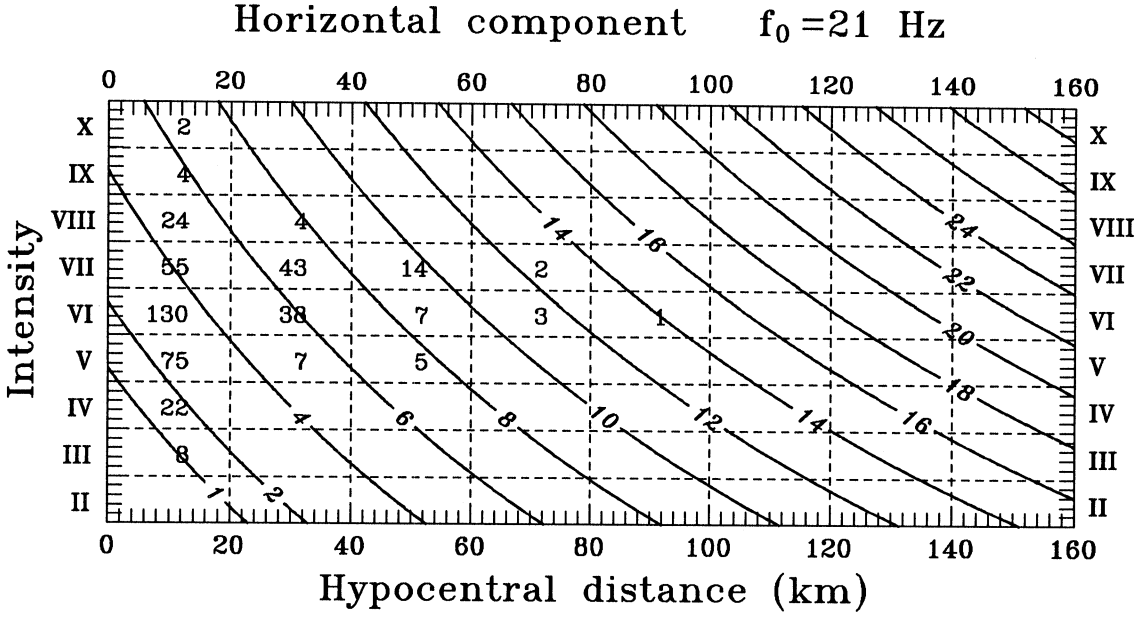

Fig. 3.2f Channel #12: isolines of the duration (in seconds) of the horizontal component of strong earthquake ground motion as predicted by the model in Eq. (3.2). The numbers in the dashed "boxes" designate the number of the data points used in the analysis for the particular range of intensities, I_{MM}, and hypocentral distances, Δ'.

For each fixed I_{MM}, the duration grows with Δ'. The dependence of the duration on the intensity for fixed hypocentral distance depends on the frequency and on the distance: the duration grows with I_{MM} for the high frequency channels and decreases for the low frequency channels. A smooth transition from one pattern to another can be seen for the intermediate channels, where *dur* grows with increasing I_{MM} for large Δ', and decreases with increasing I_{MM} for small Δ'. See Fig. 2.2 for comparison with the actual data.

the spectrum at the site. Long and short period waves attenuate with different rates, so that a severe earthquake felt at a larger distance might have short period amplitudes smaller and long period amplitudes higher, than a smaller shock, recorded at a smaller distance. As a result, the behavior of the intensity scale at low frequencies may seem "contradictory" at first. For long period waves (channels #2 and #3, $f_0 = 0.12 \div 0.21$ Hz), the influence of the earthquake magnitude is not "felt" (Novikova and Trifunac, 1993), and the increase in I_{MM} (for fixed distance) causes the decrease of the duration. For high frequencies ($f_0 \geq 2.5$ Hz), the dispersion does not play as important role as for low and for intermediate frequencies (Novikova and Trifunac, 1993). As a result, the duration increases with the increasing intensity, because the latter is caused primarily by a growing magnitude. In the intermediate frequency range (channels #4 $\div$ 7, $f_0 = 0.37 \div 1.7$ Hz), the behavior of the duration as a function of intensity for a fixed distance is of intermediate and dual nature. For large distances it resembles the behavior typical for the high frequency channels. For short distances, the dependence of the duration on intensity (when the distance to the source is fixed) appears to be similar to that for low frequencies. The definitions of "long" and "short" should be scaled by the wavelength of the channel considered. Once this scaling is taken into account, it is easy to understand why the "transition" distance (where "short" distance borders with "long" distance) moves towards the source when the frequency of motion becomes higher.

The model discussed above has the distance to the earthquake source as one of the parameters. We assume that the depth of the hypocenter can be obtained from teleseismic records, from the macroseismic field, or from geological field studies. The location of the epicenter can also be estimated, if the intensities are known at many locations surrounding the epicenter. However, the model which does not include any distance to the source as a parameter, may appear to be more useful in practice. Such a model would also be less region dependent, as it does not assume (explicitly at least) any region specific dispersion or attenuation law. We next consider such a model:

$$\left\{ \begin{array}{c} dur^{(h)}(f) \\ dur^{(v)}(f) \end{array} \right\} = \max \left[\left(\left\{ \begin{array}{c} a_1^{(h)}(f) \\ a_1^{(v)}(f) \end{array} \right\} + a_{19}(f) \cdot I_{MM} \right), 1 \right] . \tag{3.3}$$

Table 3.2 and Fig. 3.3 show the results of the regression analysis with this model, which was performed in two steps, similar to those for the model in Eq. (3.2). The behavior of the coefficient $a_{19}(f)$ can easily be explained now by comparison with Fig. 3.2 (Eq. (3.2)) and by recalling the discussion on the nature of the dependence of the duration on the intensity and the distance in the previous model. The duration decreases with growth of intensity for low and intermediate frequencies, when the increase of intensity corresponds to a decrease of distance. In the high frequency range ($f_0 \geq 2.5$ Hz), the duration becomes longer when the intensity increases, and this shows that, for these frequencies, the intensity is governed more by the magnitude, than by the distance to the source.

Table 3.2 Results of the regression analysis of the model in Eq. (3.3).

Channel number	f_0 (Hz)	# of data points N(f)	Coeff. a_i and their ("σ–interval")			σ_{dur} (sec)	dur_{av} (sec)
			$a_1^{(h)}$ $\pm\sigma_1^{(h)}$	$a_1^{(v)}$ $\pm\sigma_1^{(v)}$	a_{19} $\pm\sigma_{19}$		
1	0.075	37	40.8 ±2.0	32.5 ±3.1	.0	10.2	38.3
2	0.12	311	54.1 ±5.2	53.6 ±5.6	-3.88 ±.79	11.5	28.3
3	0.21	962	52.3 ±2.7	54.2 ±2.8	-4.74 ±.40	8.7	21.4
4	0.37	1499	42.3 ±1.8	43.2 ±1.8	-3.33 ±.27	8.4	21.0
5	0.63	2035	35.8 ±1.6	37.9 ±1.7	-2.75 ±.25	9.2	18.7
6	1.1	2636	27.7 ±1.2	30.9 ±1.3	-2.05 ±.19	8.6	15.6
7	1.7	3119	15.9 ±0.9	18.8 ±0.9	-.71 ±.14	7.1	12.4
8	2.5	3418	9.2 ±0.6	11.2 ±0.6	-.12 ±.10	5.3	9.1
9	4.2	2739	3.1 ±0.6	4.7 ±0.6	.66 ±.10	4.9	7.6
10	7.2	2576	-0.3 ±0.5	0.5 ±0.6	1.06 ±.09	4.5	6.4
11	13	1584	-2.5 ±0.5	-2.0 ±0.5	1.22 ±.08	3.5	5.1
12	21	735	-3.2 ±0.6	-2.8 ±0.6	1.19 ±.10	2.9	4.2
			1 horiz	1 vert	I_{MM}		
			Corr. parameters				

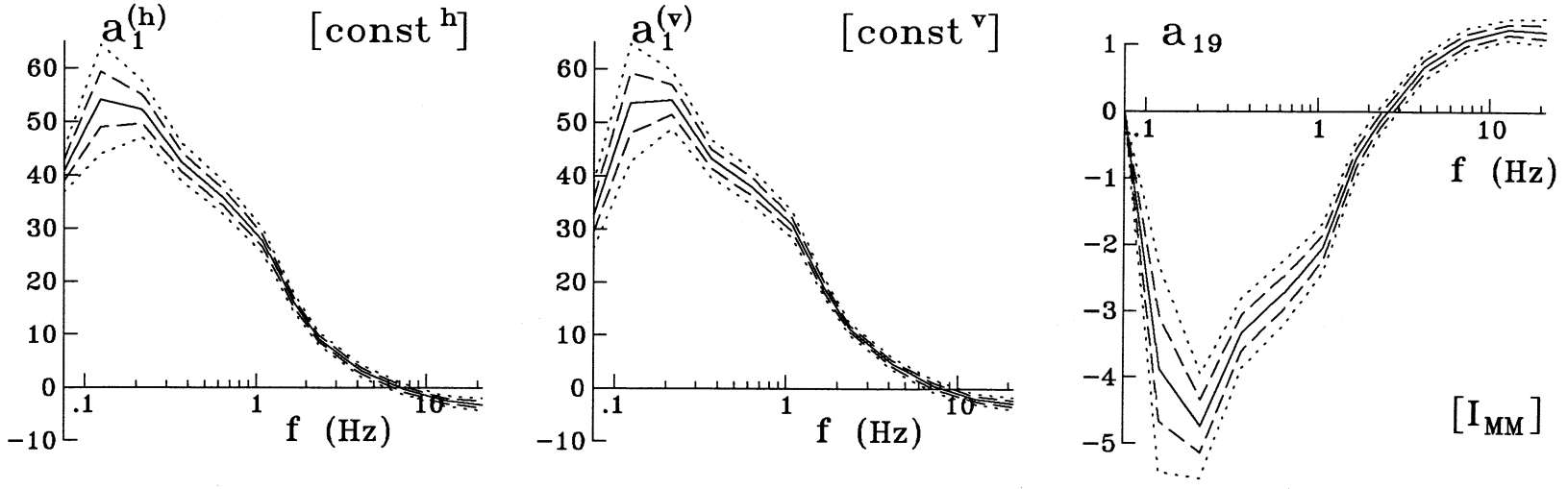

Fig. 3.3 The coefficients $a_i(f)$ in the model in Eq. (3.3), plotted versus the central frequency of the channels (solid lines). The coefficients are bounded by their "σ-intervals" (dashed lines) and by their estimated 95% confidence intervals (dotted lines).

III.2 Models $dur = dur(I_{MM}, \Delta', I_{MM}\Delta', s)$, $dur = dur(I_{MM}, s)$

So far, we considered the sum of the first two terms, $\tau_0 + \tau_\Delta$, from the general description of the duration of strong ground motion (Eq.(1.1)). We will call "basic" models those models that only include these two terms. We now turn to the models which include the site conditions term, τ_{rs}. We will start from the simplest models, which only consider the influence of the geological conditions at the site, expressed through the parameter s (see Eqs. (2.9)–(2.10)). When Eq. (3.2) is taken as a "basic" equation, the model has the form:

$$\left\{ \begin{array}{l} dur^{(h)}(f) \\ dur^{(v)}(f) \end{array} \right\} = \max \left[\left(\left\{ \begin{array}{l} a_1^{(h)(f)} \\ a_1^{(v)}(f) \end{array} \right\} + a_{19}(f) \cdot I_{MM} + a_4(f) \cdot \Delta' + a_{20}(f) \cdot I_{MM}\Delta' \right), 1 \right]$$

$$+ a_{13}(f) \cdot S^{(1)} + a_{14}(f) \cdot S^{(0)}, \qquad (3.4a)$$

where Δ' is measured in kilometers and

$$S^{(1)} = \left\{ \begin{array}{ll} 1, & \text{if } s = 1, \\ 0, & \text{if } s \neq 1, \end{array} \right.$$

$$S^{(0)} = \left\{ \begin{array}{ll} 1, & \text{if } s = 0, \\ 0, & \text{if } s \neq 0. \end{array} \right. \qquad (3.4b)$$

Recall here that $s = 0$ corresponds to sites on sediments, $s = 2$ stands for sites located on basement rock and $s = 1$ designates intermediate sites (Trifunac and Brady, 1975b) .

The results of the regression analysis of Eq. (3.4) are shown in Table 3.3 and Fig. 3.4. The set of coefficients $\{a_1(f),\ a_{19}(f),\ a_4(f),\ a_{20}(f)\}$ is similar to the same set from the model in Eq. (3.2). The comparison of the last two coefficients, $a_{13}(f)$ and $a_{14}(f)$, with their counterparts from the model were the "basic duration" $\tau_0 + \tau_\Delta$ is expressed in terms of M and Δ (Novikova and Trifunac, 1993) shows remarkable similarity between these two sets of coefficients. Such a similarity provides additional support for the methods we use to construct our models, and for the models themselves. In this particular case, the assumption that $\tau_0 + \tau_\Delta$ can be modeled by Eq. (2.1) receives some additional support.

The influence of the geological conditions at the site is noticeable for the intermediate frequencies only. At low frequencies, the wavelength of the waves is too long to "feel" the presence of the sediments, and at high frequencies, the attenuation effects may overshadow the prolongation which is caused by multiple reflections in the sediments (Trifunac, 1990). These reflections may be the main reason for the duration on sediments being longer (on average) than the duration on rock sites (Novikova and Trifunac, 1993). $a_{14}(f)$ shows that, for the sites on sediments, this prolongation can be as much as about 5 sec (channel #6, $f_0 = 1.1$ Hz). $a_{13}(f)$ gives prolongation for intermediate sites of about 2.5 sec at the same frequency.

Table 3.3 Results of the regression analysis of the model in Eq. (3.4).

Channel number	f_0 (Hz)	# of data points N(f)	Coefficients a_i and their accuracy ("σ-interval")							σ_{dur} (sec)	dur_{av} (sec)
			$a_1^{(h)}$ $\pm\sigma_1^{(h)}$	$a_1^{(h)}$ $\pm\sigma_1^{(h)}$	a_{19} $\pm\sigma_{19}$	a_4 $\pm\sigma_4$	a_{20} $\pm\sigma_{20}$	a_{13} $\pm\sigma_{13}$	a_{14} $\pm\sigma_{14}$		
1	0.075	37	40.8 ±2.0	32.5 ±3.1	.0	.0	.0	.0	.0	10.2	38.3
2	0.12	311	27.7 ±5.4	28.2 ±5.7	-1.30 ±.75	.182 ±.019	.0	.0	.0	10.1	28.3
3	0.21	850	26.6 ±3.0	28.5 ±3.1	-2.51 ±.41	.191 ±.013	.0	.0	2.83 ±.64	7.9	20.7
4	0.37	1179	20.3 ±2.9	20.5 ±3.0	-1.51 ±.43	.088 ±.042	.016 ±.007	.0	2.98 ±.51	7.7	20.5
5	0.63	1647	8.5 ±2.4	11.0 ±2.5	-.55 ±.35	.127 ±.035	.012 ±.006	2.84 ±.85	5.76 ±.74	8.1	18.3
6	1.1	2189	5.8 ±1.7	8.5 ±1.8	-.23 ±.26	.093 ±.026	.014 ±.004	1.44 ±.63	3.83 ±.54	7.1	15.1
7	1.7	2645	3.8 ±1.1	6.3 ±1.1	-.09 ±.17	.039 ±.018	.021 ±.003	1.10 ±.44	2.36 ±.38	5.6	12.2
8	2.5	2931	4.2 ±0.7	5.7 ±0.7	-.19 ±.12	-.026 ±.013	.026 ±.002	.0	1.28 ±.17	4.1	9.0
9	4.2	2464	1.2 ±0.6	2.4 ±0.6	.16 ±.10	-.045 ±.013	.030 ±.002	.0	.88 ±.15	3.4	7.4
10	7.2	2576	1.0 ±0.5	1.6 ±0.5	.18 ±.08	-.070 ±.012	.035 ±.002	.0	.0	2.8	6.4
11	13	1584	-1.1 ±0.5	-1.0 ±0.5	.46 ±.08	-.028 ±.017	.027 ±.003	.0	.0	2.3	5.1
12	21	735	-3.4 ±0.7	-3.3 ±0.7	.75 ±.12	.118 ±.038	.005 ±.006	.0	.0	2.0	4.2
			1 horiz	1 vert	I_{MM}	Δ'	$I_{MM}\Delta'$	$S^{(1)}$	$S^{(0)}$		
			Corresponding parameters								

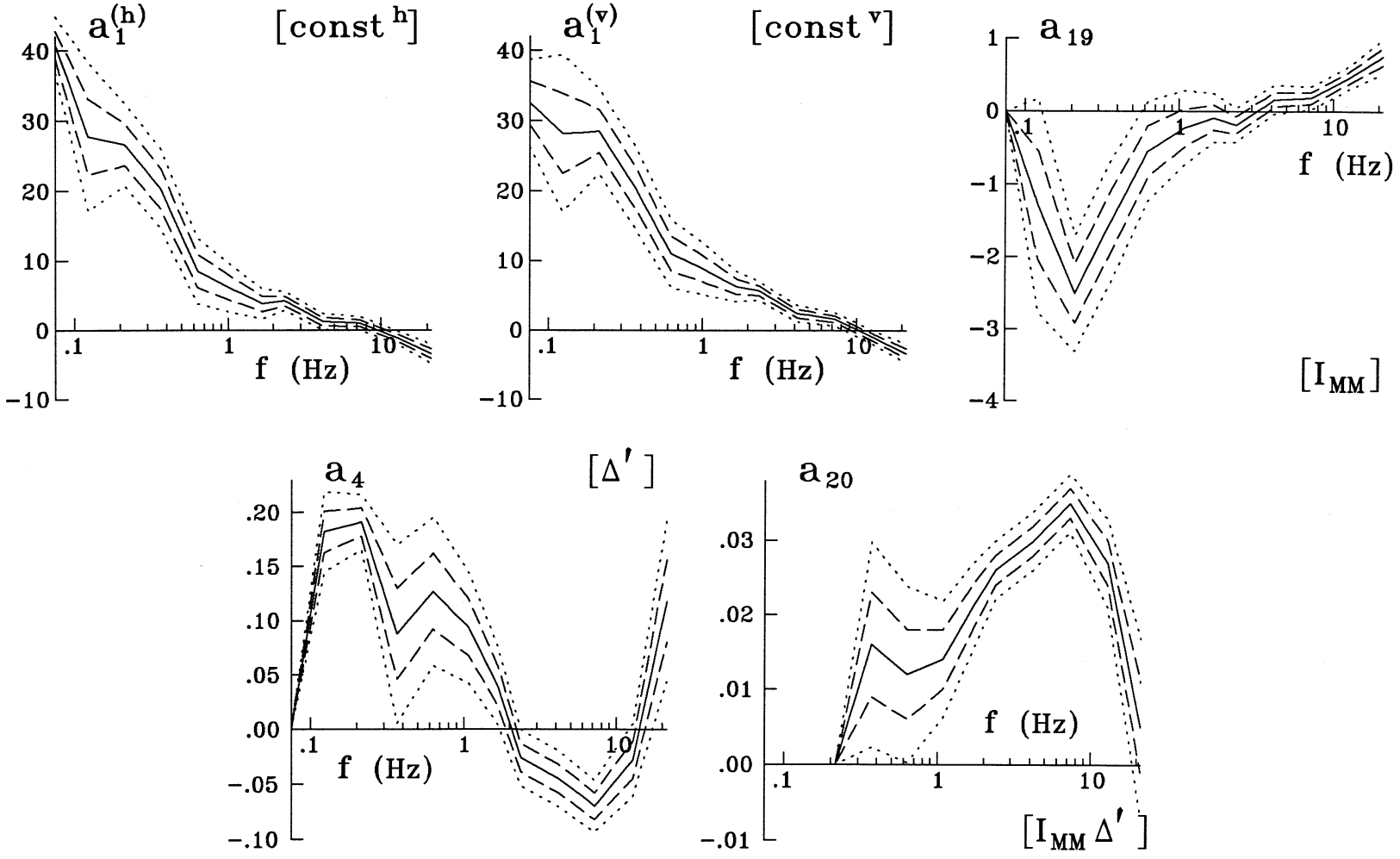

Fig. 3.4a The coefficients $a_1(f)$, $a_{19}(f)$, $a_4(f)$ and $a_{20}(f)$ in the model in Eq. (3.4), plotted versus the central frequency of the channels (solid lines). The coefficients are bounded by their "σ-intervals" (dashed lines) and by their estimated 95% confidence intervals (dotted lines).

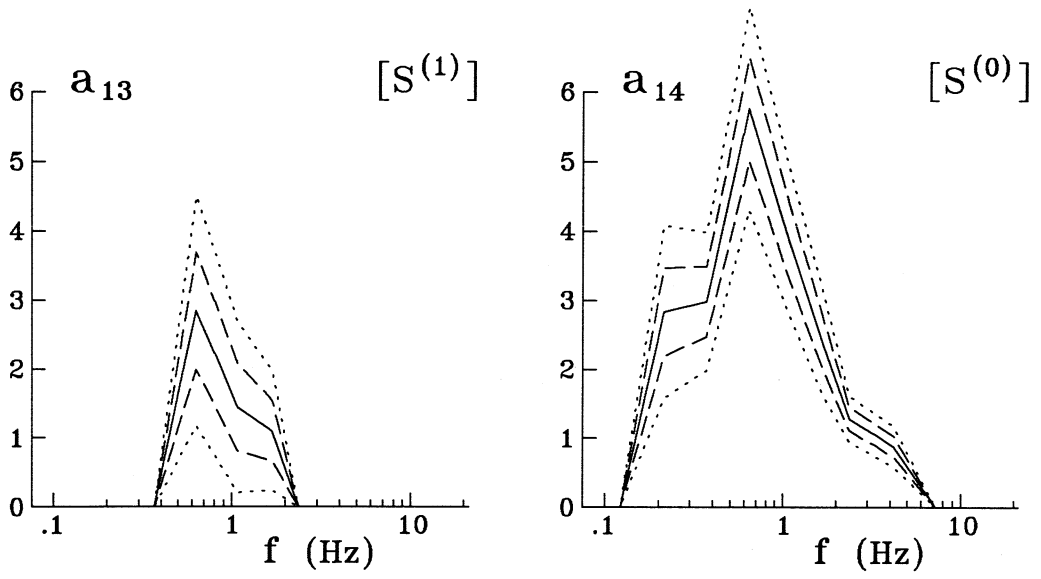

Fig. 3.4b The coefficients $a_{13}(f)$ and $a_{14}(f)$ in the model in Eq. (3.4), plotted versus the central frequency of the channels (solid lines). The coefficients are bounded by their "σ-intervals" (dashed lines) and by their estimated 95% confidence intervals (dotted lines).

Table 3.4 Results of the regression analysis of the model in Eq. (3.5).

Channel number	f_0 (Hz)	# of data points N(f)	Coefficients a_i and their accuracy ("σ-interval")				σ_{dur} (sec)	dur_{av} (sec)
			$a_1^{(h)}$ $\pm\sigma_1^{(h)}$	$a_1^{(h)}$ $\pm\sigma_1^{(h)}$	a_{19} $\pm\sigma_{19}$	a_{13} $\pm\sigma_{13}$		
1	0.075	37	40.8 ±2.0	32.5 ±3.1	.0	.0	10.2	38.3
2	0.12	311	54.1 ±5.2	53.6 ±5.6	-3.88 ±.79	.0	11.5	28.3
3	0.21	850	44.4 ±3.3	46.3 ±3.4	-4.10 ±.46	1.92 ±.53	8.9	20.7
4	0.37	1179	37.2 ±2.2	38.0 ±2.2	-3.20 ±.31	2.60 ±.40	8.8	20.5
5	0.63	1647	28.7 ±1.9	31.3 ±2.0	-2.58 ±.27	3.52 ±.38	9.7	18.3
6	1.1	2189	21.2 ±1.4	24.4 ±1.5	-1.79 ±.21	2.73 ±.29	8.7	15.1
7	1.7	2645	12.7 ±1.0	15.4 ±1.0	-.69 ±.15	1.83 ±.22	7.3	12.2
8	2.5	2931	7.5 ±0.7	9.3 ±0.7	-.14 ±.11	1.12 ±.16	5.5	9.0
9	4.2	2464	1.8 ±0.6	3.3 ±0.7	.64 ±.10	.74 ±.14	4.9	7.4
10	7.2	2374	-0.8 ±0.6	-0.2 ±0.6	1.07 ±.09	.21 ±.13	4.4	6.2
11	13	1500	-2.4 ±0.5	-2.0 ±0.6	1.20 ±.09	.04 ±.13	3.4	5.1
12	21	735	-3.2 ±0.6	-2.8 ±0.6	1.19 ±.10	.0	2.9	4.2
			1 horiz	1 vert	I_{MM}	s		
			Corresponding parameters					

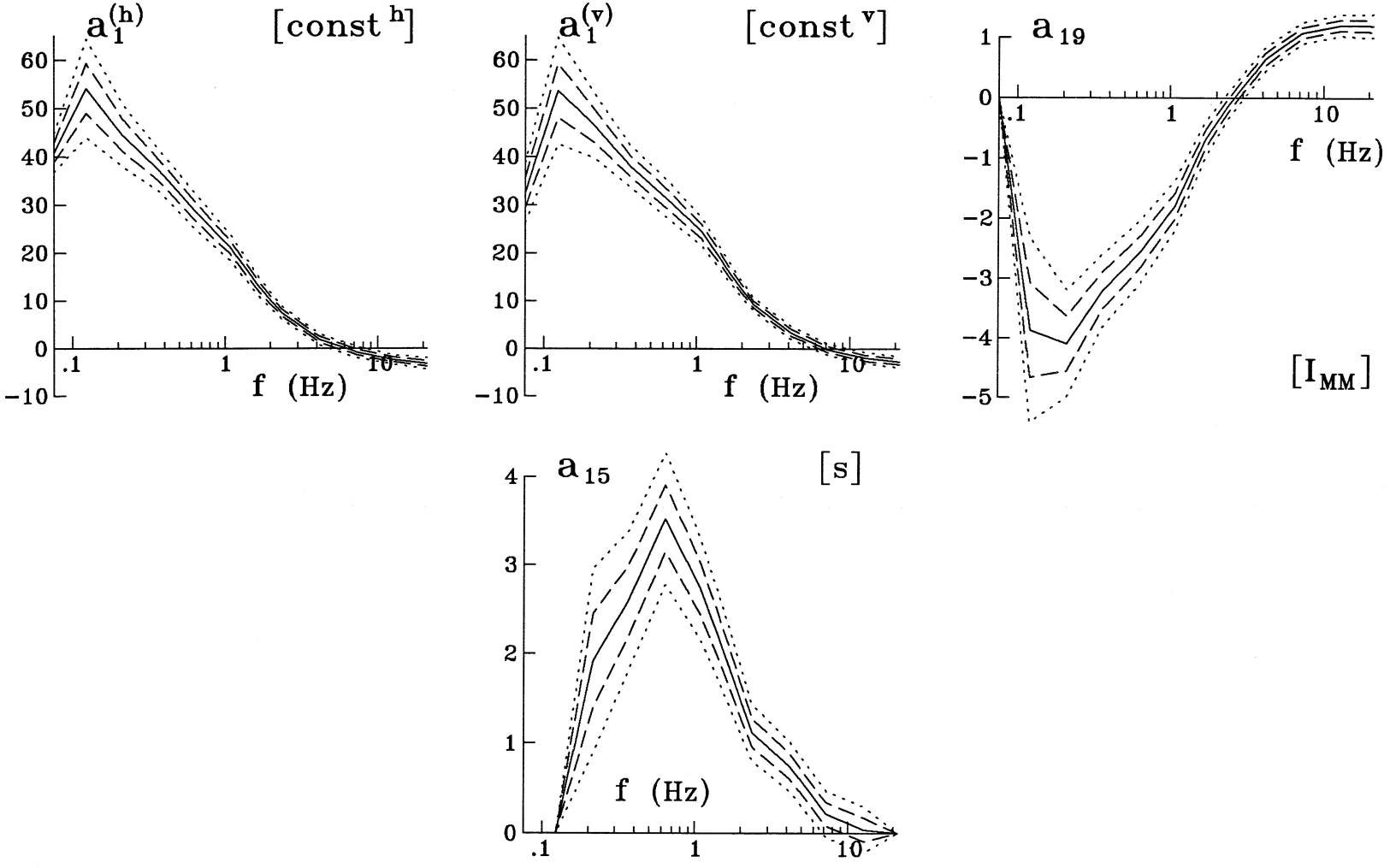

Fig. 3.5 The coefficients $a_i(f)$ in the model in Eq. (3.5), plotted versus the central frequency of the channels (solid lines). The coefficients are bounded by their "σ-intervals" (dashed lines) and by their estimated 95% confidence intervals (dotted lines).

We now turn to the second model which includes the influence of the geological conditions at the recording site on the duration of strong ground motion. The "basic" model in this case is the model in Eq. (3.3). The preliminary analysis showed that the representation of the site-specific term in the form $a_{13}(f)\cdot S^{(1)} + a_{14}(f)\cdot S^{(0)}$ causes instability of the inversion. So, we considered then the geological parameter s as a "regular" quantitative variable. The corresponding model equation is, then:

$$\left\{ \begin{array}{c} dur^{(h)}(f) \\ dur^{(v)}(f) \end{array} \right\} = \max \left[\left(\left\{ \begin{array}{c} a_1^{(h)}(f) \\ a_1^{(v)}(f) \end{array} \right\} + a_{19}(f)\cdot I_{MM} \right), 1 \right] + a_{15}(f)\cdot(2-s). \qquad (3.5)$$

We use here the term $a_{15}(f)\cdot(2-s)$ instead of $a_{15}(f)\cdot s$ because we want the coefficient $a_{15}(f)$ to be positive if the duration on sediments ($s = 0$) and on intermediate sites ($s = 1$) is longer than the duration on basement rock sites ($s = 2$). The results of the analysis of this model are given in Table 3.4 and Fig. 3.5. All the results agree with the previously discussed models. The first three coefficients are very similar to those for the model in Eq. (3.3), and

$$a_{15}(f) \approx 0.5\cdot\{a_{13}(f) + 0.5\cdot a_{14}(f)\}$$

where $a_{13}(f)$ and $a_{14}(f)$ are taken from the model in Eq. (3.4). The last relationship is what might be expected when the effect of the geology is described in two different ways; one way accounts for the qualitative nature of the parameter s (and gives the coefficients a_{13} and a_{14}), and the other one treats the parameter s as any other quantitative parameter.

III.3 Models $dur(I_{MM}, \Delta', I_{MM}\Delta', s, s_L)$ and $dur = dur(I_{MM}, s, s_L)$

We next consider the influence of the local soil conditions at the recording site. This influence was not considered before in the regression models of the duration of strong ground motion with the Modified Mercalli intensity as the main scaling parameter. Recall that $s_L = 2$ for deep soil sites, $s_L = 1$ for stiff soil sites and $s_L = 0$ for local "rock" sites. The attempt to use the "prolongation" term τ_{rs} in the form suggested by Eqs. (2.8) and (2.10), i.e.

$$\tau_{rs} = a_{11}(f)\cdot S_L^{(1)} + a_{12}(f)\cdot S_L^{(2)} + a_{13}(f)\cdot S^{(1)} + a_{14}(f)\cdot S^{(0)},$$

where $S^{(1)}$, $S^{(0)}$, $S_L^{(1)}$ and $S_L^{(2)}$ are defined by Eqs. (2.8) and (2.10), fails due to instability of the regression. So, we use the model with simplified $\tau_{rs}^{(s)}$ part:

$$\left\{ \begin{array}{c} dur^{(h)}(f) \\ dur^{(v)}(f) \end{array} \right\} = \max \left[\left(\left\{ \begin{array}{c} a_1^{(h)(f)} \\ a_1^{(v)}(f) \end{array} \right\} + a_{19}(f)\cdot I_{MM} + a_4(f)\cdot\Delta' + a_{20}(f)\cdot I_{MM}\Delta' \right), 1 \right]$$

$$+ a_{15}(f)\cdot(2-s) + a_{11}(f)\cdot S_L^{(1)} + a_{12}(f)\cdot S_L^{(2)}, \qquad (3.6a)$$

where the hypocentral distance Δ' is measured in kilometers and

$$S_L^{(1)} = \begin{cases} 1, & \text{if } s_L = 1, \\ 0, & \text{if } s_L \neq 1, \end{cases}$$
$$S_L^{(2)} = \begin{cases} 1, & \text{if } s_L = 2, \\ 0, & \text{if } s_L \neq 2. \end{cases} \qquad (3.6b)$$

All the terms which include s or s_L were chosen in such a way, that the corresponding coefficients, coming out positive as a result of the regression analysis, would show prolongation of the duration on sedimentary and soft soil sites, compared to the basement rock locations or soil "rock" sites.

The results of the analysis of the model in Eq. (3.6) are shown in Table 3.5 and Fig. 3.6. The coefficients $a_1(f)$, $a_{19}(f)$, $a_4(f)$, $a_{20}(f)$ and $a_{15}(f)$ have functional forms similar to those found in the previous models. The new coefficients, $a_{11}(f)$ and $a_{12}(f)$, can be compared with their counterparts in the model which accounts for the geological and local soil conditions and has the magnitude of the earthquake as the "master" parameter of the model (Novikova and Trifunac, 1993). The behavior of $a_{11}(f)$ and $a_{12}(f)$ in the current model and in this "magnitude" model are remarkably similar, and the additional duration (in both models) at the soft soil sites (compared with "rock") is about 7 sec for frequencies about 1 Hz, and about $3.5 \div 4$ sec at stiff soil sites for frequencies $1 \div 2$ Hz. The influence of the geological parameter is more prominent at lower frequencies, with maximum contributions at channel #4 ($f_0 = 0.37$ Hz). The difference in the range of frequencies where the influence of the geological and the local soil conditions is noticeable might come from the difference of the characteristic depth of the corresponding "soft" layer (up to several kilometers in the case of sediments and not more than several hundred feet in the case of local soils). Notice that the consideration of the influence of the local soil condition on the duration of the strong ground motion at the site is important. The prolongation of duration due to the presence of soft soils under the station may be more prominent at some frequencies than the prolongation due to the presence of deep sedimentary deposits.

The next model we consider is the simplified form of the previous one. Instead of Eq. (3.2), the Eq. (3.3) is taken as the "basic" model:

$$\begin{Bmatrix} dur^{(h)}(f) \\ dur^{(v)}(f) \end{Bmatrix} = \max \left[\left(\begin{Bmatrix} a_1^{(h)}(f) \\ a_1^{(v)}(f) \end{Bmatrix} + a_{19}(f) \cdot I_{MM} \right), 1 \right] + a_{15}(f) \cdot (2 - s) + a_{16}(f) \cdot s_L. \qquad (3.7)$$

The results of the regression analysis of this model are presented in Table 3.6 and Fig.3.7. This "rough" model is hardly able to detect the influence of the local soil conditions on the duration of strong ground motion, although the previous model in Eq. (3.6) allows one to detect this influence.

Table 3.5 Results of the regression analysis of the model in Eq. (3.6).

Channel number	f_0 (Hz)	# of data points N(f)	Coefficients a_i and their accuracy ("σ-interval")								σ_{dur} (sec)	dur_{av} (sec)
			$a_1^{(h)}$ $\pm\sigma_1^{(h)}$	$a_1^{(h)}$ $\pm\sigma_1^{(h)}$	a_{19} $\pm\sigma_{19}$	a_4 $\pm\sigma_4$	a_{20} $\pm\sigma_{20}$	a_{15} $\pm\sigma_{15}$	a_{11} $\pm\sigma_{11}$	a_{12} $\pm\sigma_{12}$		
1	0.075	37	40.8 ±2.0	32.5 ±3.1	.0	.0	.0	.0	.0	.0	10.2	38.3
2	0.12	311	27.7 ±5.4	28.2 ±5.7	-1.30 ±.75	.182 ±.019	.0	.0	.0	.0	10.1	28.3
3	0.21	850	27.5 ±3.2	29.3 ±3.2	-2.58 ±.42	.194 ±.013	.0	.95 ±.48	.0	.0	8.0	20.7
4	0.37	1179	19.3 ±3.0	19.5 ±3.0	-1.47 ±.43	.090 ±.043	.016 ±.007	1.81 ±.35	.0	.0	7.7	20.5
5	0.63	1139	15.1 ±3.1	17.5 ±3.2	-1.73 ±.46	.059 ±.040	.027 ±.007	1.29 ±.53	1.99 ±.89	4.42 ±1.01	7.7	19.0
6	1.1	1376	12.1 ±2.5	15.1 ±2.6	-1.51 ±.38	.075 ±.032	.019 ±.006	.23 ±.42	3.80 ±.70	7.22 ±.80	7.0	16.7
7	1.7	1550	8.0 ±1.9	10.4 ±1.9	-.97 ±.29	.048 ±.025	.020 ±.004	.0	3.78 ±.44	5.47 ±.42	5.6	14.1
8	2.5	1574	5.8 ±1.4	7.4 ±1.4	-.65 ±.21	-.008 ±.019	.023 ±.003	.0	2.40 ±.33	3.45 ±.31	4.2	10.5
9	4.2	1159	1.2 ±1.4	2.5 ±1.4	.04 ±.22	.005 ±.021	.022 ±.004	.0	2.02 ±.32	2.36 ±.30	3.7	9.3
10	7.2	1093	2.2 ±1.3	2.8 ±1.3	.04 ±.20	-.056 ±.022	.029 ±.004	.0	.92 ±.29	.74 ±.27	3.2	8.3
11	13	628	-2.5 ±1.8	-2.6 ±1.8	.80 ±.27	.025 ±.045	.015 ±.007	.0	.27 ±.31	0.92 ±.29	2.7	7.1
12	21	284	-4.7 ±1.5	-4.7 ±1.5	1.02 ±.21	.034 ±.010	.0	.0	.0	0.96 ±.30	2.5	6.3
			1 horiz	1 vert	I_{MM}	Δ'	$I_{MM}\Delta'$	s	$S_L^{(1)}$	$S_L^{(2)}$		
			Corresponding parameters									

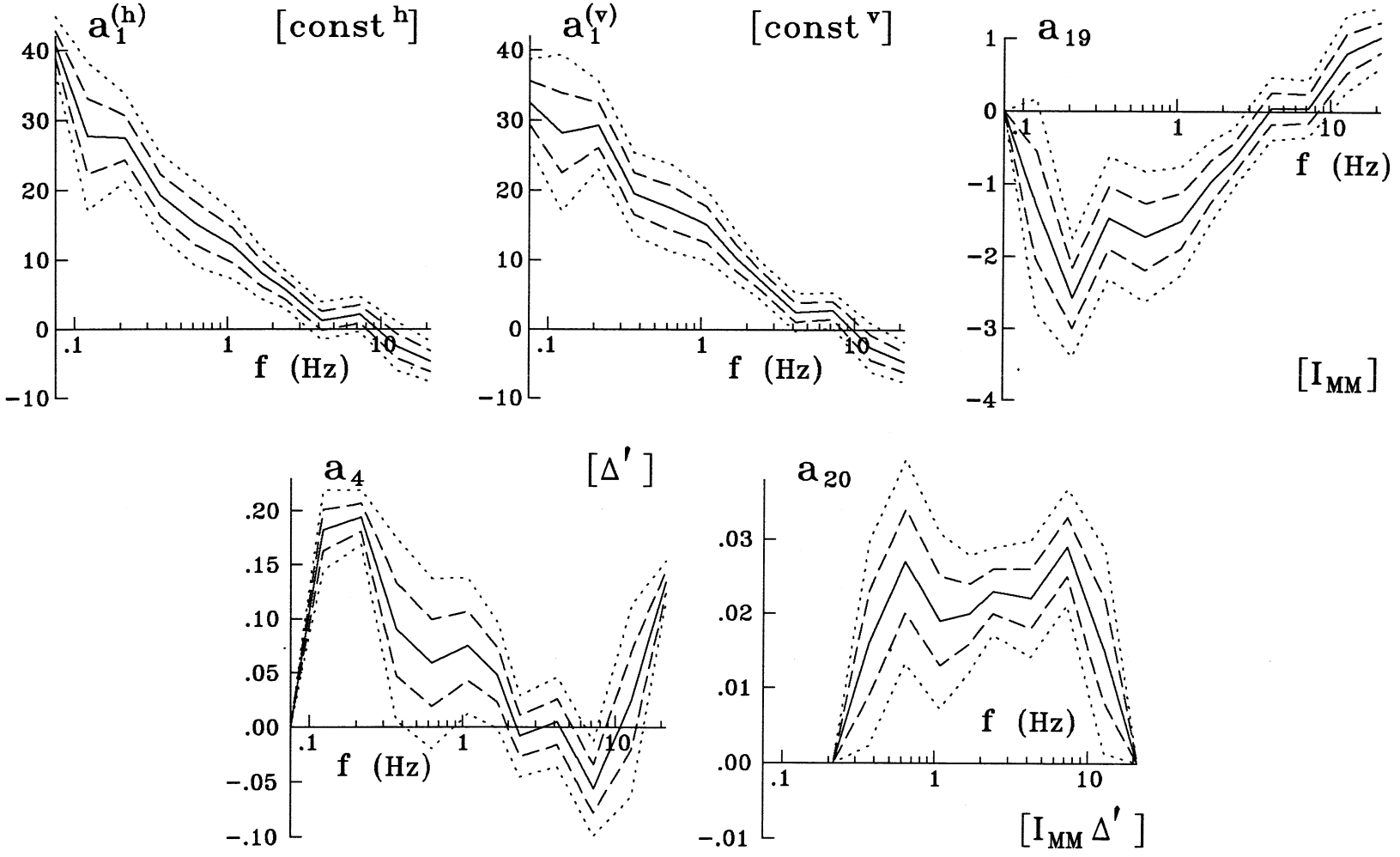

Fig. 3.6a The coefficients $a_1(f)$, $a_{19}(f)$, $a_4(f)$ and $a_{20}(f)$ in the model in Eq. (3.6), plotted versus the central frequency of the channels (solid lines). The coefficients are bounded by their "σ-intervals" (dashed lines) and by their estimated 95% confidence intervals (dotted lines).

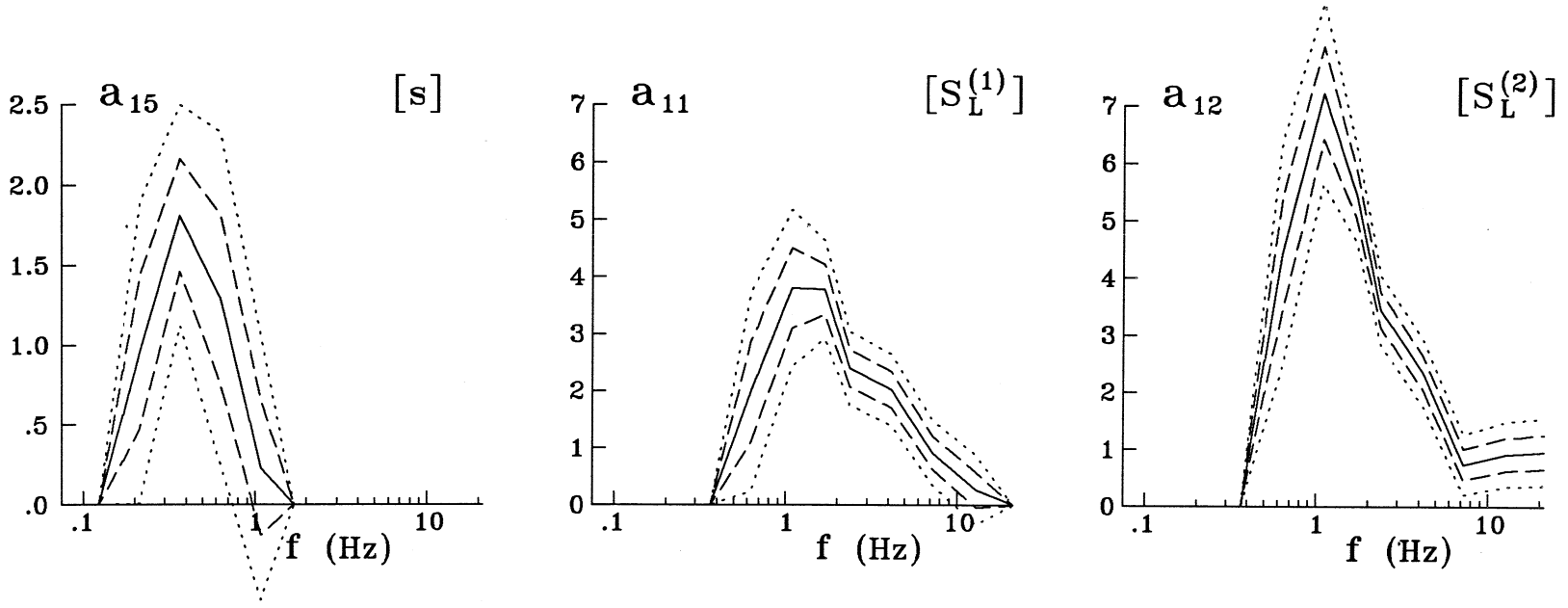

Fig. 3.6b The coefficients $a_{15}(f)$, $a_{11}(f)$ and $a_{12}(f)$ in the model in Eq. (3.6), plotted versus the central frequency of the channels (solid lines). The coefficients are bounded by their "σ-intervals" (dashed lines) and by their estimated 95% confidence intervals (dotted lines).

Table 3.6 Results of the regression analysis of the model in Eq. (3.7).

Channel number	f_0 (Hz)	# of data points N(f)	Coefficients a_i and their accuracy ("σ-interval")					σ_{dur} (sec)	dur_{av} (sec)
			$a_1^{(h)}$ $\pm\sigma_1^{(h)}$	$a_1^{(h)}$ $\pm\sigma_1^{(h)}$	a_{19} $\pm\sigma_{19}$	a_{15} $\pm\sigma_{15}$	a_{13} $\pm\sigma_{13}$		
1	0.075	37	40.8 ±2.0	32.5 ±3.1	.0	.0	.0	10.2	38.3
2	0.12	311	54.1 ±5.2	53.6 ±5.6	-3.88 ±.79	.0	.0	11.5	28.3
3	0.21	850	44.4 ±3.6	46.3 ±3.6	-4.10 ±.49	1.92 ±.57	.0	9.6	20.7
4	0.37	1179	37.2 ±2.5	38.0 ±2.5	-3.20 ±.35	2.60 ±.45	.0	9.9	20.5
5	0.63	1647	28.7 ±1.9	31.3 ±2.0	-2.58 ±.27	3.52 ±.38	.0	9.7	18.3
6	1.1	1376	28.7 ±1.8	31.8 ±1.9	-2.96 ±.27	3.17 ±.46	.84 ±.42	8.4	16.7
7	1.7	1550	24.3 ±1.4	26.5 ±1.4	-2.06 ±.21	.0	1.66 ±.26	7.3	14.1
8	2.5	1574	15.5 ±1.0	17.0 ±1.1	-1.07 ±.16	.0	.96 ±.19	5.5	10.5
9	4.2	1159	10.5 ±1.2	11.9 ±1.2	-.35 ±.18	.0	.43 ±.20	5.2	9.3
10	7.2	2576	-0.3 ±0.5	0.5 ±0.6	1.06 ±.09	.0	.0	4.5	6.4
11	13	1584	-2.5 ±0.5	-2.0 ±0.5	1.22 ±.08	.0	.0	3.5	5.1
12	21	735	-3.2 ±0.6	-2.8 ±0.6	1.19 ±.10	.0	.0	2.9	4.2
			1 horiz	1 vert	I_{MM}	s	s_L		
			Corresponding parameters						

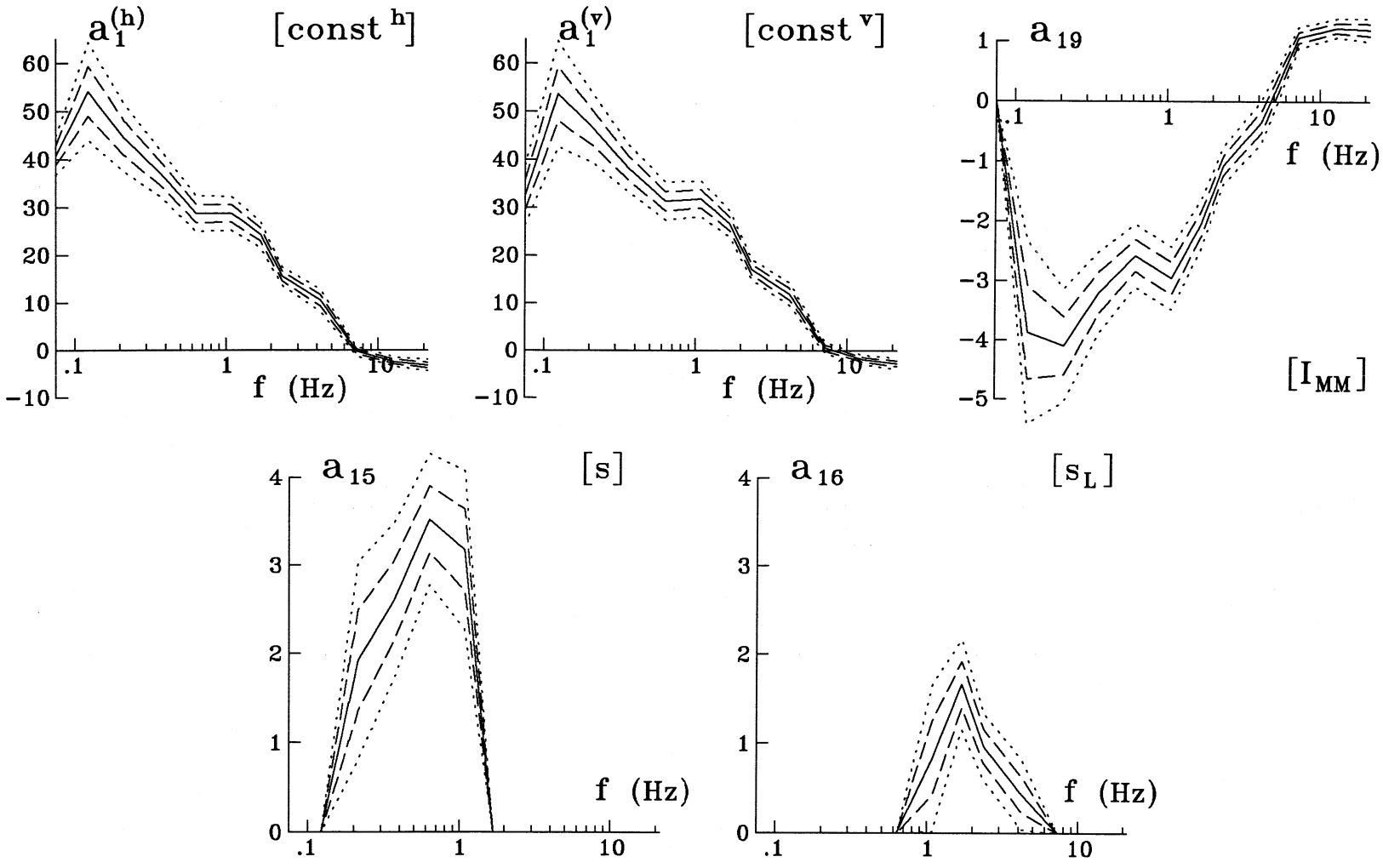

Fig. 3.7 The coefficients $a_i(f)$ in the model in Eq. (3.7), plotted versus the central frequency of the channels (solid lines). The coefficients are bounded by their "σ-intervals" (dashed lines) and by their estimated 95% confidence intervals (dotted lines).

III.4 Models $dur = dur(I_{MM}, \Delta', I_{MM}\Delta', h, R, hR, R^2, h^2, \varphi)$ and $dur = dur(I_{MM}, h, R, hR, R^2, h^2\varphi)$

We turn now to the models which utilize the detailed description of the recording site conditions trough (a) the depth of sediments under the recording site, h; (b) the distance, R, to the rocks that can reflect towards the station the waves coming from the source; and (c) the angle subtended at the station by the surface of the rocks capable of producing effective reflections. First, we consider the most "complete" model, with the "prolongation" term as in Eq. (2.5) and the "basic duration" as in the model in Eq. (3.2):

$$\left\{ \begin{array}{l} dur^{(h)}(f) \\ dur^{(v)}(f) \end{array} \right\} = \max \left[\left(\left\{ \begin{array}{l} a_1^{(h)}(f) \\ a_1^{(v)}(f) \end{array} \right\} + a_{19}(f) \cdot I_{MM} + a_4(f) \cdot \Delta' + a_{20}(f) \cdot I_{MM}\Delta' \right), 1 \right]$$

$$+ \left\{ \begin{array}{l} \left[a_5^{(h)}(f) \cdot h + a_6^{(h)}(f) \cdot R + a_7^{(h)}(f) \cdot hR + a_8^{(h)}(f) \cdot R^2 + a_9^{(h)}(f) \cdot h^2 + a_{10}^{(h)}(f) \cdot \varphi \right]_+ \\ \left[a_5^{(v)}(f) \cdot h + a_6^{(v)}(f) \cdot R + a_7^{(v)}(f) \cdot hR + a_8^{(v)}(f) \cdot R^2 + a_9^{(v)}(f) \cdot h^2 + a_{10}^{(v)}(f) \cdot \varphi \right]_+ \end{array} \right\}, \tag{3.8a}$$

where all the distances are measured in kilometers and the sum of the terms involving h, R and φ and designated earlier as $\tau_{\rm rs}$, is considered only if it is positive:

$$[\tau_{\rm rs}(f)]_+ = \max\{0, \tau_{\rm rs}(f)\}. \tag{3.8b}$$

The values of h, R and φ are assumed to be zero if the site is located on rock.

Eq. (3.8) was fit to the data in tree steps. The first two steps were similar to what was used in the analysis of the model in Eq. (3.2), and the subscript "+" in Eq. (3.8a) was not taken into account at these stages. During the third step, $\tau_{\rm rs}$ was estimated using the results of the second iteration, and the final set of coefficients was obtained. As before, all three sets of the coefficients—the results of the three step fitting—are very similar to each other.

The numerical results of the regression analysis are summarized in Table 3.7 and in Fig. 3.8. The set of coefficients, responsible for scaling the duration in terms of the intensity and the distance, $\{a_1(f), a_{19}(f), a_4(f), a_{20}(f)\}$, is very similar to what was obtained in the model in Eq. (3.2), which did not include any geological parameters (compare Figs. 3.1 and 3.8a). The coefficients $\{a_5(f) \div a_{10}(f)\}$ are similar to their counterparts in the "magnitude model" (Novikova and Trifunac, 1993), which scaled the duration as $dur = dur(M, M^2, \Delta, h, R, hR, R^2, h^2, \varphi)$. Fig. 3.9 gives the prolongation of duration on sediments, as a function of R and h, when predicted by the model in Eq. (3.8). As in the case of "magnitude-type" "basic duration," this prolongation can be only noticed at moderate frequencies ($.5 \div 5$ Hz), where the seismic waves are not long enough to pass through the sediments without "noticing" them, and not short

Table 3.7 Results of the regression analysis of the model in Eq. (3.8).

Channel number	f_0 (Hz)	# of data points N(f)	Coefficients a_i and their accuracy ("σ-interval")																σ_{dur} (sec)	dur_{av} (sec)
			$a_1^{(h)}$ $\pm\sigma_1^{(h)}$	$a_1^{(v)}$ $\pm\sigma_1^{(v)}$	a_{19} $\pm\sigma_{19}$	a_4 $\pm\sigma_4$	a_{20} $\pm\sigma_{20}$	$a_5^{(h)}$ $\pm\sigma_5^{(h)}$	$a_6^{(h)}$ $\pm\sigma_6^{(h)}$	$a_7^{(h)}$ $\pm\sigma_7^{(h)}$	$a_8^{(h)}$ $\pm\sigma_8^{(h)}$	$a_9^{(h)}$ $\pm\sigma_9^{(h)}$	$a_{10}^{(h)}$ $\pm\sigma_{10}^{(h)}$	$a_5^{(v)}$ $\pm\sigma_5^{(v)}$	$a_6^{(v)}$ $\pm\sigma_6^{(v)}$	$a_7^{(v)}$ $\pm\sigma_7^{(v)}$	$a_8^{(v)}$ $\pm\sigma_8^{(v)}$	$a_9^{(v)}$ $\pm\sigma_9^{(v)}$	$a_{10}^{(v)}$ $\pm\sigma_{10}^{(v)}$		
1	0.075	37	40.8 ±2.0	32.5 ±3.1	.0	.0	.0	.0	.0	.0	.0	.0	.0	.0	.0	.0	.0	.0	.0	10.2	38.3
2	0.12	311	27.7 ±5.4	28.2 ±5.7	-1.30 ±.75	.182 ±.019	.0	.0	.0	.0	.0	.0	.0	.0	.0	.0	.0	.0	.0	10.1	28.3
3	0.21	962	33.3 ±2.7	35.3 ±2.7	-3.17 ±.37	.195 ±.012	.0	.0	.0	.0	.0	.0	.0	.0	.0	.0	.0	.0	.0	7.8	21.4
4	0.37	1364	17.1 ±2.8	17.9 ±2.9	-1.25 ±.40	.169 ±.044	.012 ±.007	.0	.0	.0	.0	.0	.0185 ±.0044	.0	.0	.0	.0	.0	.0162 ±.0072	7.1	20.7
5	0.63	1182	14.8 ±4.1	18.5 ±4.3	-1.89 ±.63	.215 ±.067	.013 ±.011	.0	.343 ±.056	.0265 ±.0110	-.0055 ±.0008	-.32 ±.08	.0282 ±.0062	1.49 ±1.14	.101 ±.107	.0657 ±.0186	-.0037 ±.0016	-.75 ±.17	.0265 ±.0105	7.6	19.4
6	1.1	1472	6.0 ±3.2	9.5 ±3.3	-1.06 ±.52	.156 ±.069	.018 ±.011	.84 ±.56	.351 ±.053	.0213 ±.0096	-.0061 ±.0008	-.35 ±.09	.0360 ±.0047	1.16 ±.81	.107 ±.076	.0520 ±.0159	-.0032 ±.0012	-.54 ±.14	.0310 ±.0074	6.4	15.7
7	1.7	1879	7.2 ±1.5	10.4 ±1.7	-.83 ±.26	.010 ±.023	.027 ±.004	1.53 ±.41	.181 ±.039	.0233 ±.0068	-.0037 ±.0006	-.41 ±.07	.0139 ±.0032	2.41 ±.60	.042 ±.056	.0246 ±.0106	-.0016 ±.0008	-.51 ±.10	.0	5.4	13.4
8	2.5	2053	6.7 ±1.0	8.1 ±1.1	-.81 ±.17	-.037 ±.016	.028 ±.003	.0	.146 ±.019	.0053 ±.0019	-.0022 ±.0003	.0	.0105 ±.0021	1.99 ±.40	.075 ±.037	.0070 ±.0068	-.0015 ±.0006	-.32 ±.06	.0	3.8	9.8
9	4.2	2295	1.6 ±0.6	2.8 ±0.7	.05 ±.11	-.026 ±.014	.027 ±.002	.0	.074 ±.013	.0	-.0009 ±.0002	.0	.0046 ±.0015	1.30 ±.27	.0	.0	.0	-.16 ±.05	.0	3.2	7.6
10	7.2	2576	1.0 ±0.5	1.6 ±0.5	.18 ±.08	-.070 ±.012	.035 ±.002	.0	.0	.0	.0	.0	.0	.0	.0	.0	.0	.0	.0	2.8	6.4
11	13	1584	-1.1 ±0.5	-1.0 ±0.5	.46 ±.08	-.028 ±.017	.027 ±.003	.0	.0	.0	.0	.0	.0	.0	.0	.0	.0	.0	.0	2.3	5.1
12	21	735	-3.4 ±0.7	-3.3 ±0.7	.75 ±.12	.118 ±.038	.005 ±.006	.0	.0	.0	.0	.0	.0	.0	.0	.0	.0	.0	.0	2.0	4.2
			1 horiz	1 vert	I_{MM}	Δ'	$I_{MM}\Delta'$	h	R	hR	R^2	h^2	φ	h	R	hR	R^2	h^2	φ		
								horizontal component						vertical component							
			Corresponding parameters																		

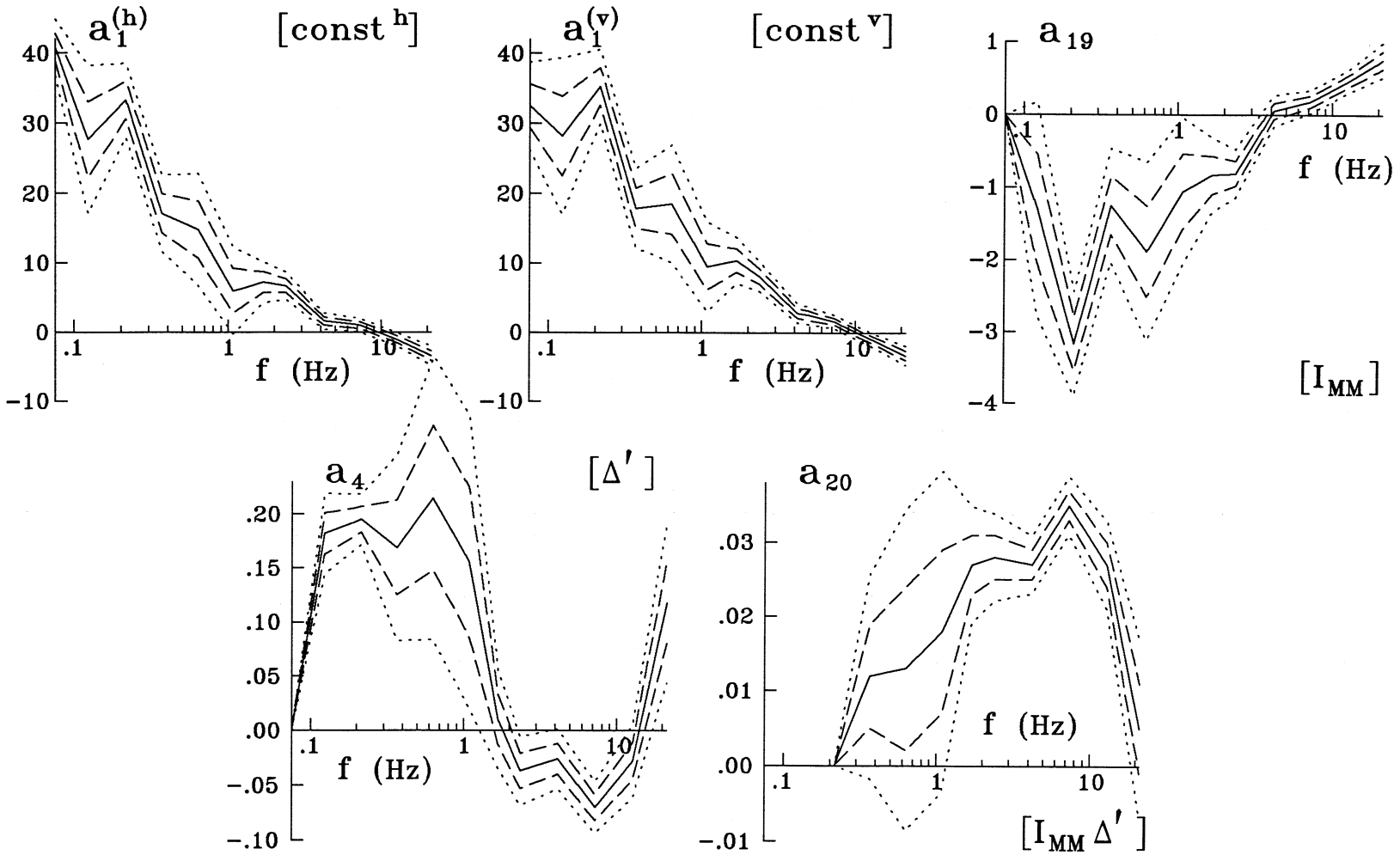

Fig. 3.8a The coefficients $a_1(f)$, $a_{19}(f)$, $a_4(f)$ and $a_{20}(f)$ in the model in Eq. (3.8), plotted versus the central frequency of the channels (solid lines). The coefficients are bounded by their "σ-intervals" (dashed lines) and by their estimated 95% confidence intervals (dotted lines).

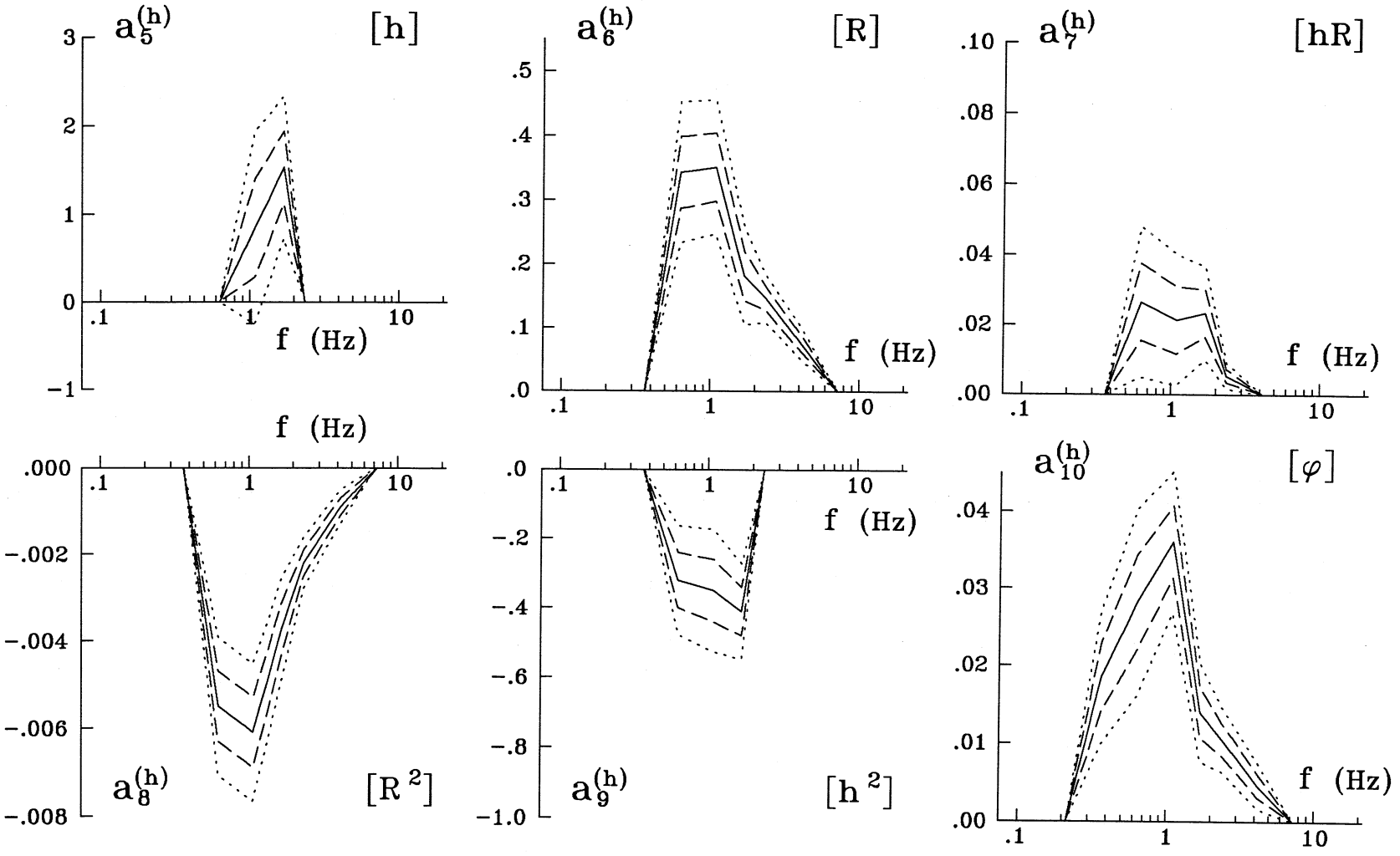

Fig. 3.8b The coefficients $a_5(f)$, $a_6(f)$, $a_7(f)$, $a_8(f)$, $a_9(f)$ and $a_{10}(f)$ for the horizontal component of motion in the model in Eq. (3.8), plotted versus the central frequency of the channels (solid lines). The coefficients are bounded by their "σ-intervals" (dashed lines) and by their estimated 95% confidence intervals (dotted lines).

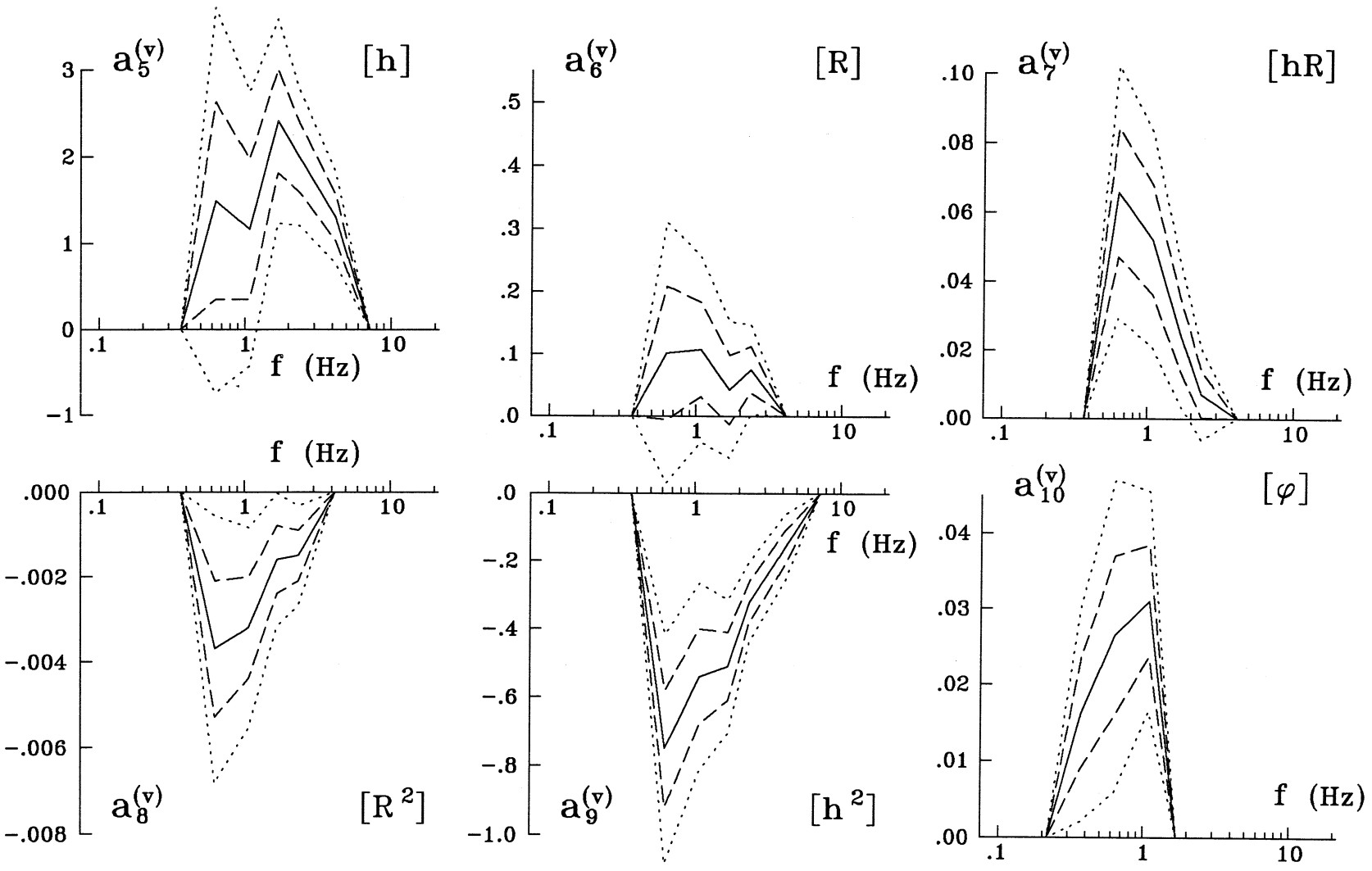

Fig. 3.8c The coefficients $a_5(f)$, $a_6(f)$, $a_7(f)$, $a_8(f)$, $a_9(f)$ and $a_{10}(f)$ for the vertical component of motion in the model in Eq. (3.8), plotted versus the central frequency of the channels (solid lines). The coefficients are bounded by their "σ-intervals" (dashed lines) and by their estimated 95% confidence intervals (dotted lines).

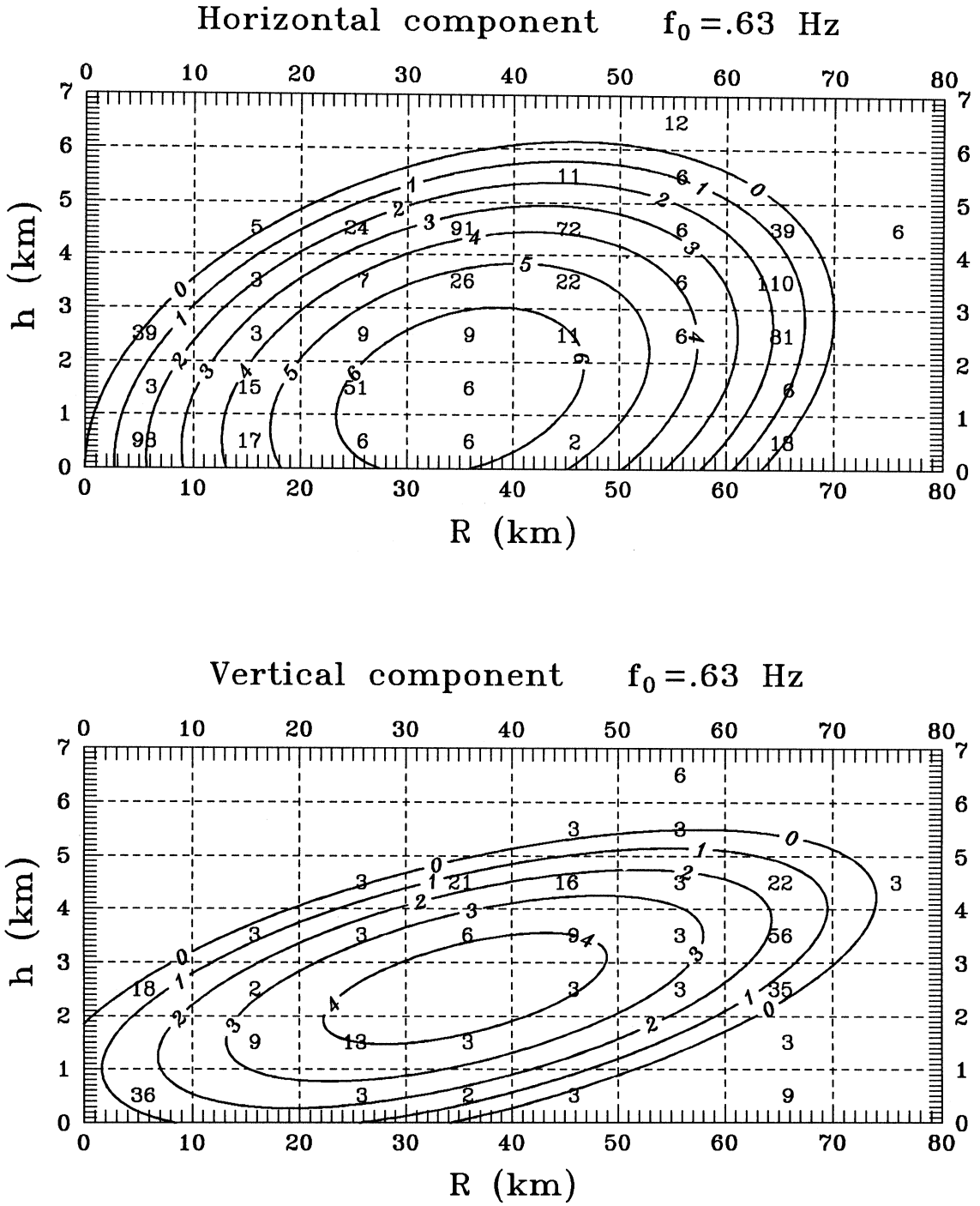

Fig. 3.9a Channel #5: isolines of the additional (relative to the basement rock sites) duration (in seconds) of strong ground motion due to the specific geometry of the sedimentary basin, as predicted by the model in Eq. (3.8). Only the positive contribution of the terms $a_5 \cdot h + a_6 \cdot R + a_7 \cdot hR + a_8 \cdot R^2 + a_9 \cdot h^2 + a_{10}$ is considered. The numbers in the dashed "boxes" designate the number of the data points used in the analysis for the particular range of R and h.

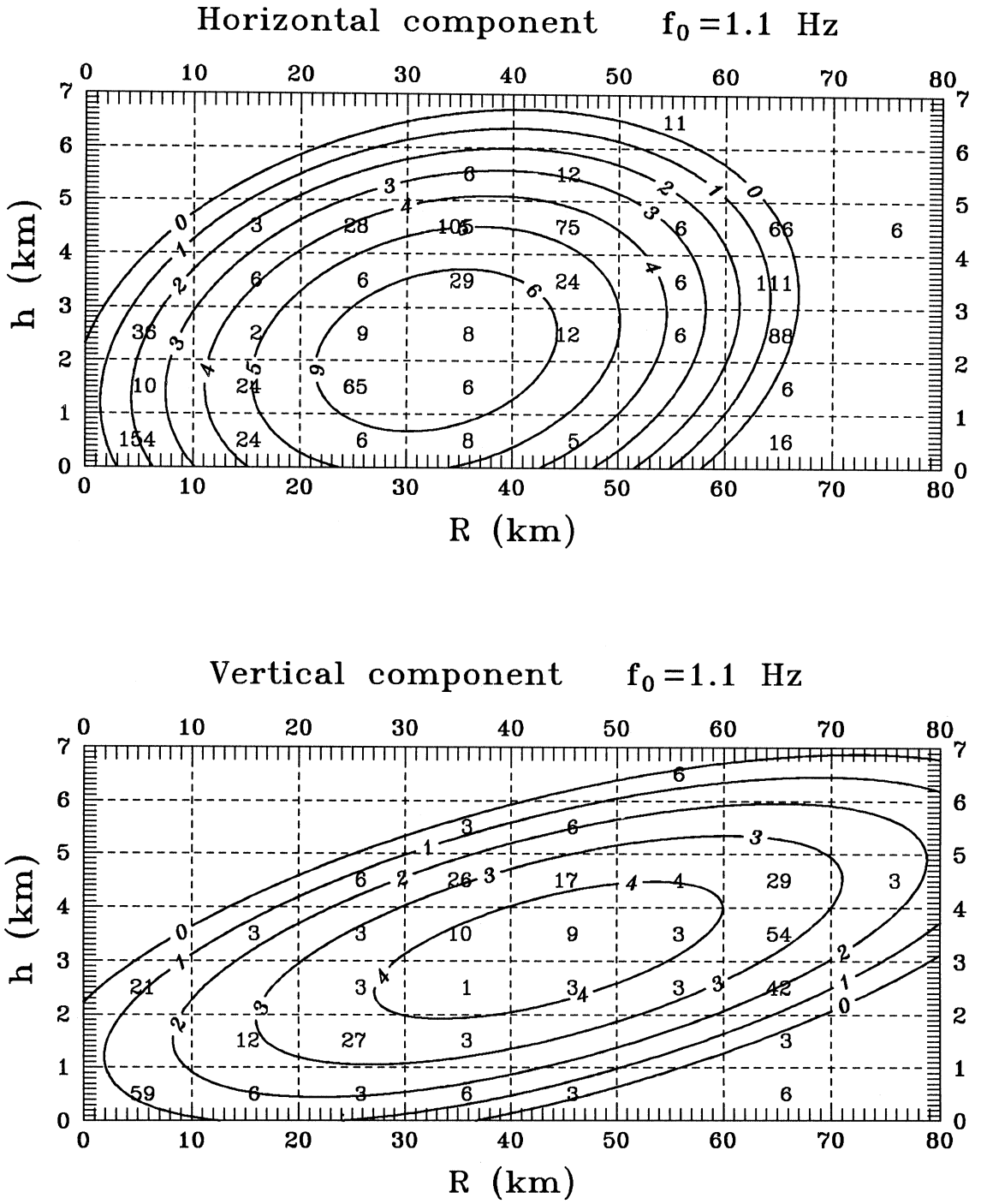

Fig. 3.9b Channel #6: isolines of the additional (relative to the basement rock sites) duration (in seconds) of strong ground motion due to the specific geometry of the sedimentary basin, as predicted by the model in Eq. (3.8). Only the positive contribution of the terms $a_5 \cdot h + a_6 \cdot R + a_7 \cdot hR + a_8 \cdot R^2 + a_9 \cdot h^2 + a_{10}$ is considered. The numbers in the dashed "boxes" designate the number of the data points used in the analysis for the particular range of R and h.

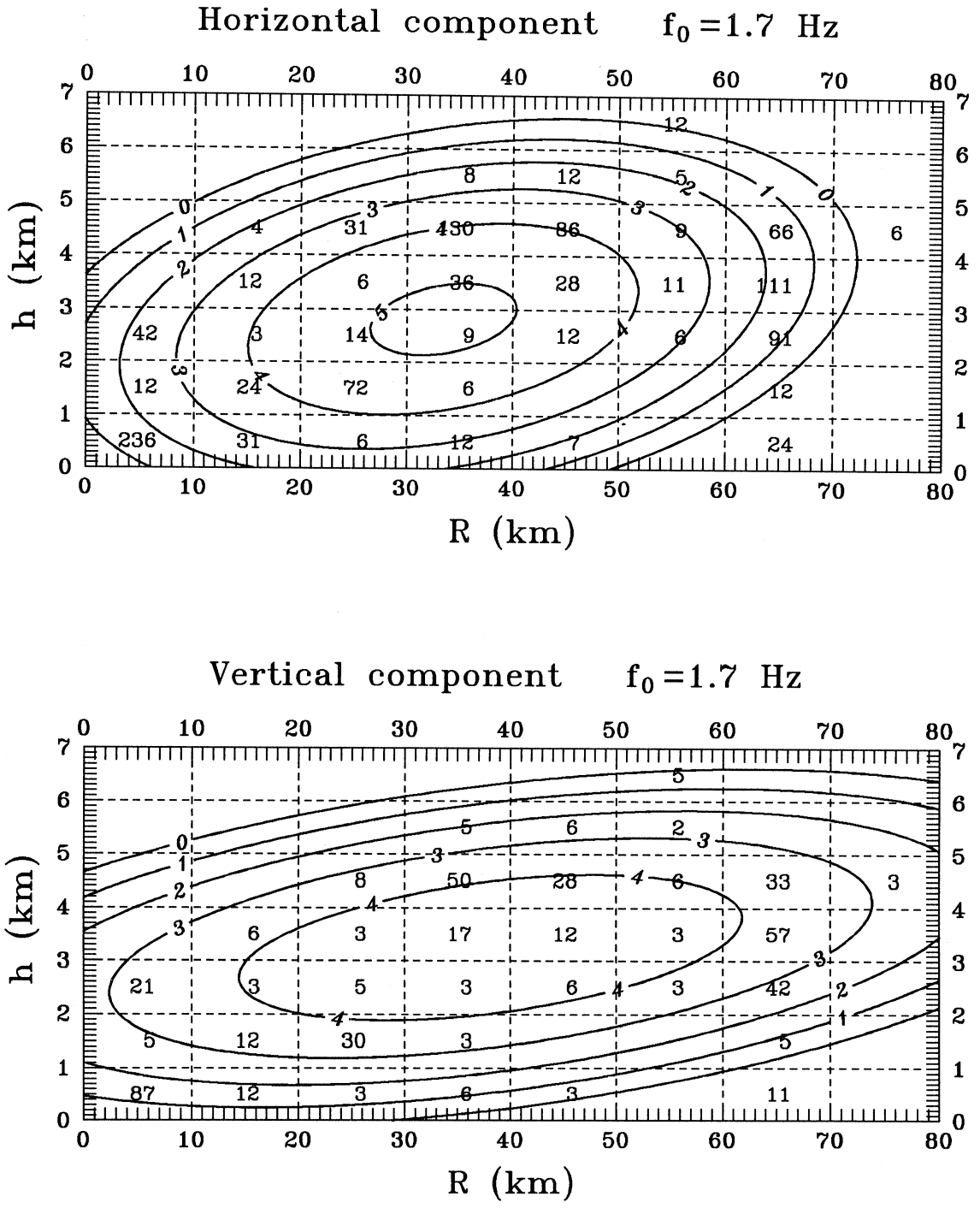

Fig. 3.9c Channel #7: isolines of the additional (relative to the basement rock sites) duration (in seconds) of strong ground motion due to the specific geometry of the sedimentary basin, as predicted by the model in Eq. (3.8). Only the positive contribution of the terms $a_5 \cdot h + a_6 \cdot R + a_7 \cdot hR + a_8 \cdot R^2 + a_9 \cdot h^2 + a_{10}$ is considered. The numbers in the dashed "boxes" designate the number of the data points used in the analysis for the particular range of R and h.

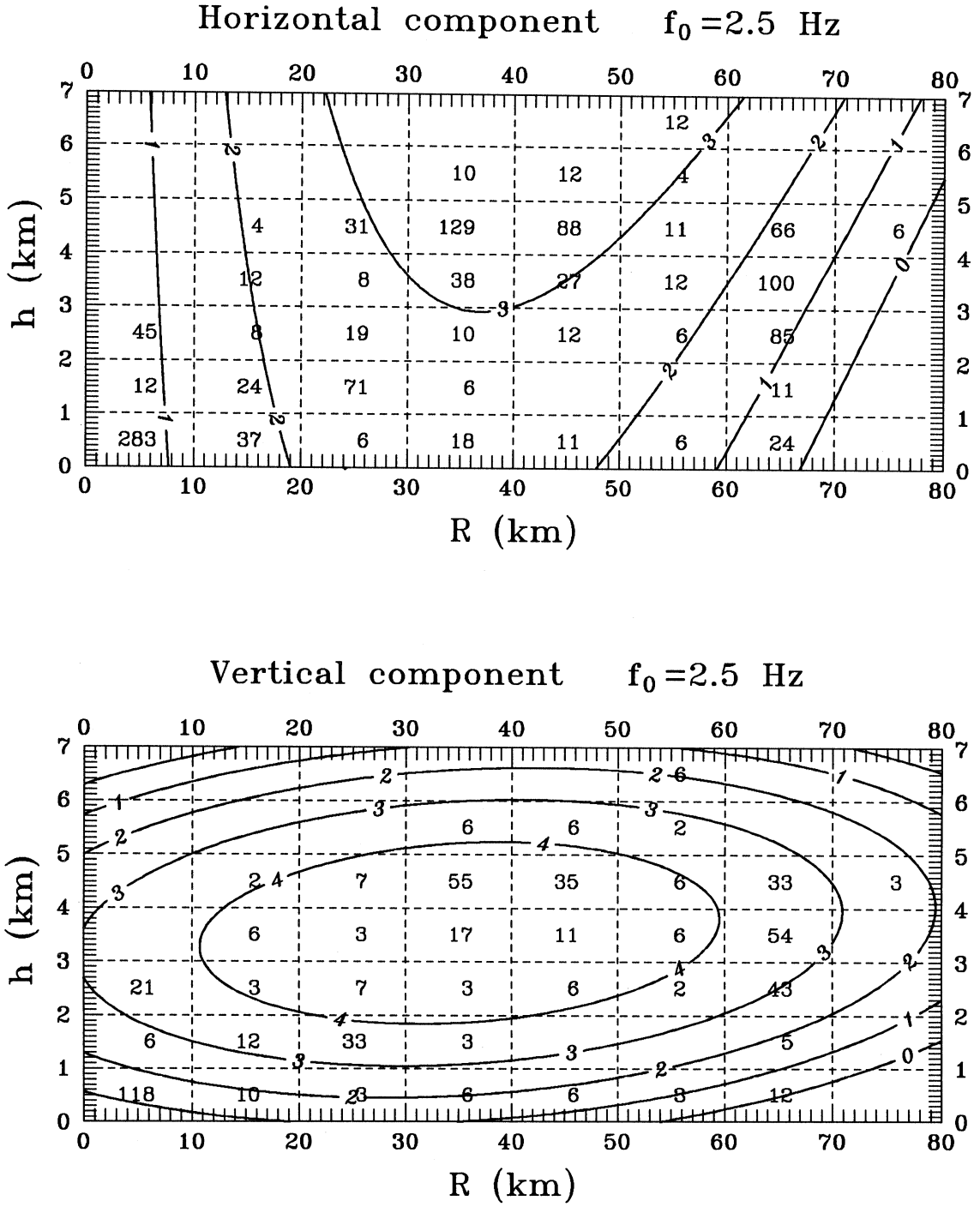

Fig. 3.9d Channel #8: isolines of the additional (relative to the basement rock sites) duration (in seconds) of strong ground motion due to the specific geometry of the sedimentary basin, as predicted by the model in Eq. (3.8). Only the positive contribution of the terms $a_5 \cdot h + a_6 \cdot R + a_7 \cdot hR + a_8 \cdot R^2 + a_9 \cdot h^2 + a_{10}$ is considered. The numbers in the dashed "boxes" designate the number of the data points used in the analysis for the particular range of R and h.

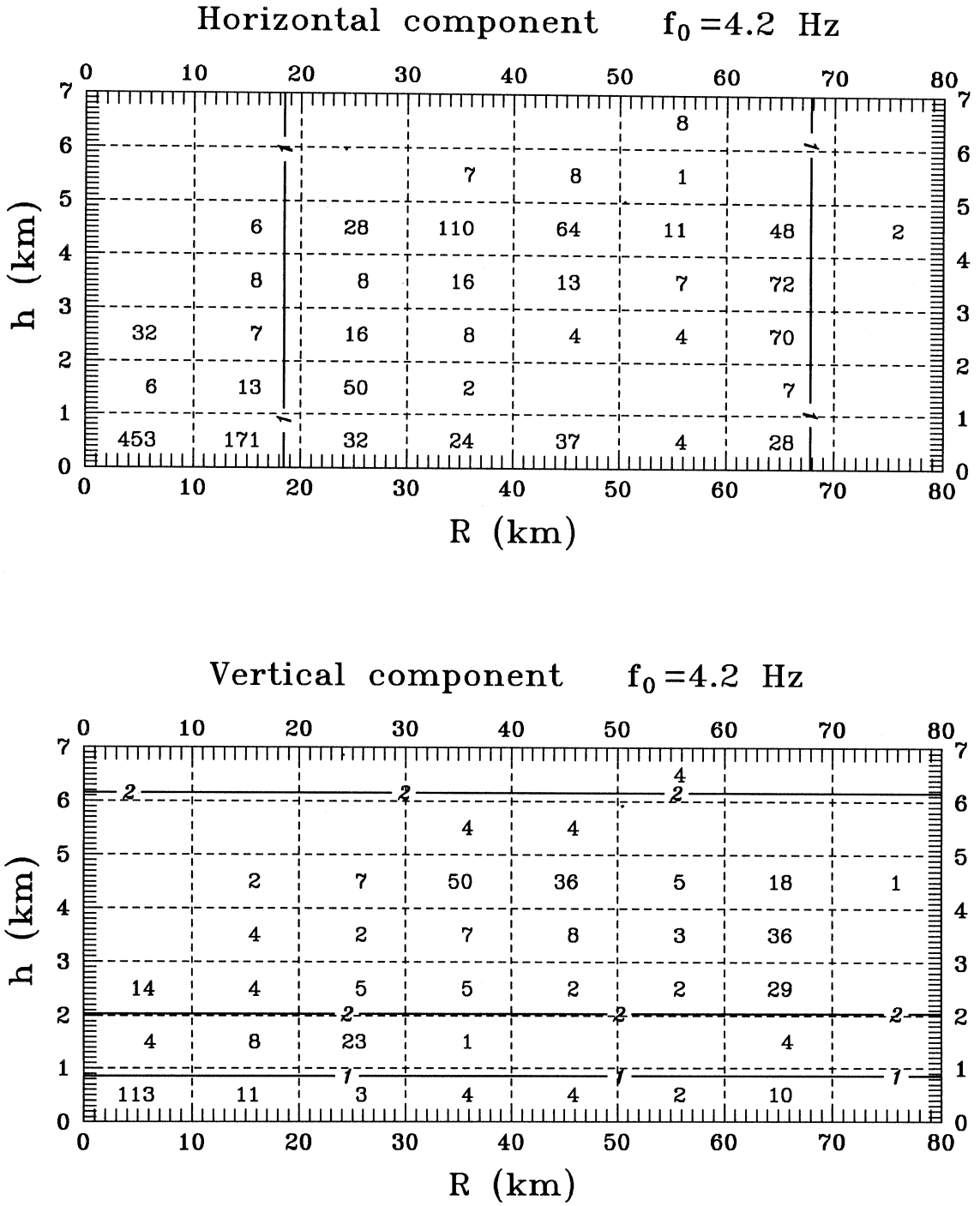

Fig. 3.9e Channel #9: isolines of the additional (relative to the basement rock sites) duration (in seconds) of strong ground motion due to the specific geometry of the sedimentary basin, as predicted by the model in Eq. (3.8). Only the positive contribution of the terms $a_5 \cdot h + a_6 \cdot R + a_7 \cdot hR + a_8 \cdot R^2 + a_9 \cdot h^2 + a_{10}$ is considered. The numbers in the dashed "boxes" designate the number of the data points used in the analysis for the particular range of R and h.

enough to get significantly attenuated on the way through the sediments. The maximum prolongation occurs at moderate depths ($2 \div 3$ km) and widths ($30 \div 50$ km) of sediments. The additional duration can be as much as $5 \div 6$ sec at frequencies near 1 Hz. One of the features, common for the "intensity-type" model and the "magnitude-type" model, is the higher sensitivity of the horizontal motion to the horizontal dimension of the sedimentary valley, R, and the greater influence of the depth of sediments (vertical dimension) h, on the vertical component of motion. Notice also that practically all the data points in Fig. 3.9 fall into the area where $\tau_{rs}(R,h) > 0$. Consequently, $\tau_{rs}(R,h,\varphi) = \tau_{rs}(R,h) + \{\text{contribution due to } \varphi\}$ is greater than zero for even more data points. This verifies our assumptions about how the presence of a sedimentary basin can influence the duration of strong ground motion and provides additional support for our models.

We next turn to a simplified companion of the model just discussed which does not include the source-to-station distance as a parameter:

$$\begin{Bmatrix} dur^{(h)}(f) \\ dur^{(v)}(f) \end{Bmatrix} = \max\left[\left(\begin{Bmatrix} a_1^{(h)}(f) \\ a_1^{(v)}(f) \end{Bmatrix} + a_{19}(f)\cdot I_{MM}\right), 1\right] +$$

$$+ \begin{Bmatrix} \left[a_5^{(h)}(f)\cdot h + a_6^{(h)}(f)\cdot R + a_7^{(h)}(f)\cdot hR + a_8^{(h)}(f)\cdot R^2 + a_9^{(h)}(f)\cdot h^2 + a_{10}^{(h)}(f)\cdot\varphi\right]_+ \\ \left[a_5^{(v)}(f)\cdot h + a_6^{(v)}(f)\cdot R + a_7^{(v)}(f)\cdot hR + a_8^{(v)}(f)\cdot R^2 + a_9^{(v)}(f)\cdot h^2 + a_{10}^{(v)}(f)\cdot\varphi\right]_+ \end{Bmatrix}, \tag{3.9a}$$

where all the distances are measured in kilometers, and τ_{rs} is accounted for only if it is positive:

$$[\tau_{rs}(f)]_+ = \max\{0, \tau_{rs}(f)\} \tag{3.9b}$$

As before, the values of h, R and φ are assumed to be zero if the site is located on rock. Exactly as in the case of the previous model, Eq. (3.9) was fit to the data in tree steps, results of which appear to be very similar to each other. The results of the regression analysis are given in Table 3.8 and in Fig. 3.10. Recall, that the parameter R was not "felt" that well by the vertical component of motion in the previous model. In the current equation, this parameter cannot be "detected" at all by the vertical component, and the coefficients $a_6^{(v)}(f)$ and $a_8^{(v)}(f)$ are equal to zero. In other respects, the set $\{a_5(f) \div a_{10}(f)\}$ from Eq. (3.9) is similar to the set $\{a_5(f) \div a_{10}(f)\}$ from Eq. (3.8), but the coefficients are well defined in somewhat smaller frequency range. This is what should be expected, because the removal of the distance to the source from the set of the parameters of the model leads to higher scattering of data around the model's prediction and to additional uncertainties in the calculation of the very sensitive coefficients $\{a_5(f) \div a_{10}(f)\}$. The first three coefficients, $a_1^{(h)}(f)$, $a_1^{(v)}(f)$, and $a_{19}(f)$ practically coincide with their counterparts from the model in Eq. (3.3), which scaled duration as $dur = dur(I_{MM})$.

Table 3.8 Results of the regression analysis of the model in Eq. (3.9).

Channel number	f_0 (Hz)	# of data points N(f)	Coefficients a_i and their accuracy ("σ-interval")															σ_{dur} (sec)	dur_{av} (sec)
			$a_1^{(h)}$ $\pm\sigma_1^{(h)}$	$a_1^{(v)}$ $\pm\sigma_1^{(v)}$	a_{19} $\pm\sigma_{19}$	$a_5^{(h)}$ $\pm\sigma_5^{(h)}$	$a_6^{(h)}$ $\pm\sigma_6^{(h)}$	$a_7^{(h)}$ $\pm\sigma_7^{(h)}$	$a_8^{(h)}$ $\pm\sigma_8^{(h)}$	$a_9^{(h)}$ $\pm\sigma_9^{(h)}$	$a_{10}^{(h)}$ $\pm\sigma_{10}^{(h)}$	$a_5^{(v)}$ $\pm\sigma_5^{(v)}$	$a_6^{(v)}$ $\pm\sigma_6^{(v)}$	$a_7^{(v)}$ $\pm\sigma_7^{(v)}$	$a_8^{(v)}$ $\pm\sigma_8^{(v)}$	$a_9^{(v)}$ $\pm\sigma_9^{(v)}$	$a_{10}^{(v)}$ $\pm\sigma_{10}^{(v)}$		
1	0.075	37	40.8 ±2.0	32.5 ±3.1	.0	.0	.0	.0	.0	.0	.0	.0	.0	.0	.0	.0	.0	10.2	38.3
2	0.12	311	54.1 ±5.2	53.6 ±5.6	-3.88 ±.79	.0	.0	.0	.0	.0	.0	.0	.0	.0	.0	.0	.0	11.5	28.3
3	0.21	962	52.3 ±2.7	54.2 ±2.8	-4.74 ±.40	.0	.0	.0	.0	.0	.0	.0	.0	.0	.0	.0	.0	8.7	21.4
4	0.37	1399	42.8 ±1.9	43.9 ±1.9	-3.45 ±.28	.0	.0	.0	.0	.0	.0010 ±.0051	.0	.0	.0	.0	.0	.0	8.2	20.7
5	0.63	1657	35.3 ±2.0	37.6 ±2.5	-2.94 ±.29	.0	.0	.0	.0	.0	.0163 ±.0050	1.40 ±1.18	.0	.0234 ±.0111	.0	-.48 ±.16	.0078 ±.0124	9.3	18.4
6	1.1	1472	25.3 ±2.3	30.2 ±2.5	-2.86 ±.37	1.81 ±.74	.304 ±.069	.0243 ±.0126	-.0041 ±.0010	-.63 ±.12	.0394 ±.0060	2.61 ±.91	.0	.0254 ±.0092	.0	-.59 ±.13	.0264 ±.0096	8.4	15.7
7	1.7	1879	17.9 ±1.3	23.1 ±1.5	-1.94 ±.22	1.93 ±.55	.204 ±.052	.0005 ±.0091	-.0019 ±.0008	-.41 ±.09	.0293 ±.0042	3.04 ±.66	.0	.0170 ±.0068	.0	-.61 ±.10	.0062 ±.0062	7.3	13.4
8	2.5	2836	9.9 ±0.7	11.7 ±0.8	-.76 ±.11	.0	.108 ±.017	.0	-.0006 ±.0003	.0	.0187 ±.0019	2.95 ±.42	.0	.0088 ±.0043	.0	-.48 ±.07	.0062 ±.0039	4.9	9.1
9	4.2	2567	3.7 ±0.6	5.2 ±0.6	-.39 ±.10	.0	.0	.0	.0	.0	.0158 ±.0020	.0	.0	.0	.0	.0	.0165 ±.0030	4.7	7.6
10	7.2	2576	-0.3 ±0.5	0.5 ±0.6	1.09 ±.09	.0	.0	.0	.0	.0	.0	.0	.0	.0	.0	.0	.0	4.5	6.4
11	13	1584	-2.5 ±0.5	-2.0 ±0.5	1.22 ±.08	.0	.0	.0	.0	.0	.0	.0	.0	.0	.0	.0	.0	3.5	5.1
12	21	735	-3.2 ±0.6	-2.8 ±0.6	1.19 ±.10	.0	.0	.0	.0	.0	.0	.0	.0	.0	.0	.0	.0	2.9	4.2
			1 horiz	1 vert	I_{MM}	h	R	hR	R^2	h^2	φ	h	R	hR	R^2	h^2	φ		
						horizontal component						vertical component							
			Corresponding parameters																

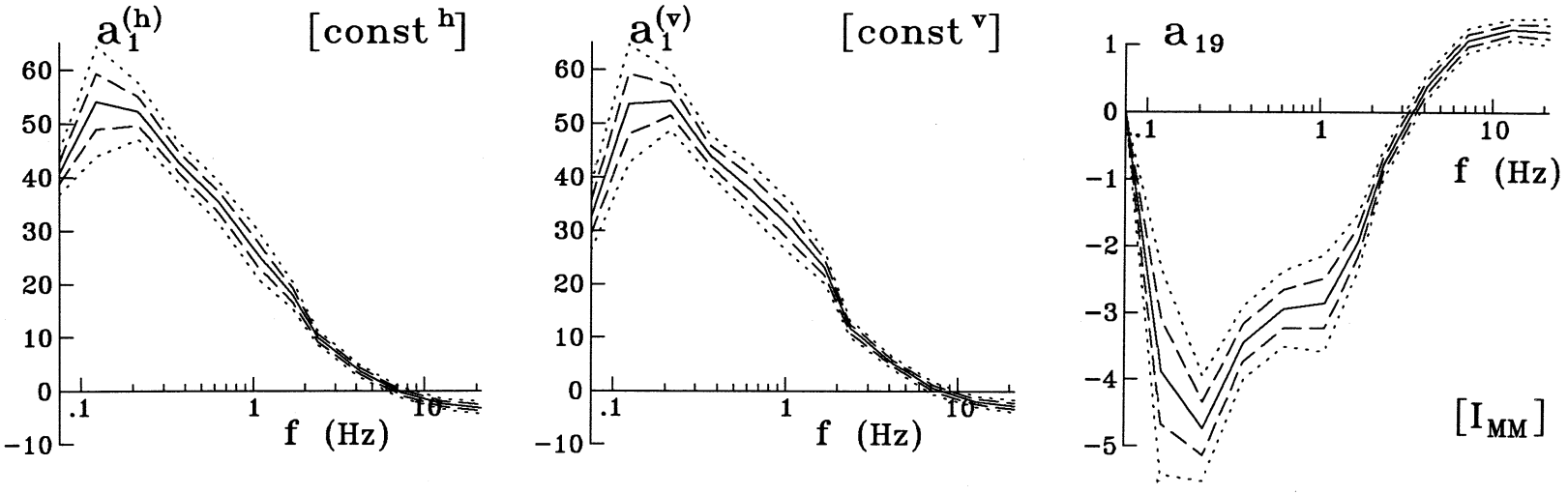

Fig. 3.10a The coefficients $a_1(f)$ and $a_{19}(f)$ in the model in Eq. (3.9), plotted versus the central frequency of the channels (solid lines). The coefficients are bounded by their "σ-intervals" (dashed lines) and by their estimated 95% confidence intervals (dotted lines).

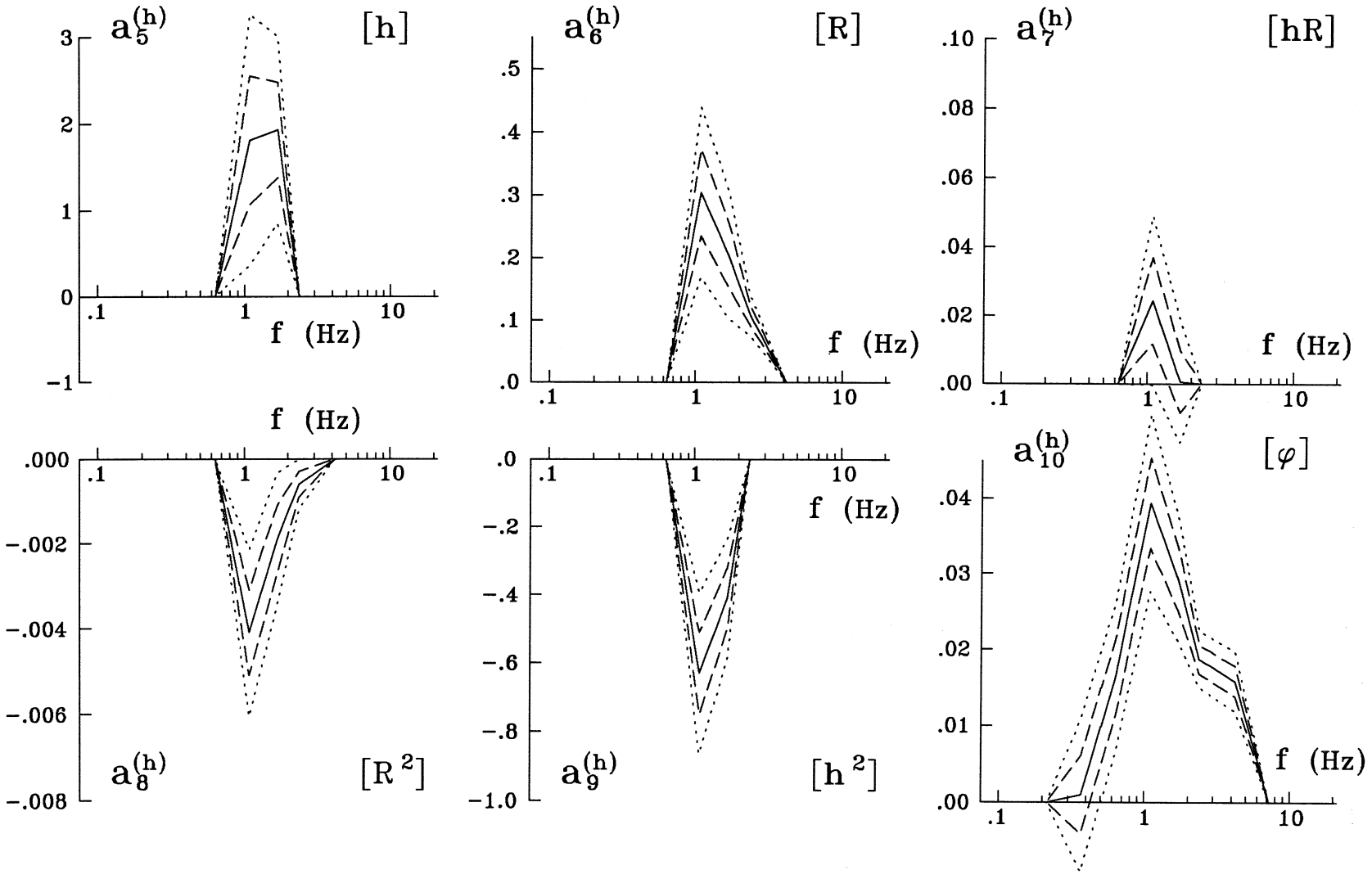

Fig. 3.10b The coefficients $a_5(f)$, $a_6(f)$, $a_7(f)$, $a_8(f)$, $a_9(f)$ and $a_{10}(f)$ for the horizontal component of motion in the model in Eq. (3.9), plotted versus the central frequency of the channels (solid lines). The coefficients are bounded by their "σ-intervals" (dashed lines) and by their estimated 95% confidence intervals (dotted lines).

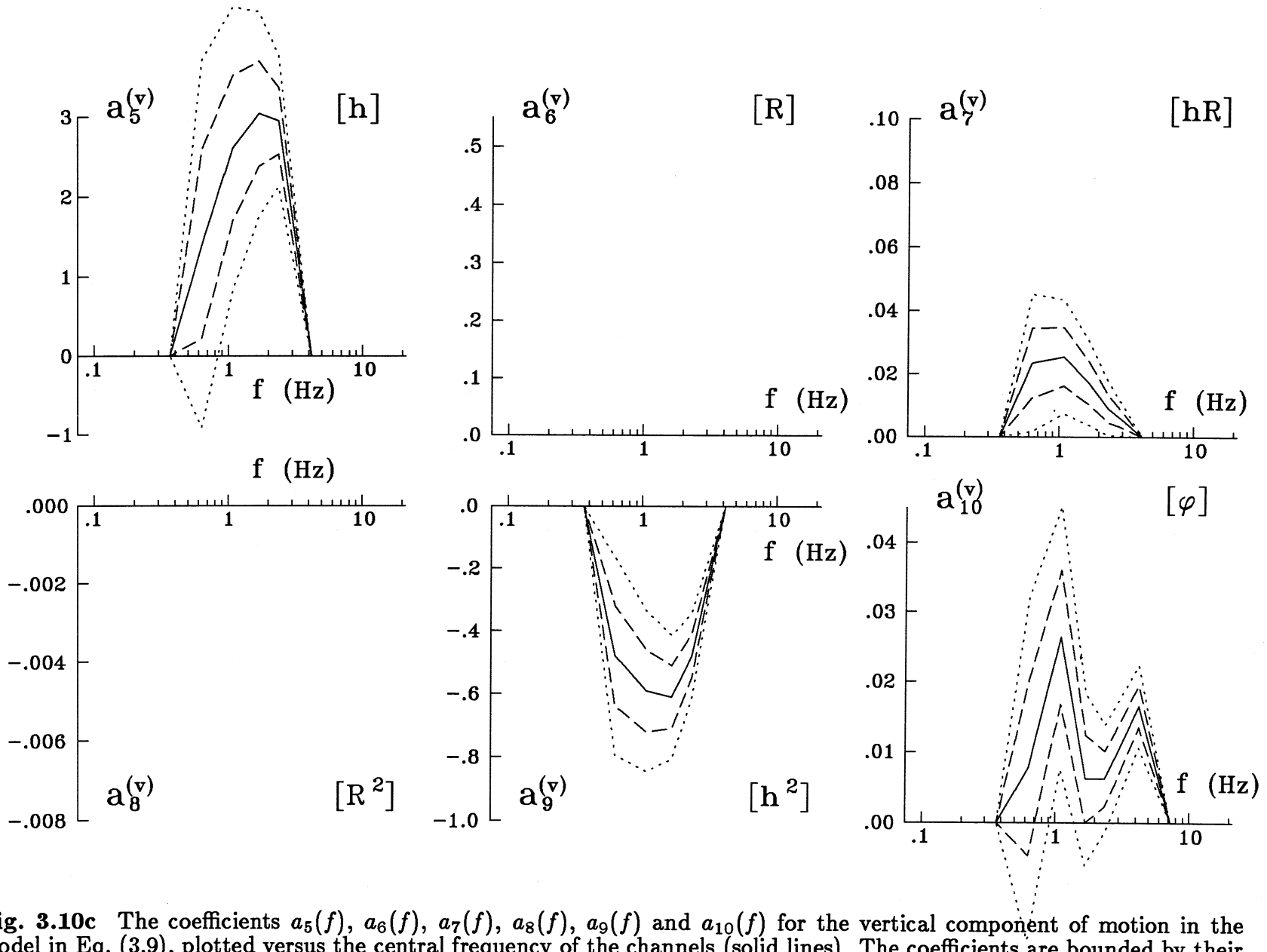

Fig. 3.10c The coefficients $a_5(f)$, $a_6(f)$, $a_7(f)$, $a_8(f)$, $a_9(f)$ and $a_{10}(f)$ for the vertical component of motion in the model in Eq. (3.9), plotted versus the central frequency of the channels (solid lines). The coefficients are bounded by their "σ-intervals" (dashed lines) and by their estimated 95% confidence intervals (dotted lines).

III.5 Models $dur = dur(I_{MM}, \Delta', I_{MM}\Delta', R, R^2, \varphi)$, $dur = dur(I_{MM}, R, R^2, \varphi)$, $dur = dur(I_{MM}, \Delta', I_{MM}\Delta', h, h^2)$ **and** $dur = dur(I_{MM}, h, h^2)$

It is not always possible to obtain complete information about all the parameters, involved in the description of a sedimentary basin, required for the models in Eqs. (3.8)–(3.9). We will present here four "truncated" models, which use the τ_{rs} term (see Eq. (1.1) in the form defined by Eqs. (2.6) or (2.7). The first two models deal with the case when the depth of sediments under the recording station is not known, but the distribution of rocks around it is available in terms of R and φ. The more complete model is as follows:

$$\left\{ \begin{array}{l} dur^{(h)}(f) \\ dur^{(v)}(f) \end{array} \right\} = \max \left[\left(\left\{ \begin{array}{l} a_1^{(h)}(f) \\ a_1^{(v)}(f) \end{array} \right\} + a_{19}(f) \cdot I_{MM} + a_4(f) \cdot \Delta' + a_{20}(f) \cdot I_{MM}\Delta' \right), 1 \right]$$

$$+ \left\{ \begin{array}{l} \left[a_6^{(h)}(f) \cdot R + a_8^{(h)}(f) \cdot R^2 + a_{10}^{(h)}(f) \cdot \varphi \right]_+ \\ \left[a_6^{(v)}(f) \cdot R + a_8^{(v)}(f) \cdot R^2 + a_{10}^{(v)}(f) \cdot \varphi \right]_+ \end{array} \right\}, \qquad (3.10a)$$

where all the distances are measured in kilometers and

$$[\cdot]_+ = \max\{0, [\cdot]\}. \qquad (3.10b)$$

The results of the regression analysis for this model are presented in Table 3.9 and in Fig. 3.11. As expected, the set of coefficients $\{a_1(f), a_{19}(f), a_4(f), a_{20}(f)\}$ is similar to that in the model in Eq. (3.2), and the set $\{a_6(f), a_8(f), a_{10}(f)\}$ repeats the main features of the same set from the model $dur = dur(M, M^2, \Delta, R, R^2, \varphi)$ (Novikova and Trifunac, 1993). Fig. 3.12 displays the positive contribution of the terms $a_6(f) \cdot R + a_8(f) \cdot R^2$ to the total duration, predicted by Eq. (3.10), for horizontal and vertical motions. In the $dur(I_{MM}, \Delta', I_{MM}\Delta', R, R^2, \varphi)$ model (Eq. (3.10)), the additional duration τ_{rs} appears to be "averaged" over the depth of sediments h, when compared to the term τ_{rs} from the model $dur(I_{MM}, \Delta', I_{MM}\Delta', h, R, hR, R^2, h^2, \varphi)$, in Eq. (3.8).

The simplified version of the model in Eq. (3.10) is

$$\left\{ \begin{array}{l} dur^{(h)}(f) \\ dur^{(v)}(f) \end{array} \right\} = \max \left[\left(\left\{ \begin{array}{l} a_1^{(h)}(f) \\ a_1^{(v)}(f) \end{array} \right\} + a_{19}(f) \cdot I_{MM} \right), 1 \right] +$$

$$+ \left\{ \begin{array}{l} \left[a_6^{(h)}(f) \cdot R + a_8^{(h)}(f) \cdot R^2 + a_{10}^{(h)}(f) \cdot \varphi \right]_+ \\ \left[a_6^{(v)}(f) \cdot R + a_8^{(v)}(f) \cdot R^2 + a_{10}^{(v)}(f) \cdot \varphi \right]_+ \end{array} \right\}, \qquad (3.11a)$$

where all the distances are measured in kilometers and

$$[\cdot]_+ = \max\{0, [\cdot]\}. \qquad (3.11b)$$

Table 3.9 Results of the regression analysis of the model in Eq. (3.10).

Channel number	f_0 (Hz)	# of data points N(f)	Coefficients a_i and their accuracy ("σ-interval")											σ_{dur} (sec)	dur_{av} (sec)
			$a_1^{(h)}$ $\pm\sigma_1^{(h)}$	$a_1^{(v)}$ $\pm\sigma_1^{(v)}$	a_{19} $\pm\sigma_{19}$	a_4 $\pm\sigma_4$	a_{20} $\pm\sigma_{20}$	$a_6^{(h)}$ $\pm\sigma_6^{(h)}$	$a_8^{(h)}$ $\pm\sigma_8^{(h)}$	$a_{10}^{(h)}$ $\pm\sigma_{10}^{(h)}$	$a_6^{(v)}$ $\pm\sigma_6^{(v)}$	$a_8^{(v)}$ $\pm\sigma_8^{(v)}$	$a_{10}^{(v)}$ $\pm\sigma_{10}^{(v)}$		
1	0.075	37	40.8 ±2.0	32.5 ±3.1	.0	.0	.0	.0	.0	.0	.0	.0	.0	10.2	38.3
2	0.12	311	27.7 ±5.4	28.2 ±5.6	-1.30 ±.74	.182 ±.019	.0	.0	.0	.0	.0	.0	.0	10.1	28.3
3	0.21	962	33.3 ±2.7	35.3 ±2.7	-3.17 ±.37	.195 ±.012	.0	.0	.0	.0	.0	.0	.0	7.8	21.4
4	0.37	1364	17.1 ±2.8	17.9 ±2.9	-1.25 ±.40	.169 ±.044	.012 ±.007	.0	.0	.0185 ±.0044	.0	.0	.0162 ±.0072	7.1	20.7
5	0.63	1897	7.8 ±2.2	9.2 ±2.3	-.56 ±.32	.096 ±.032	.023 ±.005	.288 ±.033	-.0042 ±.0005	.0211 ±.0039	.262 ±.055	-.0035 ±.0008	.0274 ±.0066	7.4	18.5
6	1.1	2443	6.1 ±1.5	8.7 ±1.6	-.61 ±.23	.049 ±.024	.026 ±.004	.328 ±.024	-.0051 ±.0004	.0251 ±.0029	.217 ±.040	-.0029 ±.0006	.0297 ±.0047	6.2	15.4
7	1.7	2906	4.6 ±1.0	7.0 ±1.0	-.35 ±.15	.033 ±.017	.023 ±.003	.208 ±.018	-.0031 ±.0003	.0132 ±.0021	.172 ±.027	-.0021 ±.0004	.0109 ±.0031	5.0	12.3
8	2.5	3185	4.7 ±0.7	6.4 ±0.7	-.41 ±.11	-.020 ±.013	.025 ±.002	.141 ±.013	-.0020 ±.0002	.0078 ±.0014	.141 ±.019	-.0018 ±.0003	.0048 ±.0022	3.7	9.1
9	4.2	2567	1.9 ±0.6	3.8 ±0.6	-.03 ±.10	-.032 ±.013	.029 ±.002	.076 ±.012	-.0009 ±.0002	.0044 ±.0014	.0	.0	.0065 ±.0021	3.2	7.6
10	7.2	2576	1.0 ±0.5	1.6 ±0.5	.18 ±.08	-.070 ±.012	.035 ±.002	.0	.0	.0	.0	.0	.0	2.8	6.4
11	13	1584	-1.1 ±0.5	-1.0 ±0.5	.46 ±.08	-.028 ±.017	.027 ±.003	.0	.0	.0	.0	.0	.0	2.3	5.1
12	21	735	-3.4 ±0.7	-3.3 ±0.7	.75 ±.12	.118 ±.038	.005 ±.006	.0	.0	.0	.0	.0	.0	2.0	4.2
			1 horiz	1 vert	I_{MM}	Δ'	$I_{MM}\Delta'$	R	R^2	φ	R	R^2	φ		
								horizontal			vertical				
			Corresponding parameters												

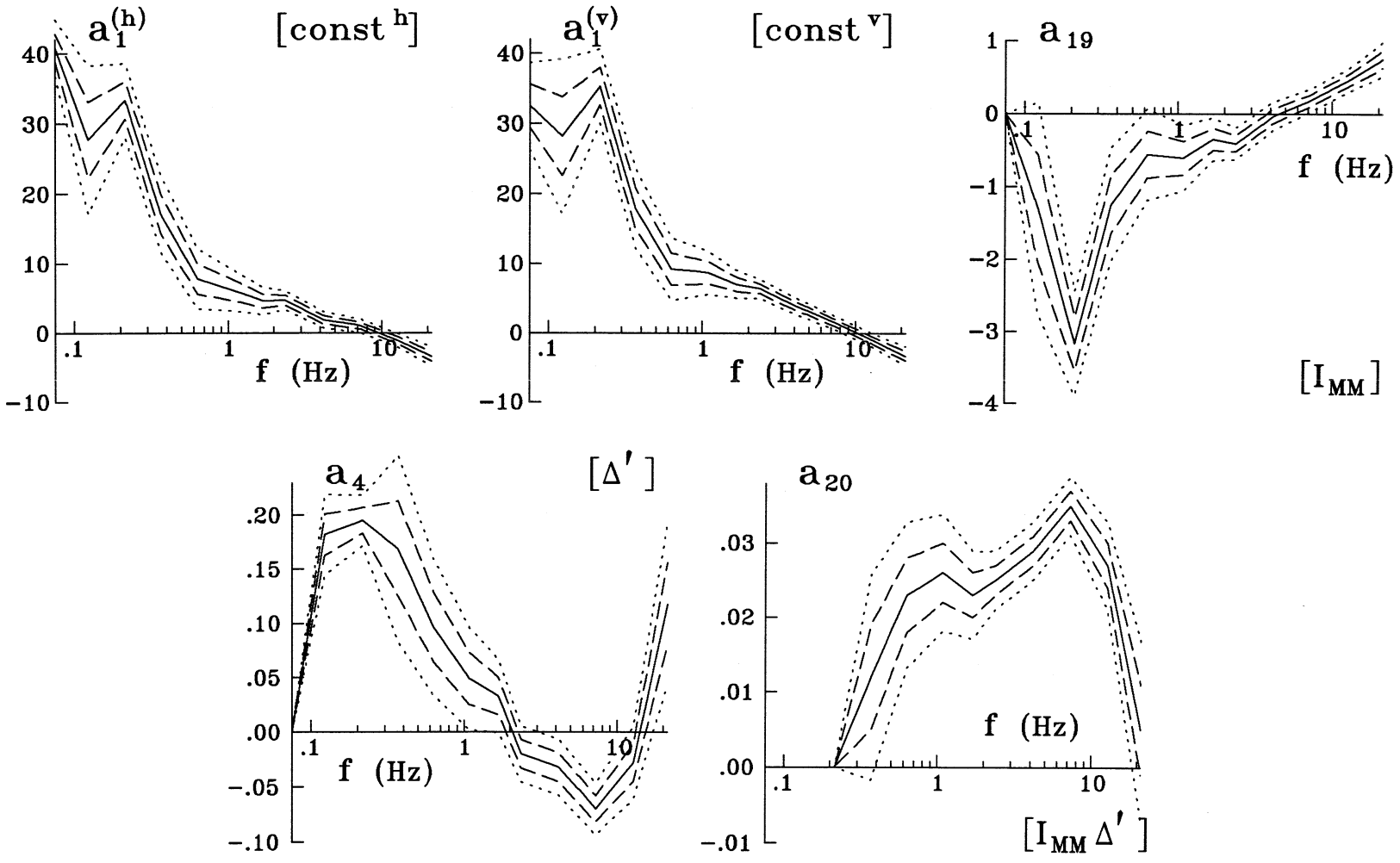

Fig. 3.11a The coefficients $a_1(f)$, $a_{19}(f)$, $a_4(f)$ and $a_{20}(f)$ in the model in Eq. (3.10), plotted versus the central frequency of the channels (solid lines). The coefficients are bounded by their "σ-intervals" (dashed lines) and by their estimated 95% confidence intervals (dotted lines).

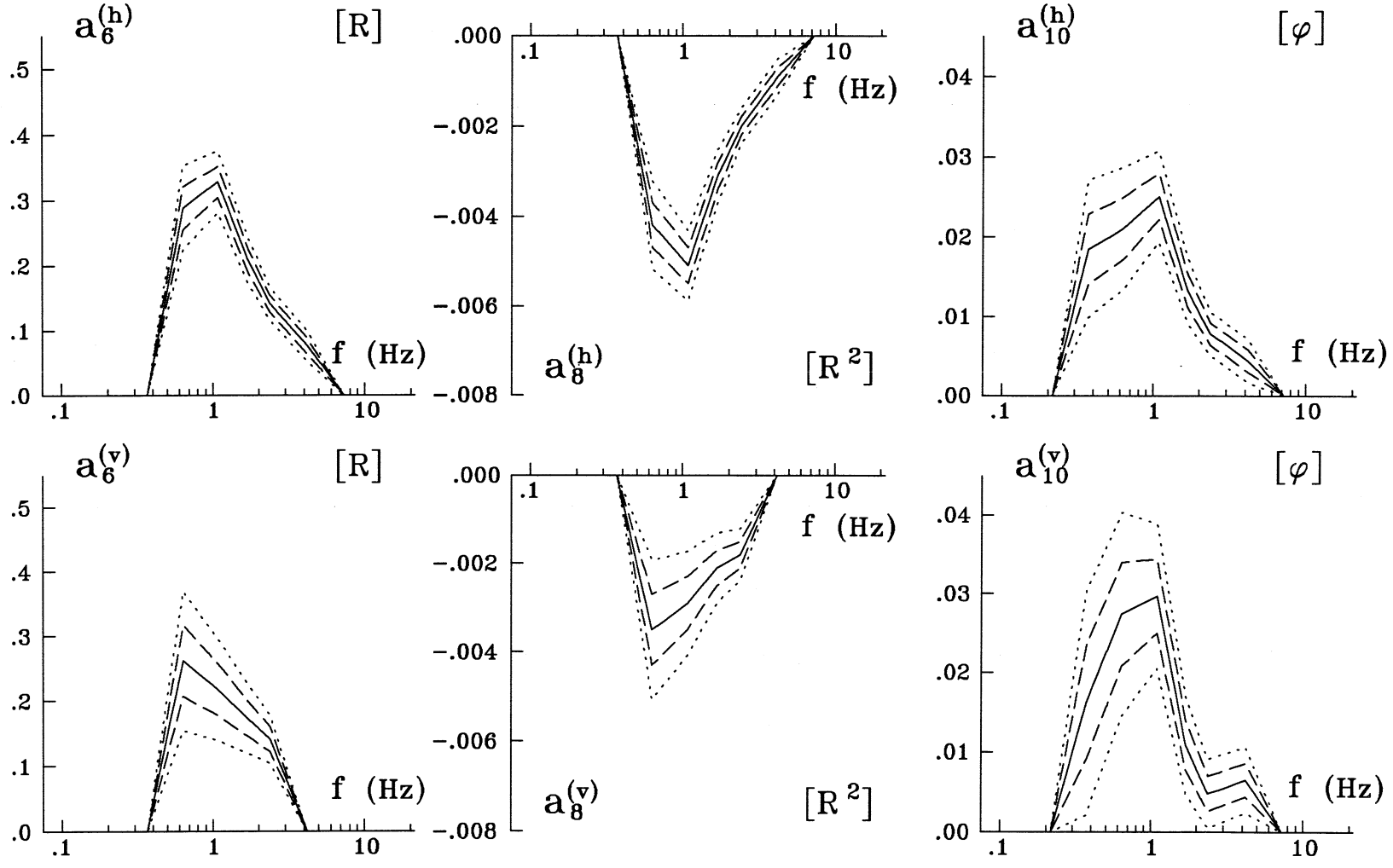

Fig. 3.11b The coefficients $a_6(f)$, $a_8(f)$ and $a_{10}(f)$ for the horizontal (top) and vertical (bottom) component of motion in the model in Eq. (3.10), plotted versus the central frequency of the channels (solid lines). The coefficients are bounded by their "σ-intervals" (dashed lines) and by their estimated 95% confidence intervals (dotted lines).

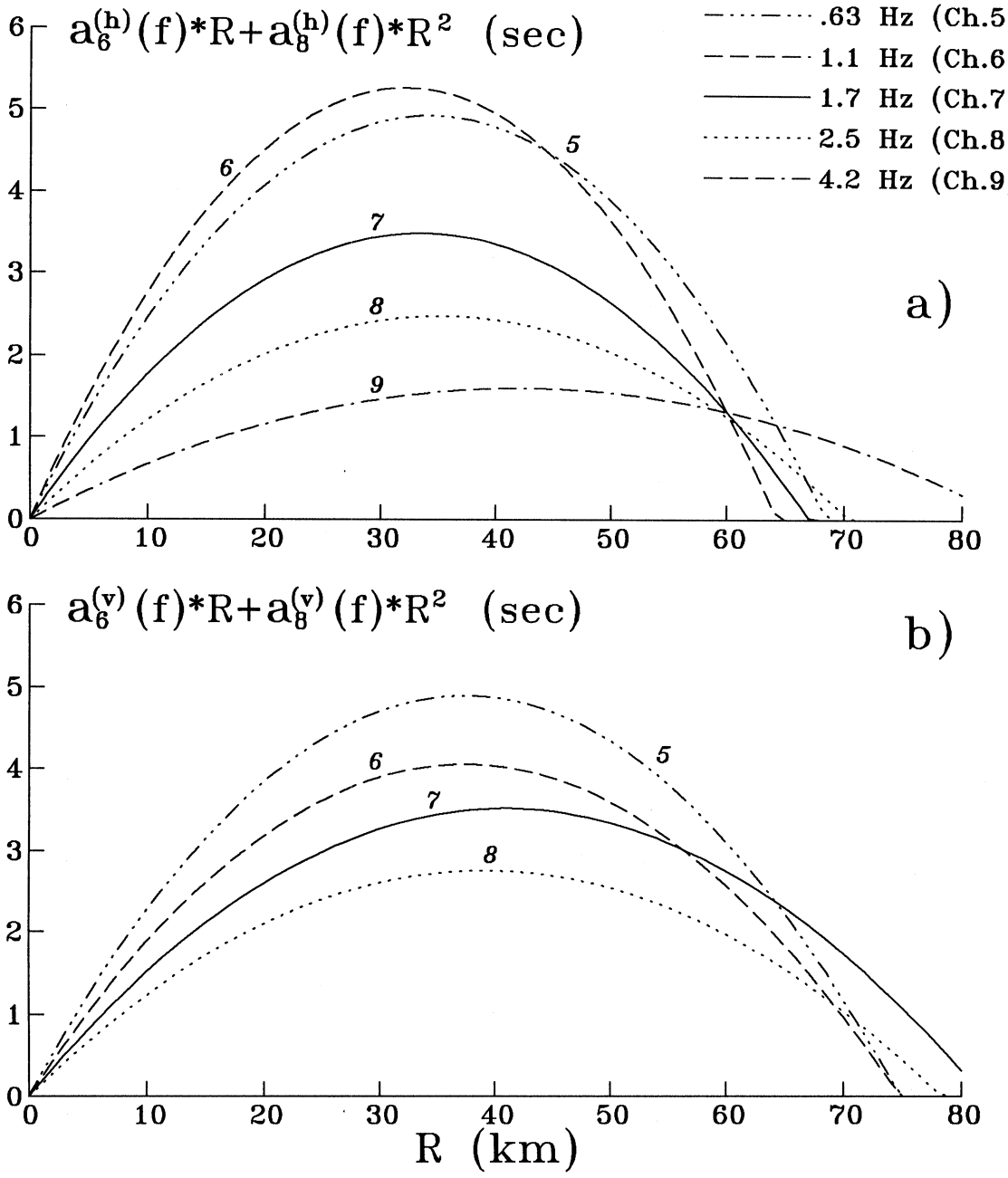

Fig. 3.12 Additional (relative to the basement rock sites) duration (in seconds) due to the specific horizontal characteristic dimension of the sedimentary valley, R, as predicted by the model in Eq. (3.10):

a) horizontal component;

b) vertical component.

This "truncated" model preserves the main features of the "complete" model (Eq. (3.8), Fig. 3.9) regarding the behavior of the terms which describe the prolongation of duration due to the specific geometry of a sedimentary basin.

Table 3.10 Results of the regression analysis of the model in Eq. (3.11).

Channel number	f_0 (Hz)	# of data points N(f)	Coefficients a_i and their accuracy ("σ-interval")									σ_{dur} (sec)	dur_{av} (sec)
			$a_1^{(h)}$ $\pm\sigma_1^{(h)}$	$a_1^{(v)}$ $\pm\sigma_1^{(v)}$	a_{19} $\pm\sigma_{19}$	$a_6^{(h)}$ $\pm\sigma_6^{(h)}$	$a_8^{(h)}$ $\pm\sigma_8^{(h)}$	$a_{10}^{(h)}$ $\pm\sigma_{10}^{(h)}$	$a_6^{(v)}$ $\pm\sigma_6^{(v)}$	$a_8^{(v)}$ $\pm\sigma_8^{(v)}$	$a_{10}^{(v)}$ $\pm\sigma_{10}^{(v)}$		
1	0.075	37	40.8 ±2.0	32.5 ±3.1	.0	.0	.0	.0	.0	.0	.0	10.2	38.3
2	0.12	311	54.1 ±5.2	53.6 ±5.6	-3.88 ±.79	.0	.0	.0	.0	.0	.0	11.5	28.3
3	0.21	962	52.3 ±2.7	54.2 ±2.8	-4.74 ±.40	.0	.0	.0	.0	.0	.0	8.7	21.4
4	0.37	1399	42.8 ±1.9	43.9 ±1.9	-3.45 ±.28	.0	.0	.0010 ±.0051	.0	.0	.0	8.2	20.7
5	0.63	1851	33.0 ±1.8	35.3 ±2.0	-2.58 ±.27	.0	.0	.0170 ±.0049	.0	.0	.0147 ±.0080	9.1	18.3
6	1.1	2344	20.9 ±1.4	24.2 ±1.5	-1.99 ±.21	.213 ±.030	-.0022 ±.0005	.0386 ±.0037	.130 ±.050	-.0006 ±.0007	.0391 ±.0059	7.7	14.9
7	1.7	2805	12.3 ±0.9	15.0 ±1.0	-.87 ±.14	.126 ±.022	-.0008 ±.0003	.0259 ±.0027	.104 ±.034	-.0002 ±.0005	.0254 ±.0039	6.2	11.8
8	2.5	3185	10.2 ±0.6	12.4 ±0.7	-.82 ±.10	.107 ±.016	-.0005 ±.0003	.0188 ±.0019	.095 ±.025	-.0003 ±.0004	.0151 ±.0028	4.8	9.1
9	4.2	2567	3.7 ±0.6	5.2 ±0.6	.39 ±.10	.0	.0	.0158 ±.0020	.0	.0	.0165 ±.0030	4.7	7.6
10	7.2	2576	-0.3 ±0.5	0.5 ±0.6	1.06 ±.09	.0	.0	.0	.0	.0	.0	4.5	6.4
11	13	1584	-2.5 ±0.5	-2.0 ±0.5	1.22 ±.08	.0	.0	.0	.0	.0	.0	3.5	5.1
12	21	735	-3.2 ±0.6	-2.8 ±0.6	1.19 ±.10	.0	.0	.0	.0	.0	.0	2.9	4.2
			1 horiz	1 vert	I_{MM}	R	R^2	φ	R	R^2	φ		
						horizontal			vertical				
			Corresponding parameters										

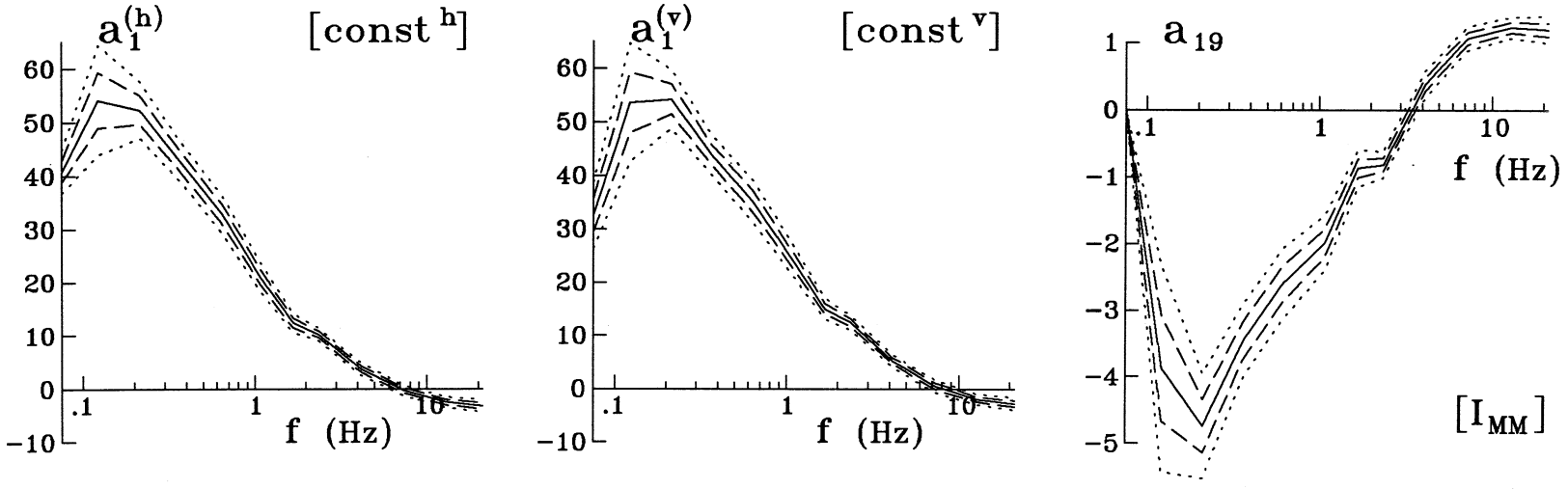

Fig. 3.13a The coefficients $a_1(f)$ and $a_{19}(f)$ in the model in Eq. (3.11), plotted versus the central frequency of the channels (solid lines). The coefficients are bounded by their "σ-intervals" (dashed lines) and by their estimated 95% confidence intervals (dotted lines).

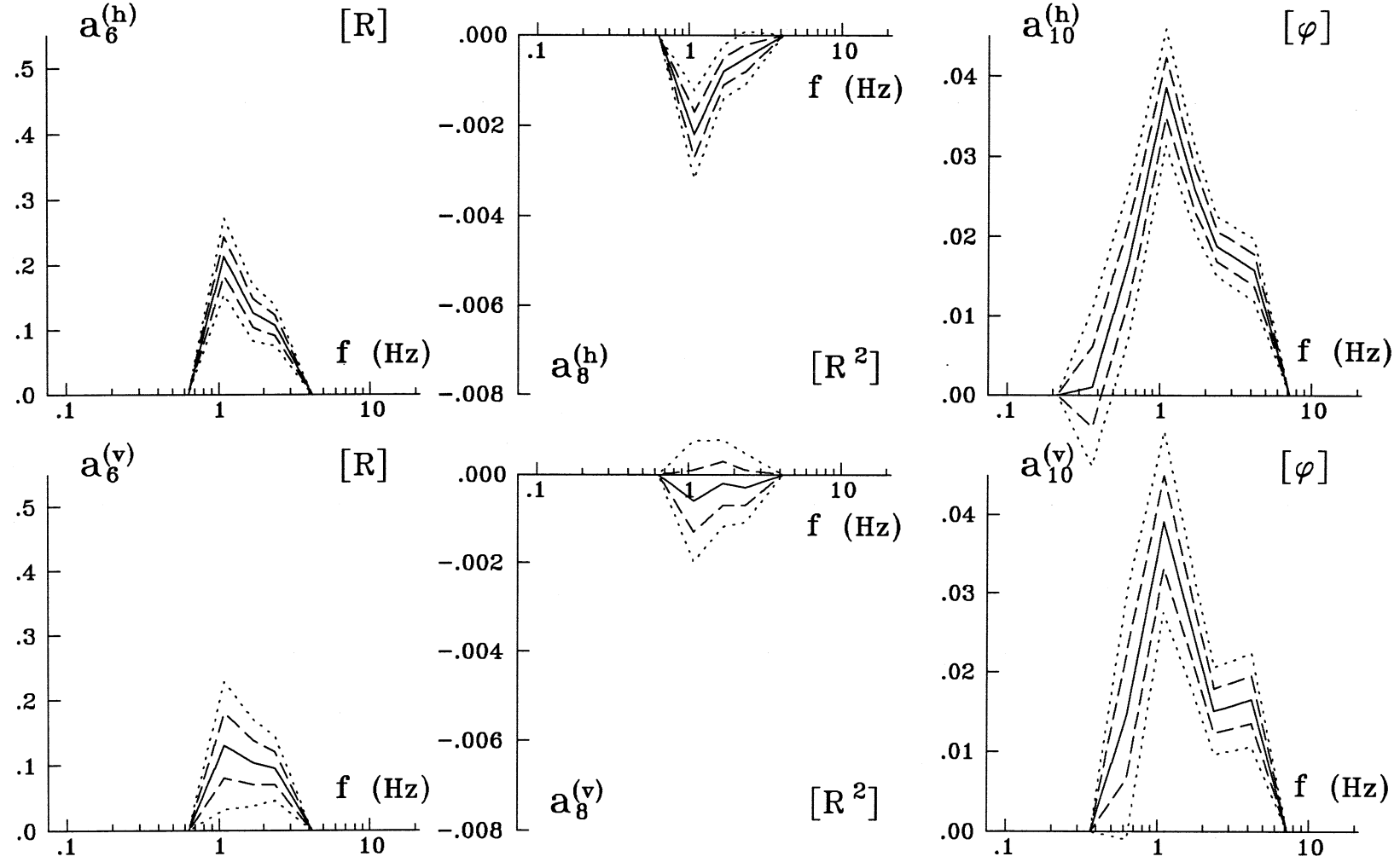

Fig. 3.13b The coefficients $a_6(f)$, $a_8(f)$ and $a_{10}(f)$ for the horizontal (top) and vertical (bottom) component of motion in the model in Eq. (3.11), plotted versus the central frequency of the channels (solid lines). The coefficients are bounded by their "σ-intervals" (dashed lines) and by their estimated 95% confidence intervals (dotted lines).

The results of the regression analysis of this model are given in Table 3.10 and in Fig. 3.13. The coefficients $a_1(f)$ and $a_{19}(f)$ behave as expected, i.e. are similar to their counterparts from the model in Eq. (3.3), where a_1 and a_{19} are the only coefficients present. However, the rest of the coefficients in the present model in Eq. (3.11) do not quite follow the behavior of the corresponding coefficients from the more complete "intensity model" in Eq. (3.10) or the "magnitude model" $dur = dur(M, M^2, \Delta, R, R^2, \varphi)$ Eq. (4.14). The lack of information about the distance to the source makes the equation very approximate, and the results of the regression analysis are less precise.

The models

$$\left\{ \begin{matrix} dur^{(h)}(f) \\ dur^{(v)}(f) \end{matrix} \right\} = \max \left[\left(\left\{ \begin{matrix} a_1^{(h)}(f) \\ a_1^{(v)}(f) \end{matrix} \right\} + a_{19}(f) \cdot I_{MM} + a_4(f) \cdot \Delta' + a_{20}(f) \cdot I_{MM} \Delta' \right), 1 \right] + \left\{ \begin{matrix} \left[a_7^{(h)}(f) \cdot h + a_9^{(h)}(f) \cdot h^2 \right]_+ \\ \left[a_7^{(v)}(f) \cdot h + a_9^{(v)}(f) \cdot h^2 \right]_+ \end{matrix} \right\}, \tag{3.12a}$$

where

$$[\cdot]_+ = \max\{0, [\cdot]\}, \tag{3.12b}$$

and

$$\left\{ \begin{matrix} dur^{(h)}(f) \\ dur^{(v)}(f) \end{matrix} \right\} = \max \left[\left(\left\{ \begin{matrix} a_1^{(h)}(f) \\ a_1^{(v)}(f) \end{matrix} \right\} + a_{19}(f) \cdot I_{MM} \right), 1 \right] + \left\{ \begin{matrix} \left[a_7^{(h)}(f) \cdot h + a_9^{(h)}(f) \cdot h^2 \right]_+ \\ \left[a_7^{(v)}(f) \cdot h + a_9^{(v)}(f) \cdot h^2 \right]_+ \end{matrix} \right\}, \tag{3.13a}$$

where again

$$[\cdot]_+ = \max\{0, [\cdot]\}, \tag{3.13b}$$

give the prediction of the duration when the depth of sediments, h, is available and the parameters R and φ are not known. The results of the regression analysis, performed for the first model, Eq. (3.12), are shown in Table 3.11 and in Figs. 3.14–3.15. The results for the second model, Eq. (3.13), can be found in Table 3.12 and in Fig. 3.16. The contribution to the overall duration occurring due to the presence of sediments, $\tau_{rs}(h)$, is similar to that in the model $dur = dur(M, M^2, \Delta, h, h^2)$ (Novikova and Trifunac, 1993). Also, the similarity holds when the last two models are compared with Eqs. (3.8)–(3.9). Thus, in the model $dur(I_{MM}, \Delta', I_{MM}\Delta', h, h^2,)$ (Eq. (3.12)), the additional duration τ_{rs} appears to be "averaged" over the characteristic horizontal dimension of the sediments, R, when compared to the term τ_{rs} from the model $dur(I_{MM}, \Delta', I_{MM}\Delta', h, R, hR, R^2, h^2, \varphi)$ (Eq. (3.8))

Table 3.11 Results of the regression analysis of the model in Eq. (3.12).

Channel number	f_0 (Hz)	# of data points N(f)	Coefficients a_i and their accuracy ("σ-interval")									σ_{dur} (sec)	dur_{av} (sec)
			$a_1^{(h)}$ $\pm\sigma_1^{(h)}$	$a_1^{(h)}$ $\pm\sigma_1^{(h)}$	a_{19} $\pm\sigma_{19}$	a_4 $\pm\sigma_4$	a_{20} $\pm\sigma_{20}$	$a_5^{(h)}$ $\pm\sigma_5^{(\eta)}$	$a_9^{(h)}$ $\pm\sigma_9^{(h)}$	$a_5^{(v)}$ $\pm\sigma_5^{(v)}$	$a_9^{(v)}$ $\pm\sigma_9^{(v)}$		
1	0.075	37	40.8 ±2.0	32.5 ±3.1	.0	.0	.0	.0	.0	.0	.0	10.2	38.3
2	0.12	311	27.7 ±5.4	28.2 ±5.7	-1.30 ±.75	.182 ±.019	.0	.0	.0	.0	.0	10.1	28.3
3	0.21	962	33.3 ±2.7	35.3 ±2.7	-3.17 ±.37	.195 ±.012	.0	.0	.0	.0	.0	7.8	21.4
4	0.37	1499	23.8 ±2.6	24.2 ±2.6	-1.73 ±.39	.084 ±.040	.018 ±.007	.0	.0	.0	.0	7.3	21.0
5	0.63	2035	13.7 ±2.1	15.6 ±2.1	-.62 ±.32	.134 ±.033	.012 ±.006	.0	.0	.0	.0	7.8	18.7
6	1.1	1612	9.9 ±2.7	12.4 ±2.8	-.55 ±.43	.122 ±.035	.009 ±.006	1.73 ±.45	-.30 ±.08	1.83 ±.67	-.28 ±.12	7.6	16.7
7	1.7	1930	4.8 ±1.5	7.0 ±1.6	-.12 ±.25	.080 ±.023	.013 ±.004	1.76 ±.33	-.26 ±.06	2.07 ±.48	-.30 ±.09	5.9	13.6
8	2.5	2107	4.7 ±1.0	5.6 ±1.1	-.26 ±.17	-.001 ±.016	.021 ±.003	.85 ±.22	-.08 ±.04	1.70 ±.32	-.22 ±.06	4.2	10.0
9	4.2	2411	1.5 ±0.6	1.5 ±0.7	.22 ±.10	-.032 ±.013	.028 ±.002	.0	.0	1.43 ±.29	-.18 ±.05	3.3	7.6
10	7.2	2576	1.0 ±0.5	1.6 ±0.5	.18 ±.08	-.070 ±.012	.035 ±.002	.0	.0	.0	.0	2.8	6.4
11	13	1584	-1.1 ±0.5	-1.0 ±0.5	.46 ±.08	-.028 ±.017	.027 ±.003	.0	.0	.0	.0	2.3	5.1
12	21	735	-3.4 ±0.7	-3.3 ±0.7	.75 ±.12	.118 ±.038	.005 ±.006	.0	.0	.0	.0	2.0	4.2
			1 horiz	1 vert	I_{MM}	Δ'	$I_{MM}\Delta'$	h	h^2	h	h^2		
								horizontal		vertical			
			Corresponding parameters										

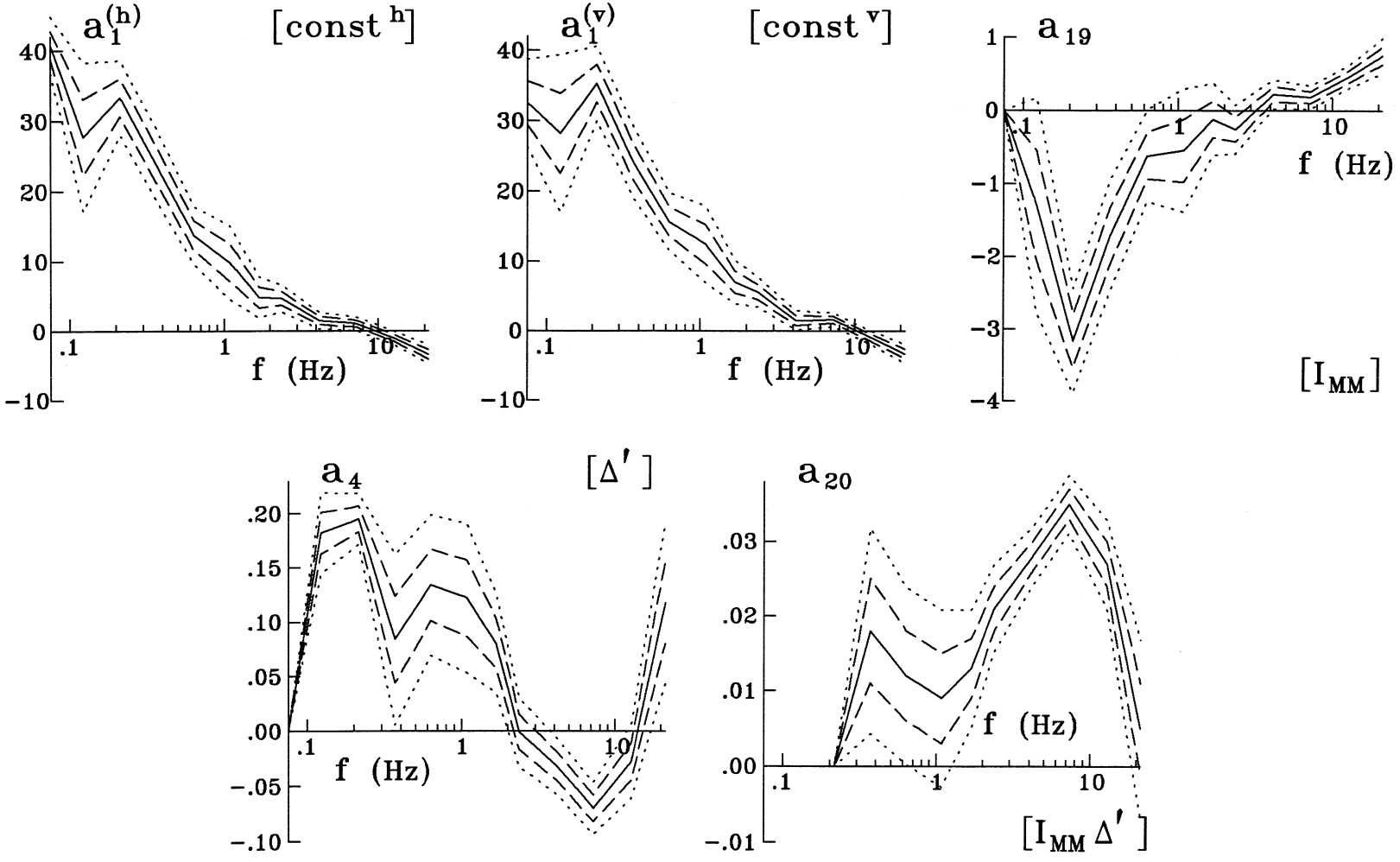

Fig. 3.14a The coefficients $a_1(f)$, $a_{19}(f)$, $a_4(f)$ and $a_{20}(f)$ in the model in Eq. (3.12), plotted versus the central frequency of the channels (solid lines). The coefficients are bounded by their "σ-intervals" (dashed lines) and by their estimated 95% confidence intervals (dotted lines).

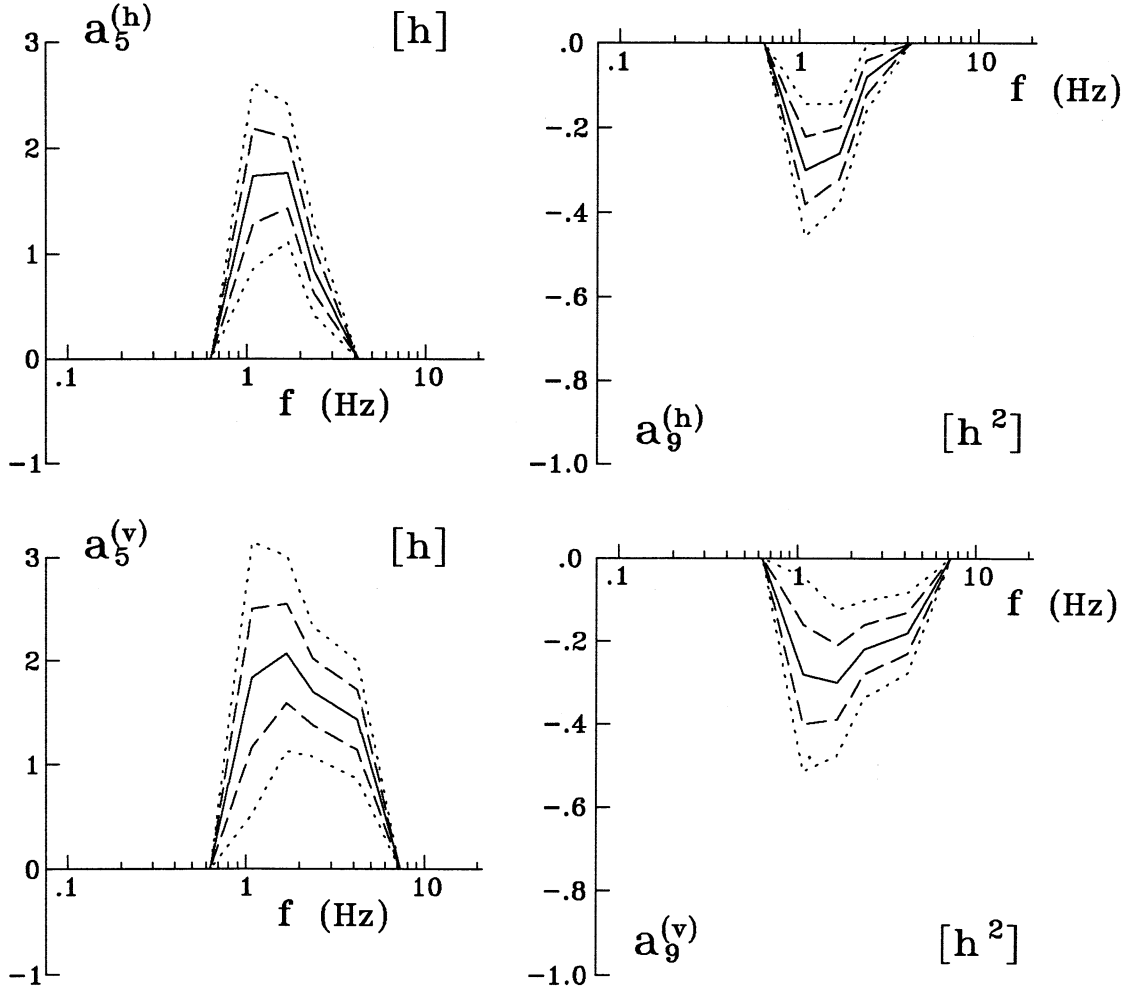

Fig. 3.14b The coefficients $a_5(f)$ and $a_9(f)$ for the horizontal (top) and vertical (bottom) component of motion in the model in Eq. (3.12), plotted versus the central frequency of the channels (solid lines). The coefficients are bounded by their "σ-intervals" (dashed lines) and by their estimated 95% confidence intervals (dotted lines).

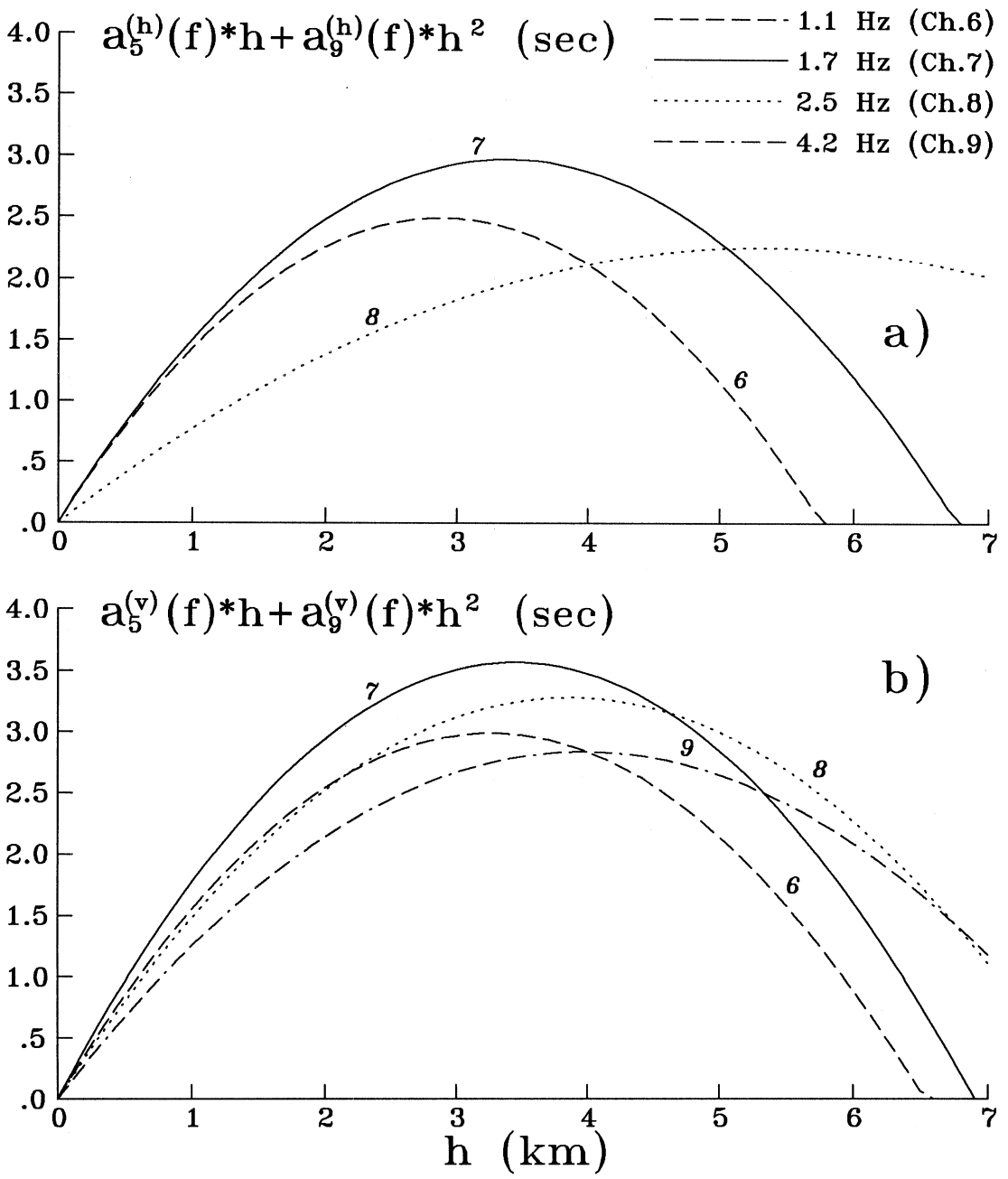

Fig. 3.15 Additional (relative to the basement rock sites) duration (in seconds) due to the depth of sediments under the recording site, h, as predicted by the model in Eq. (3.12):

a) horizontal component;

b) vertical component.

This "truncated" model preserves the main features of the complete model (Eq. (3.8), Fig. 3.9) regarding the behavior of the terms which describe the prolongation of the duration due to the specific geometry of a sedimentary basin.

Table 3.12 Results of the regression analysis of the model in Eq. (3.13).

Channel number	f_0 (Hz)	# of data points N(f)	Coefficients a_i and their accuracy ("σ-interval")							σ_{dur} (sec)	dur_{av} (sec)
			$a_1^{(h)}$ $\pm\sigma_1^{(h)}$	$a_1^{(h)}$ $\pm\sigma_1^{(h)}$	a_{19} $\pm\sigma_{19}$	$a_5^{(h)}$ $\pm\sigma_5^{(h)}$	$a_9^{(h)}$ $\pm\sigma_9^{(h)}$	$a_5^{(v)}$ $\pm\sigma_5^{(v)}$	$a_9^{(v)}$ $\pm\sigma_9^{(v)}$		
1	0.075	37	40.8 ±2.0	32.5 ±3.1	.0	.0	.0	.0	.0	10.2	38.3
2	0.12	311	54.1 ±5.2	53.6 ±5.6	-3.88 ±.79	.0	.0	.0	.0	11.5	28.3
3	0.21	962	52.3 ±2.7	54.2 ±2.8	-4.74 ±.40	.0	.0	.0	.0	8.7	21.4
4	0.37	1499	42.3 ±1.8	43.2 ±1.8	-3.33 ±.27	.0	.0	.0	.0	8.4	21.0
5	0.63	1756	34.6 ±1.9	36.1 ±2.3	-2.59 ±.29	.0	.0	2.37 ±1.01	-.41 ±.17	9.3	18.6
6	1.1	1522	22.1 ±2.1	25.6 ±2.2	-1.63 ±.33	4.00 ±.54	-.70 ±.10	3.17 ±.81	-.48 ±.14	9.0	16.0
7	1.7	1930	14.9 ±1.2	18.1 ±1.4	-1.06 ±.20	4.19 ±.41	-.64 ±.07	3.59 ±.61	-.52 ±.11	7.5	13.6
8	2.5	2107	8.3 ±0.8	9.7 ±0.9	-.35 ±.14	2.74 ±.29	-.36 ±.05	3.23 ±.42	-.44 ±.08	5.5	10.0
9	4.2	1667	1.5 ±0.8	2.6 ±0.9	.56 ±.14	2.68 ±.29	-.36 ±.05	3.33 ±.43	-.48 ±.08	4.8	8.4
10	7.2	2576	-0.3 ±0.5	0.5 ±0.6	1.06 ±.09	.0	.0	.0	.0	4.5	6.4
11	13	1584	-2.5 ±0.5	-2.0 ±0.5	1.22 ±.08	.0	.0	.0	.0	3.5	5.1
12	21	735	-3.2 ±0.6	-2.8 ±0.6	1.19 ±.10	.0	.0	.0	.0	2.9	4.2
			1 horiz	1 vert	I_{MM}	h	h^2	h	h^2		
						horizontal		vertical			
			Corresponding parameters								

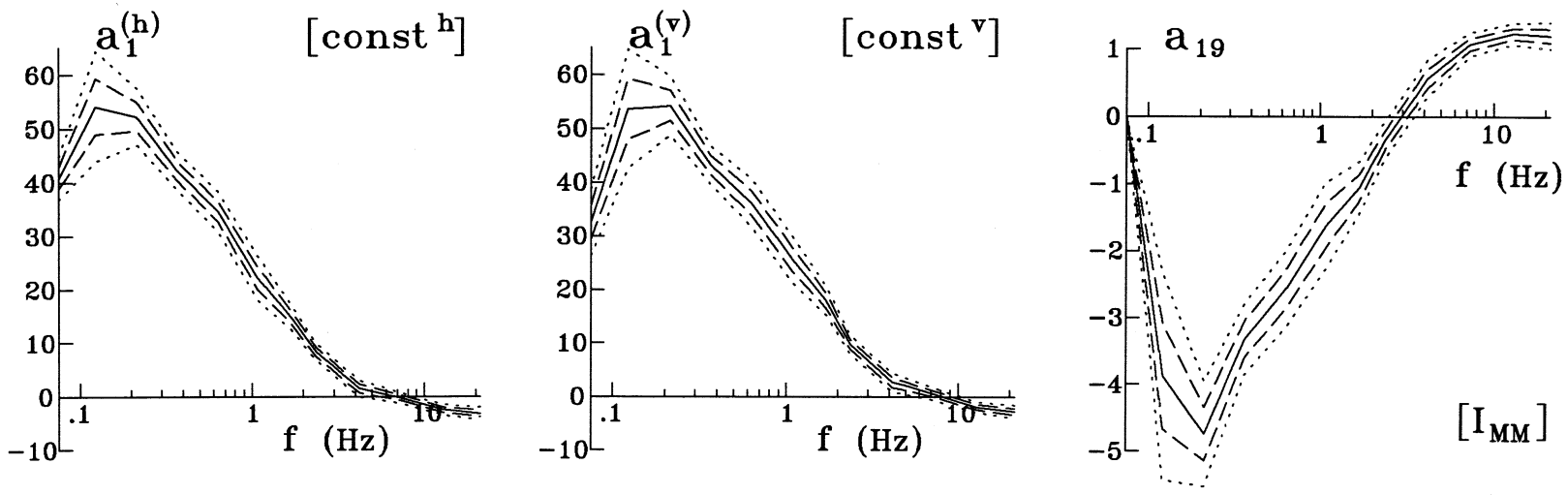

Fig. 3.16a The coefficients $a_1(f)$ and $a_{19}(f)$ in the model in Eq. (3.13), plotted versus the central frequency of the channels (solid lines). The coefficients are bounded by their "σ-intervals" (dashed lines) and by their estimated 95% confidence intervals (dotted lines).

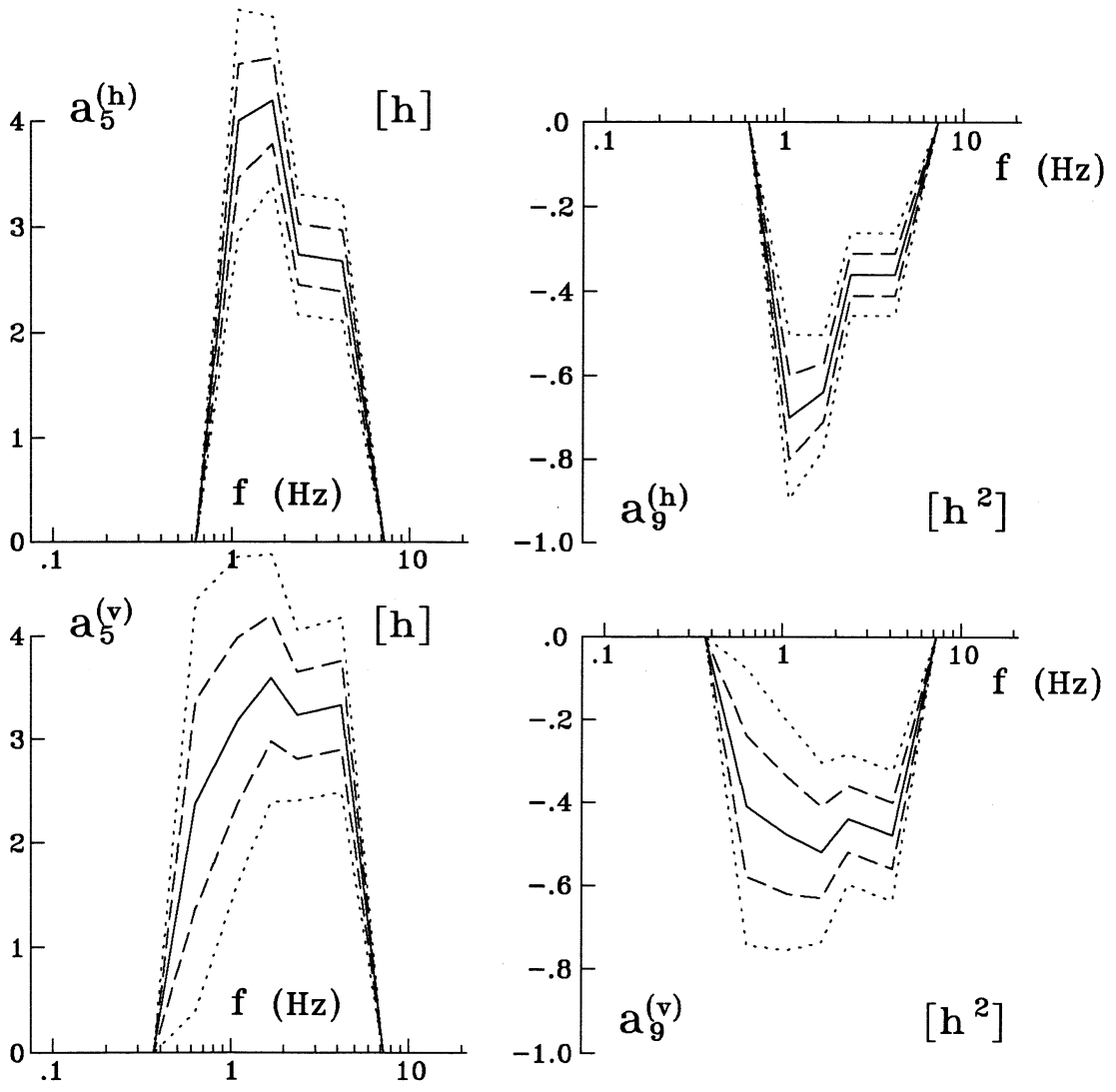

Fig. 3.16b The coefficients $a_5(f)$ and $a_9(f)$ for the horizontal (top) and vertical (bottom) component of motion in the model in Eq. (3.13), plotted versus the central frequency of the channels (solid lines). The coefficients are bounded by their "σ-intervals" (dashed lines) and by their estimated 95% confidence intervals (dotted lines).

In the present database, any attempt to include s_L in the equations dealing with the parameters h, R and φ, failed due to instability of the solution of the regression equations.

III.6 How to Choose the Proper Model

We emphasize once again that our regression models (with the coefficients we obtained) should not be used to estimate the strong motion duration in a region different from the one where the data were collected. It might (and it will) happen that different geological environment can change the prevailing earthquake mechanism, the distribution of the hypocentral depths of the sources, the velocities and the attenuation factors, and other possible conditions that influence the values of the regression coefficients. Another restriction in the application of our models comes from the "completeness" of the database. It covers only a restricted range of the Modified Mercalli intensities, observed at a site, distances to the earthquake source and other parameters. We assume that only predictions coming from interpolation, not extrapolation, may be acceptable.

In this work, we presented 12 regression equations for modelling the duration of strong earthquake ground motion. Fig. 3.17 provides an overview for choosing the proper model in each particular case, depending on what site parameters and propagation path parameters are available. Each model is shown in this figure by specifying the set of parameters it considers. The equation number of each model is also given for easy reference to the main text. The chart summarizes the "intensity-type" models only. For the models with "magnitude-type" "basic duration" refer to Novikova and Trifunac (1993).

There are two recommendations we would like to make regarding the practical use of these models. (1) If the station is located on rock, the best model would be the one that considers the geological parameter s (without considering the local soil conditions parameter s_L). In this case, obviously, s should be taken to be equal to 2. (2) The regression coefficients were obtained at some specific set of frequencies only. If the estimate of the duration of strong motion at some frequency not present in this set is required, we would recommend to get it in two steps. First, get the estimate of duration for two nearby frequencies from our set. Second, interpolate the results linearly and get the estimate for the initially required frequency. We would recommend against interpolation of our coefficients between the central frequencies of the channels, because some correlated coefficients (such as the coefficients for I_{MM} and $I_{MM}\Delta'$, for example) can be very sensitive to such a procedure.

III.7 Distribution Function of the Residuals

It is of interest for earthquake engineering applications not only to be able to predict the expected value of the duration of the strong ground motion, but also to evaluate the

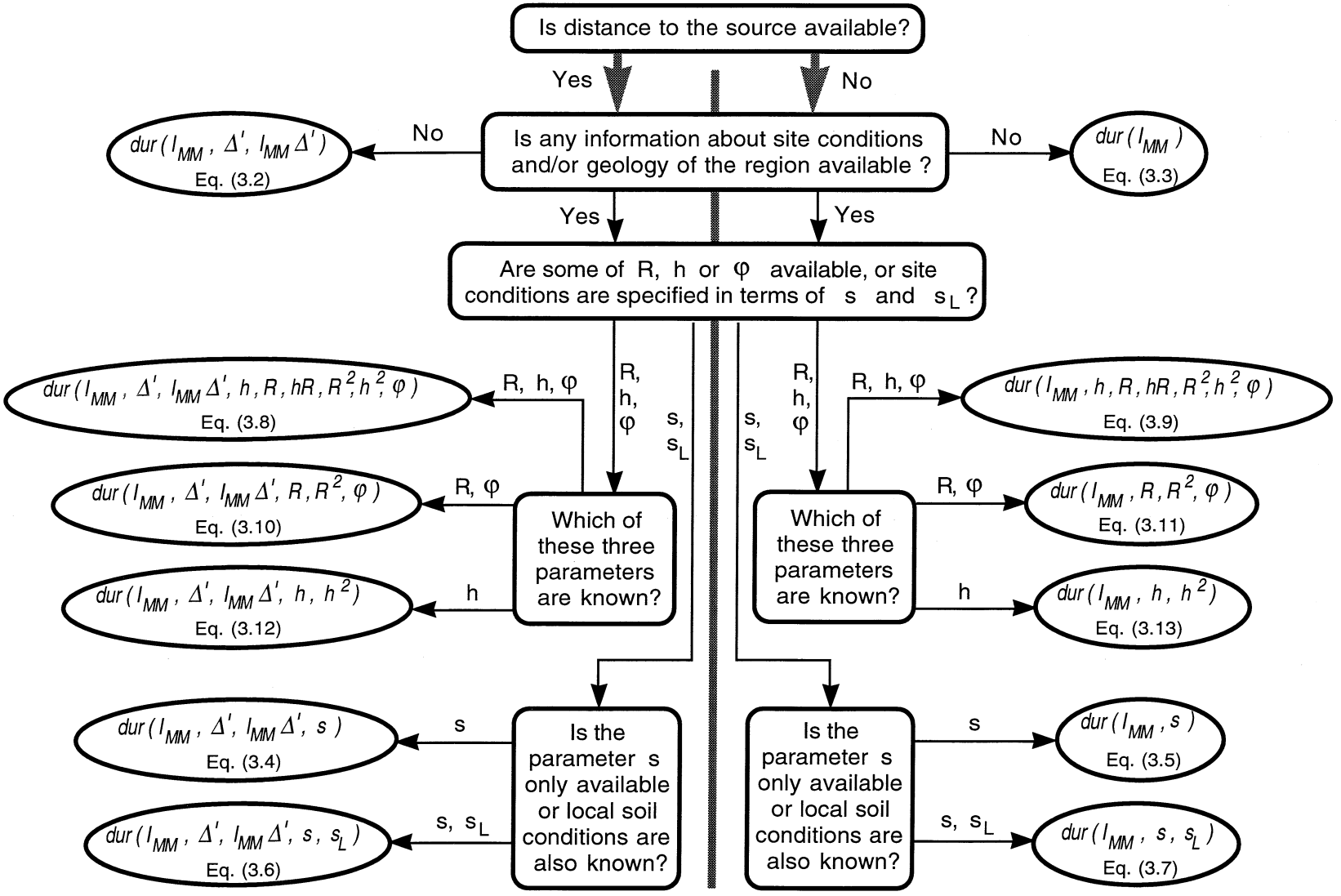

Fig. 3.17 The algorithm for choosing the proper model, based on what earthquake and site parameters are available. Each model is marked by the equation number. The chart summarizes the "intensity-type" models only. For the "magnitude-type" models refer to Novikova and Trifunac (1993).

probability of exceedance of any given duration at a particular frequency. Study of the residues allows one to estimate this probability from the distribution functions of the observed residuals.

As in our study of the "magnitude-type" models (Novikova and Trifunac, 1993), we define the residual (factor ρ, or relative residual) of a model prediction from a data point as the ratio of the observed duration of strong ground motion, dur^{obs}, to the duration, predicted by a model, dur^{model}:

$$\rho = \frac{dur^{\text{obs}}}{dur^{\text{model}}}.$$

We found that this quantity is easier to deal with than, for example the difference $dur^{\text{obs}} - dur^{\text{model}}$, because ρ has well defined lower bound (zero) and has very similar distributions for all the frequency channels. We also found that the distribution function of ρ does not depend on the parameters of the models, such as the Modified Mercalli intensity, the distance to the source and the site conditions. This distribution function, $q(\rho)$, is very similar for different models. We approximate it by:

$$q(\rho) = \frac{1}{\eta} \cdot \frac{\rho^b}{a + \rho^c}, \tag{3.14a}$$

where η is the normalizing coefficient:

$$\eta = a^{\frac{b+1}{c}-1} \cdot \frac{\pi}{c} \cdot \left[\sin \frac{(b+1)\pi}{c}\right]^{-1}. \tag{3.14b}$$

The coefficients a, b and c should be adjusted for each model at every frequency channel. We choose these coefficients so that the cumulative distribution function

$$P(\rho) = \int_0^{\rho} q(\rho) d\rho \tag{3.15}$$

stays close to the cumulative distribution function of the observed data $P^{\text{obs}}(\rho)$ (Kolmogorov-Smirnov test).

Note that the mean value of the residuals ρ is equal to 1 by the construction of all of our duration models. Thus, we could have reduced the number of coefficients in the distribution function (3.14) by setting its mean to be equal to unity. We, however, decided to allow additional flexibility in the coefficients to achieve better fit in terms of the Kolmogorov-Smirnov test. As a result, the mean of the proposed distribution differs slightly from 1 at some channels.

Table 3.13 gives the "best" values for the coefficients a, b and c for the distribution (3.14) for the models in Eqs. (3.2)–(3.13). Fig. 3.18 demonstrates the progress accomplished in the development of our regression models. The observed cumulative distribution function, $P^{\text{obs}}(\rho)$ is shown for the models in Eqs. (3.2) (the solid line), (3.3) (the dashed line) and (3.8) (the dotted line). The cumulative distribution function of an

Table 3.13a Coefficients in the distribution function (3.14) for the models in Eqs. (3.2)–(3.7).

Ch. number	f_0 (Hz)	For Eq.(3.2)			For Eq.(3.3)			For Eq.(3.4)			For Eq.(3.5)			For Eq.(3.6)			For Eq.(3.7)		
		a	b	c	a	b	c	a	b	c	a	b	c	a	b	c	a	b	c
1	0.075	2.3	3.5	12.0	2.3	3.5	12.0	2.3	3.5	12.0	2.3	3.5	12.0	2.3	3.5	12.0	2.3	3.5	12.0
2	0.12	0.6	2.7	7.4	1.9	1.7	7.4	0.6	2.7	7.4	1.9	1.7	7.4	0.6	2.7	7.4	1.9	1.7	7.4
3	0.21	0.4	3.1	7.4	0.4	2.7	6.9	0.3	3.2	7.2	0.4	2.6	6.8	0.4	3.0	7.4	0.4	2.6	6.8
4	0.37	1.2	2.5	8.3	1.1	2.3	7.6	1.1	2.4	7.9	1.5	1.8	7.1	1.2	2.4	8.1	1.5	1.8	7.1
5	0.63	2.1	1.5	7.1	2.7	1.0	6.1	1.4	1.5	6.4	4.0	0.8	6.1	1.9	1.6	7.0	4.0	0.8	6.1
6	1.1	3.5	1.1	7.1	3.5	0.7	5.6	2.7	1.1	6.6	3.7	0.6	5.4	2.7	1.3	6.9	3.5	0.9	6.1
7	1.7	2.6	1.4	7.3	4.0	0.6	5.6	2.2	1.3	6.8	2.8	0.6	5.1	2.5	1.6	7.5	2.8	1.0	6.2
8	2.5	2.4	1.6	7.6	2.1	0.8	5.3	1.7	1.5	6.8	1.6	0.8	5.0	1.8	1.7	7.2	1.5	1.3	6.0
9	4.2	4.2	1.2	7.7	2.2	0.5	4.6	1.7	1.5	6.8	2.2	0.5	4.7	2.0	1.7	7.3	2.2	1.0	5.9
10	7.2	1.7	1.4	6.5	2.0	0.3	4.1	1.7	1.4	6.5	1.9	0.4	4.3	1.7	1.8	7.2	2.0	0.3	4.1
11	13	1.3	1.6	6.5	1.4	0.5	4.2	1.3	1.6	6.5	1.4	0.5	4.2	3.1	1.5	7.7	1.4	0.5	4.2
12	21	1.4	1.5	6.4	1.0	0.6	4.2	1.4	1.5	6.4	1.0	0.6	4.2	1.1	2.1	7.4	1.0	0.6	4.2

Table 3.13b Coefficients in the distribution function (3.14) for the models in Eqs. (3.8)–(3.13).

Ch. number	f_0 (Hz)	For Eq.(3.8)			For Eq.(3.9)			For Eq.(3.10)			For Eq.(3.11)			For Eq.(3.12)			For Eq.(3.13)		
		a	b	c	a	b	c	a	b	c	a	b	c	a	b	c	a	b	c
1	0.075	2.3	3.5	12.0	2.3	3.5	12.0	2.3	3.5	12.0	2.3	3.5	12.0	2.3	3.5	12.0	2.3	3.5	12.0
2	0.12	0.6	2.7	7.4	1.9	1.7	7.4	0.6	2.7	7.4	1.9	1.7	7.4	0.6	2.7	7.4	1.9	1.7	7.4
3	0.21	0.4	3.1	7.4	0.4	2.7	6.9	0.4	3.1	7.4	0.4	2.7	6.9	0.4	3.1	7.4	0.4	2.7	6.9
4	0.37	0.9	2.7	8.1	1.1	2.2	7.4	0.9	2.7	8.1	1.1	2.2	7.4	1.2	2.5	8.3	1.1	2.3	7.6
5	0.63	1.9	1.5	7.0	2.7	1.0	6.1	2.5	1.5	7.4	2.7	1.0	6.1	2.1	1.5	7.1	2.7	1.0	6.1
6	1.1	1.6	1.6	6.8	2.0	0.8	5.2	1.8	1.7	7.3	2.6	0.9	5.8	1.7	1.2	6.1	2.2	0.7	5.1
7	1.7	2.2	1.6	7.5	1.6	1.0	5.4	2.8	1.6	8.0	2.2	1.0	5.8	2.2	1.4	7.0	1.8	0.9	5.4
8	2.5	1.9	2.0	7.6	0.8	1.5	5.6	2.5	1.7	7.7	1.2	1.3	5.7	1.1	2.1	7.3	0.7	1.5	5.5
9	4.2	2.6	1.5	7.3	2.2	0.6	4.9	3.1	1.5	7.8	2.2	0.6	4.9	3.5	1.3	7.6	0.6	1.4	5.2
10	7.2	1.7	1.4	6.5	2.0	0.3	4.1	1.7	1.4	6.5	2.0	0.3	4.1	1.7	1.4	6.5	2.0	0.3	4.1
11	13	1.3	1.6	6.5	1.4	0.5	4.2	1.3	1.6	6.5	1.4	0.5	4.2	1.3	1.6	6.5	1.4	0.5	4.2
12	21	1.4	1.5	6.4	1.0	0.6	4.2	1.4	1.5	6.4	1.0	0.6	4.2	1.4	1.5	6.4	1.0	0.6	4.2

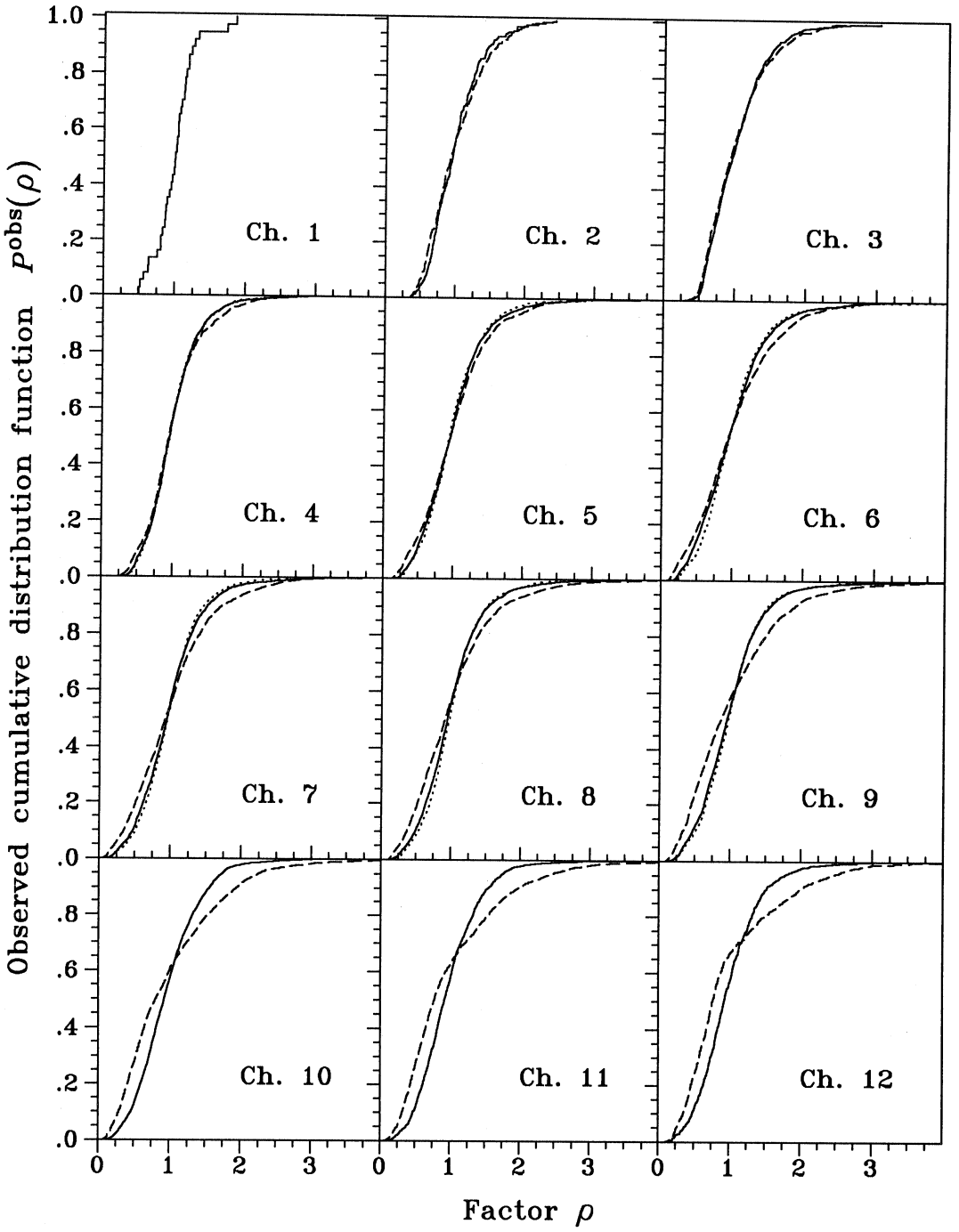

Fig. 3.18 The cumulative distribution function of the observed data, $P^{obs}(\rho)$ is plotted versus the residual factor ρ for the models in Eqs. (3.2) (solid line), (3.3) (dashed line) and (3.8) (dotted line).

The model $dur = dur(I_{MM})$, Eq. (3.3,) has the "worst" cumulative distribution function. The model $dur = dur(I_{MM}, \Delta', I_{MM}\Delta')$, Eq. (3.2), represents the duration of strong motion substantially better, and the most "complete" model $dur = dur(I_{MM}, \Delta', I_{MM}\Delta', h, R, hR, R^2, h^2, \varphi)$ (Eq. (3.8)) is the best one among those presented. The "quality" of the model can be measured by the "closeness" to the "ideal" cumulative distribution function which is equal to zero if $\rho < 0$ and equal to one if $\rho > 0$.

"ideal" model, which would predict the duration with absolute accuracy, should be equal to zero if $\rho < 0$ and equal to one if $\rho > 0$, i.e. should have zero standard deviation. As it is seen from Fig. 3.18, the model $dur = dur(I_{MM})$, Eq. (3.3), has the "worst" cumulative distribution function. The model $dur = dur(I_{MM}, \Delta', I_{MM}\Delta')$ (Eq. (3.2)) represents the duration of strong motion substantially better, as its cumulative distribution function is much closer to the "ideal" distribution than that of the model $dur = dur(I_{MM})$. The introduction of the "prolongation due to site conditions" term in the form of a function of R, h and φ makes some further refinements: the cumulative distribution function of the most "complete" model $dur = dur(I_{MM}, \Delta', I_{MM}\Delta', h, R, hR, R^2, h^2, \varphi)$ (Eq. (3.8)) is "better" than that of the model in Eq. (3.2).

Having the distribution function of ρ, we can predict the duration of strong ground motion which will not be exceeded with a given probability at the site with known properties during on earthquake with given parameters. For a probability P, the value of ρ_P, such that $P = P(\rho_P)$ can be found from Eqs. (3.14)–(3.15). The duration not to be exceeded with probability P is then $dur_P = dur \cdot \rho_P$, where dur^{model} is the duration of strong motion predicted by the model we have chosen.

IV. CONCLUSIONS

This report presents twelve empirical regression models of frequency dependent duration of strong ground motion with the Modified Mercalli intensity at the site as the main scaling parameter. The duration is considered as a sum of two parts: (1) the duration of strong motion that would be observed at a recording station located on basement rocks, and (2) the prolongation of this duration for stations, located on sediments. The first part is called "basic duration," and the second part is called "prolongation" term.

With respect to the "basic duration," two groups of regression equations are considered: one explicitly includes the dependence of the duration of strong ground motion on the distance to the source, the other excludes this dependence. The Modified Mercalli intensity is present as a parameter in both types of models. The models of the first type are more descriptive, but are also more region dependent, because the regional dispersion and attenuation laws are "built into" the frequency dependent regression coefficients. For the fixed intensity, the duration grows when the separation of the source and the recording site increases. For the fixed distance, the dependence of the duration on the intensity is more complex. At low frequencies, the duration of strong motion decreases when the intensity increases, at high frequencies it grows with the increasing intensity. A smooth transition from one to the other type of dependence occurs at intermediate frequencies.

With respect to the "prolongation due to the site conditions" term, also two groups of models are considered. One group utilizes the rough qualitative description of the recording site conditions. The site is considered as being located on rocks, on sediments or on intermediate geology, with soft soils, stiff soils or local "rock" covering the geological structure. In the second group of models, the depth of sediments under the station, the distance from the station to the rocks, surrounding it, and the angular measure of the size of those rocks (as seen from the station) are chosen as the parameters for the modelling of the prolongation of the duration. Those parameters describe the geology under and around the station in greater detail, than the qualitative classification "sediments–rock." In terms of the "rough classification," the duration of strong motion at sedimentary sites is prolonged by about 5 sec at frequencies near 1 Hz, when compared to the basement rock sites. The prolongation of duration on the soft soils can be as mush as 7 sec. The influence of the type of soils on the duration of strong ground motion is stronger at higher frequencies ($f = 0.3 \div 25$ Hz), while the presence of sedimentary deposits can be observed at lower frequencies ($f = 0.15 \div 2$ Hz). In terms of the "detailed description" of the site geology, i.e. when modeled in terms of the geometry of the sedimentary basin, the prolongation of the "basic duration" can be noticed in the frequency range from $f = .5$ Hz to $f = 5$ Hz. The maximum prolongation occurs at the stations located on sediments with moderate depth ($2 \div 3$ km) and at moderate distances from the edges of the sedimentary valley ($30 \div 50$ km). The additional duration can be as much as $5 \div 6$ sec at frequencies near 1 Hz.

The collection of the new empirical regression equations of the strong earthquake ground motion is found to have good internal consistency. These models are also consistent with the empirical models of the duration which have the magnitude and the epicentral distance as the parameters of the "basic duration." An algorithm for choosing the proper model of the duration among those presented is provided. The choice of the model depends on the availability of the site and the propagation path parameters. The residuals of the empirical regression equations are found to have similar distribution functions for all the models. An explicit functional form for such distributions is proposed and the frequency dependent coefficients are found for all the models of duration. This allows one to predict (for each set of earthquake and site parameters) the probability of exceedance of any given level of the duration of strong ground motion at a given frequency.

V. REFERENCES

Amini, A., and M.D. Trifunac (1985). Statistical Extention of Response Spectrum Superposition, *Int. J. Soil Dyn. Earthquake Eng.*, **4(2)**, 54–63.

Bolt, B.A. (1973). Duration of Strong Ground Motion, *Proc. World. Conf. Earthquake Eng., 5th*, Rome, **6-D**, Paper No. 292.

Brune, J.N. (1970). Tectonic Stress and the Spectra of Seismic Shear Waves from Earthquakes, *J. Geophs. Res.*, **75**, 4997–5009.

Esteva, L., and E. Rosenblueth (1964). Spectra of Earthquakes at Moderate and Large Distances, *Bol. Soc. Mex. Ing. Seism.*, **2(1)**, 1–18 (in Spanish).

Gupta, I.D., and M.D. Trifunac (1987). Order Statistics of Peaks of Response to Multi-Component Seismic Excitation, *Bull. Ind. Soc. Earthquake Tech.*, **24**, 135–159.

Gupta, I.D., and M.D. Trifunac (1988). Order Statistics of Peaks in Earthquake Response, *ASCE, EMD*, **114**, 1605–1627.

Gupta, V.K., and M.D. Trifunac (1990a). Response of Multistoried Buildings to Ground Translation and Rocking During Earthquakes, *J. Probabilistic Eng. Mechanics*, **5**, 138–145.

Gupta, V.K., and M.D. Trifunac (1990b). Response of Multistoried Buildings to Ground Translation and Torsion During Earthquakes, *European Earthquake Eng.*, **Vol. IV-n.1**, 34–42.

Gupta V.K., and M.D. Trifunac (1991). Effect of Ground Rocking on Dynamic Response of Multistoried Building During Earthquakes, *Structural Eng./Earthquake Eng., JSCE*, **8**, 43–50.

Gupta, V.K., and M.D. Trifunac (1992). Seismic Response of Multistoried Buildings Including the Effects of Soil Structure Interaction, *Int. J. Soil Dyn. and Earthquake Eng*, **10**, 414–422.

Housner, G.W. (1965). Intensity of Ground Shaking Near Causative Fault, *Proc. World Conf. Earthquake Eng., 3rd*, New Zealand, **3**, 94–109.

Husid, R., H. Medina, and J. Rios (1969). Analysis de Terremotos Norteamericanos y Japaneses, *Revista del IDIEM 8*, Chile (in Spanish).

Kawashima, K., and K. Aizawa (1989). Bracketed and Normalized Durations of Earthquake Ground Acceleration, *Earthquake Eng. Structural Dyn.*, **18**, 1041–1051.

Lee, V.W., and M.D. Trifunac (1984). Current Developments in Data Processing of Strong Motion Accelerograms, Dept. of Civil Eng., Report No. 84-01, Univ. of Southern Calif., Los Angeles, California.

Lee, V.W., and M.D. Trifunac (1985). Uniform Risk Spectra of Strong Earthquake Ground Motion, Dept. of Civil Eng., Report No. 85-05, Univ. of Southern Calif., Los Angeles, California.

Lee, V.W., and M.D. Trifunac (1987). Strong Earthquake Ground Motion Data in EQINFOS: Part I, Dept. of Civil Eng., Report No. 87-01, Univ. of Southern Calif., Los Angeles, California.

Lee, V.W., and M.D. Trifunac (1990). Automatic Digitization and Processing of Accelerograms Using PC, Dept. of Civil Eng., Report No. 90-03, Univ. of Southern Calif., Los Angeles, California.

McCann, M.W., and H.C. Shah (1979). Determining Strong-Motion Duration of Earthquakes, *Bull. Seism. Soc. Amer.*, **69**, 1253–1265.

Mohraz, B., and M.-M. Peng (1989). Use of a Low-Pass Filter in Determining the Duration of Strong Ground Motion, *ASME, Pressure Vessels and Piping Division (Publication) PVP*, **182**, Publ. by ASME, New York, New York, 197–200.

Montgomery D.C., and Peck E.A. (1982). Introduction to Linear Regression Analysis, J. Wiley and Sons, New York.

Novikova, E.I., and M.D. Trifunac (1993). Duration of Strong Ground Motion: Physical Basis and Empirical Equations. Dept. of Civil Eng., Report No. 93-02, Univ. of Southern Calif., Los Angeles, California.

Page, R.A., D.M. Boore, W.B. Joyner, and H.W. Caulter (1972). Ground Motion Values for Use in the Seismic Design of the Trans-Alaska Pipeline System, USGS Circular 672.

Seed, H.B., C. Ugas, and J. Lysmer (1976). Site Dependent Spectra for Earthquake Resistant Design, *Bull Seism. Soc. Amer.*, **66**, 221–243.

Shebalin, N.V. (1969). Makroseismicheskoe pole i ochag silnogo zemletrjaseniya (Macroseismic field and the source of a strong earthquake) Dissertation, Inst. Physics of the Earth, Moscow.

Smith, M.B. (1964). Map Showing Distribution and Configuration of Basement Rocks in California (North Half) (South Half), Oil and Gas Investigations, Map OM-215, Dept. of the Interior United States Geological Survey, Washington, D.C.

Theofanopulos, N.A., and M. Watabe (1989). A New Definition of Strong Motion Duration and Comparison with Other Definitions, *Structural Eng./Earthquake Eng., JSCE*, **6**, 111–122.

Trifunac, M.D. (1973). Analysis of Strong Earthquake Ground Motion for Prediction of Response Spectra, *Earthquake Eng. Structural Dyn.*, **2(1)**, 59–69.

Trifunac, M.D. (1989a). Dependence of Fourier Spectrum Amplitudes of Recorded Strong Earthquake Accelerations on Magnitude, Local Soil Conditions and on Depth of Sediments, *Earthquake Eng. Structural Dyn.*, **18**, 999–1016.

Trifunac, M.D. (1989b). Empirical Scaling of Fourier Spectrum Amplitudes of Recorded Strong Earthquake Accelerations in Terms of Magnitude and Local and Geological Conditions, *Earthquake Eng. and Eng. Vibrations*, **9**, 23–44.

Trifunac, M.D. (1989c). Scaling Strong Motion Fourier Spectra by Modified Mercalli Intensity, Local Soil and Geological Site Conditions, *Structural Eng./ Earthquake Eng., JSCE*, **6**, 217–224.

Trifunac, M.D. (1990). How to Model Amplification of Strong Earthquake Motions by Local Soil and Geological Site Conditions, *Earthquake Eng. Structural Dyn.*, **19**, 833–846.

Trifunac, M.D. (1991). M_L^{SM}, *Int. J. Soil Dyn. Earthquake Eng.*, **10**, 17–25.

Trifunac, M.D., and A.G. Brady (1975a). A Study on the Duration of Strong Earthquake Ground Motion, *Bull. Seism. Soc. Amer.*, **65**, 581–626.

Trifunac, M.D., and A.G. Brady (1975b). On the Correlation of Seismic Intensity Scales with the Peaks of Recorded Strong Ground Motion, *Bull. Seism. Soc. Amer.*, **65**, 139–162.

Trifunac, M.D., and V.W. Lee (1979). Automatic Digitization and Processing of Strong Motion Accelerograms, Dept. of Civil Eng., Report No. 79-15 I and II, Univ. of Southern Calif., Los Angeles, California.

Trifunac, M.D., and V.W. Lee (1985). Frequency Dependent Attenuation of Strong Earthquake Ground Motion, Dept. of Civil Eng., Report No. 85-02, Univ. of Southern Calif., Los Angeles, California.

Trifunac, M.D., and V.W. Lee (1990). Frequency Dependent Attenuation of Strong Earthquake Ground Motion, *Int. J. Soil Dyn. Earthquake Eng.*, **9**, 3–15.

Trifunac, M.D., and M.I. Todorovska (1989). Attenuation of Seismic Intensity in Albania and Yugoslavia, *Earthquake Eng., Structural Dyn.*, **18**, 617–631.

Trifunac, M.D., and B.D. Westermo (1976). Correlations of Frequency-Dependent Duration of Strong Ground Motion with the Modified Mercalli Intensity, and the Geological Conditions at the Recording Stations, Dept. of Civil Eng., Report No. 76-03, Univ. of Southern Calif., Los Angeles, California.

Trifunac, M.D., and B.D. Westermo (1977). A Note on the Correlation of Frequency-Dependent Duration of Strong Earthquake Ground Motion with the Modified Mercalli Intensity and the Geological Conditions at the Recording Stations, *Bull. Seism. Soc. Amer.*, **67**, 917–927.

Trifunac, M.D., and B.D. Westermo (1982). Duration of Strong Earthquake Shaking, *Int J. Soil Dyn. Earthquake Eng.*, **2**, 117–121.

Udwadia, F.E., and M.D. Trifunac (1974). Characterization of Response Spectra through the Statistics of Oscillator Response, *Bull. Seism. Soc. Amer.*, **64**, 205–219.

Vanmarcke, E.H., and S.P. Lai (1980). Strong-Motion Duration and RMS Amplitude of Earthquake Records, *Bull. Seism. Soc. Amer.*, **70**, 1293–1307.

Westermo, B.D., and M.D. Trifunac (1978). Correlations of the Frequency Dependent Duration of Strong Earthquake Ground Motion with the Magnitude, Epicentral Distance, and the Depth of Sediments at the Recording Site, Dept. of Civil Eng., Report No. 78-12, Univ. of Southern Calif., Los Angeles, California.

Westermo, B.D., and M.D. Trifunac (1979). Correlations of the Frequency Dependent Duration of Strong Ground Motion with the Modified Mercalli Intensity and the Depth of Sediments at the Recording Site, Dept. of Civil Eng., Report No. 79-01, Univ. of Southern Calif., Los Angeles, California.

Wood, H.O. and F. Neumann (1931). Modified Mercalli Intensity Scale of 1931, *Bull. Siesm. Soc. Amer.*, **21**, 277–283.